UNIVERSITY OF SOUTHAMPTON

FACULTY OF PHYSICAL AND APPLIED SCIENCES

OPTOELECTRONICS RESEARCH CENTRE

Development of a High Spatial Resolution Temperature Compensated Distributed Strain Sensor

By

Mohammad Belal

Thesis submitted for the degree of Doctor of Philosophy

July 2011

UNIVERSITY OF SOUTHAMPTON
FACULTY OF PHYSICAL AND APPLIED SCIENCE
OPTOELECTRONICS RESEARCH CENTRE
Doctor of Philosophy

Development of a High Spatial Resolution Temperature Compensated Distributed Strain Sensor

Mohammad Belal

Abstract

Optical fibre sensors have offered such unrivalled distributed sensing features that they continue to be successfully exploited in various industries for performing continuous measurements of the physical parameters, such as, temperature and strain. However, there arise certain conditions in engineering or materials manufacturing and characterisation environments, when the user seeks to extract the knowledge about a single physical parameter only, say strain, whilst the environment is also subject to temperature. This thesis explores techniques to offer solutions under such conditions by developing a high spatial resolution temperature compensated distributed strain sensor.

The preliminary exploration involved exploiting the high spatial resolution Brillouin frequency based Brillouin optical correlation domain analysis technique in combination with the anti Stokes Raman intensity based optical time domain reflectometry technique. This work resulted in achieving a temperature compensated strain resolution of 46με with a spatial resolution of 24cms over a sensing length of 135m. Tackling the impact of modest pump depletion effects on the Raman backscattered signal, a beneficial normalisation protocol was identified. During discussions the possible limitation imposed by the weaker backscattered Raman signal towards achieving any better results on the strain and spatial resolution values, seemed to emerge. In order to enhance the performance of the sensor, anti Stokes

Brillouin, which is a stronger back scattered signal, was exploited for the time domain reflectometry measurements. This resulted in 22με of temperature compensated strain resolution with a spatial resolution capability of 10cms.

Although the combined performance of the Brillouin frequency in combination with Brillouin intensity proved better than the performance of the Brillouin frequency in combination with Raman intensity, but since the electronic detection system was changed together with pulse widths between the two techniques that it was unclear as to which combinatory technique was best suited for designing the sensor. It is with this view that a theoretical analysis on the performance of the R-OTDR and B-OTDR was carried under similar sensor parameters. B-OTDR is identified as a better technique compared to the R-OTDR towards providing high spatial resolution temperature compensation feature to the Brillouin frequency based distributed strain measurements.

The exploration also gave an opportunity to experimentally study for the first time the impact of simultaneously varying temperature and strain on the four Brillouin coefficients. This study proved useful in identifying the corrections to the Brillouin coefficients in order to estimate the true value of strain and temperature in a temperature controlled variable strain environment.

The thesis culminates with a summary of work, discussing the thresholds of various non linear effects together with means to improve the performance of the sensor. With the view of enhancing the sensor applicability, schemes of loss compensation are also discussed. In conclusion work for the future is highlighted.

Contents

DECLARATION OF AUTHORSHIP

I, ***Mohammad Belal***, declare that the thesis entitled ***Development of a High Spatial Resolution Temperature Compensated Distributed Strain Sensor***
and the work presented in it are my own. I confirm that:

- this work was done wholly or mainly while in candidature for a research degree at this University;

- where any part of this thesis has previously been submitted for a degree or any other qualification at this University or any other institution, this has been clearly stated;

- where I have consulted the published work of others, it is always clearly attributed;

- where I have quoted from the work of others, the source is always given. With the exception of such quotations, this thesis is entirely my own work;

- I have acknowledged all main sources of help;

- where the thesis is based on work done by myself jointly with others, I have made clear exactly what was done by others and what I have contributed myself;

- parts of this work have been published as:
  Refer to List of Publications on pages 147-149

Signed: Mohammad Belal
Date: 12/07/11

Acknowledgements

Progress in this work would not have been possible without the generous guidance and support of the following individuals/groups:

Dr. Trevor Newson – for his unstinting commitment towards helping me cross collaborate whilst also managing to maintain the desired focus with regards to achieving particular goals. His generous and wise guidance coupled with his unusual ability to educate even outside work has contributed immensely towards the understanding of this subject and the genre of research and development in entirety.

Dr. G. Brambilla – for his willingness to engage in discussions on a number of academic projects.

Prof. D. J. Richardson – for his immense support.

ORC – all members at this facility for encouraging me to engage in those enlightening discussions and special thanks to the support staff for their concerns, care and affection.

Finally, I would like to thank my dear parents for all their prayers and good wishes over the years and the ever so supportive elder brother for encouraging me towards advanced scientific research and development.

List of Acronyms

FWHM	Full width half maximum
OTDR	Optical time domain reflectometry
R-OTDR	Raman optical time domain reflectometry
B-OTDR	Brillouin optical time domain reflectometry
BGS	Brillouin gain spectrum
GVD	Group velocity dispersion
SBS	Stimulated Brillouin scattering
SRS	Stimulated Raman scattering
SPM	Self phase modulation
FBG	Fibre Bragg grating
MI	Modulation instability
ASE	Amplified spontaneous emission
NEI	Noise equivalent current
NEV	Noise equivalent voltage
NES	Noise equivalent signal
BOTDA	Brillouin optical time domain analysis
DPP-BOTDA analysis	Differential pulse width pair Brillouin optical time domain
BDG-DS	Brillouin dynamic grating distributed sensing
BOCDA	Brillouin optical correlation domain analysis
BOCDR	Brillouin optical correlation domain reflectometry
AOM	Acousto optic modulator
EOM	Electro optic modulator

EDFA	Erbium doped fibre amplifier
OSA	Optical spectrum analyser
FWM	Four wave mixing
HWHM	Half width half maximum
PC	Personal computer
PM	Polarization maintaining
STF	Standard telecommunication fibre

1. Introduction

At the very heart of modern day electronic communications lies the vast network of silica based optical fibres. The key reason for the success of these fibres rests in their capacity to transmit optical signals at 1.55µm with small transmission losses together with an integrated signal amplification capability, in the form of an erbium doped fibre amplifier. Both these features are an outcome of an extensive research activity which started in the early sixties. However, towards the late eighties some researchers unearthed another technological application of optical fibres, besides signal transmission. This novel development came to be known as distributed optical fibre sensing.

Since then rapid advances in distributed optical fibre sensing have contributed enormously towards providing maturity and reliability to the technology. Despite increasing interests in achieving more energy efficient wireless sensor networks, it is this sense of reliable performance which optical fibre sensing technology has developed amongst users that continues to hail it as a preferred choice within the domain of distributed sensing. Even whilst considering quasi distributed sensor systems, where wireless electronic sensors are continually providing improved capabilities of probing measurands such as temperature, sound, pressure etc with fair amount of reliability using rigorously compiled routing algorithms, unique features such as immunity to electromagnetic fields together with minimal post processing requirements offered by fibre optics based technology continues to rank it as an increasingly popular choice for quasi distributed sensing environments.

Distributed fibre optic sensing over short ranges, typically under a kilometre, poses a new set of challenges and certain requirements need to be met in order to enjoy the same sensor applicability, robustness and reliability as has been realised so far with long range distributed fibre optic sensing. In the past Raman and Brillouin scattering effects in optical fibres have been exploited to make distributed measurements of

temperature and strain over long sensing ranges. The same scattering processes can still be exploited, but the real challenge in order to offer distributed strain sensing capabilities over short ranges is to design a sensor, capable of probing measurands with high spatial resolution features, typically much below a meter. With increasing interests in structural health monitoring of machines or civil structures such as dams, bridges, aircraft engines etc, the idea to establish reliable high spatial resolution distributed strain measurements continues to be of immense importance.

Strain, which is understood to be a measure of physical deformation caused in a particular direction with respect to original state, does not only result from direct physical deformations as a consequence of forces applied, but also emerges due to thermal effects. For instance in cases where a structure is subject to cyclic loading as part of routine tests for material characterisation in structural health monitoring, one witnesses substantial heating of the structure. Under such circumstances it becomes critical that the sensor, capable of offering high spatial resolution distributed strain measurements, is also designed with additional features to account for thermally induced strain and also that strain measurement is independent of temperature. To address these problems witnessed in structural engineering environments, this thesis focuses on exploring the design of a temperature compensated high spatial resolution distributed strain sensor using fibre optic technology.

The work carried out in this thesis is based on the author's own research. Use of any material from other sources is clearly referenced.

The thesis is divided into seven chapters. A brief description of each chapter is given below:

Chapter 2 attempts to critically appreciate previous contributions to distributed sensing made utilising both spontaneous and stimulated Brillouin scattering. The techniques developed so far for distributed strain and temperature measurements are analysed with the view of identifying both merits and demerits of the techniques used

in the past. The subject of this thesis is briefly mentioned before the chapter embarks onto an extended literature review highlighting previous attempts with regards to making high spatial resolution distributed strain measurements with full temperature compensation. Lessons learnt from the critical analysis in this literature review were used to select, combine and develop the most promising techniques to be exploited.

Chapter 3 describes experimental work which discusses the theory, experimental layout, results, summary and conclusions of the combinatory technique of Brillouin frequency measurements and Raman intensity measurements.

Chapter 4 similarly explores the theoretical and experimental aspects along with results, summary and conclusions associated with the other proposed combinatory technique involving Brillouin frequency and Brillouin intensity measurements.

Chapter 5 dwells on the performance outcome of the Raman intensity based OTDR technique with the Brillouin intensity based OTDR technique whilst probing a sensing length of 100m with a spatial resolution of 10cms. The treatment of the two techniques in this chapter is theoretical but the outcome helps identify the superiority of one technique over the other, which could then be used for short range high spatial resolution temperature compensation measures during distributed strain measurements.

Chapter 6 is a generic study on the validity of Brillouin coefficients experimentally tested on a temperature controlled strain rig. Motivation for this emerged due to lack of any experimental evidence in literature confirming the validity of Brillouin coefficients under conditions where the sensing fibre is subject to simultaneously varying strain and temperature. It was assumed that the coefficients would remain valid under such conditions, and all the previous work exploiting Brillouin scattering for simultaneous strain and temperature sensing was based on this assumption.

Chapter 7 concludes the thesis with discussion of results and future work aimed at enhancing the sensor performance.

2. Literature Review on Brillouin based distributed sensing techniques

The field of distributed optical fibre sensing has matured enormously over the past two decades, and it is impractical to review all the techniques developed so far. This review focuses on the spontaneous and stimulated Brillouin scattering based techniques that have been used previously for distributed sensing purposes.

2.1 Brillouin Optical Time Domain Reflectometry (B-OTDR)

The optical time domain reflectometry (OTDR) [1] technique introduced the distributed measuring capabilities of fibre optics. In OTDR, as the pulse travels down the optical fibre, the most powerful scattering observed is Rayleigh scattering. This Rayleigh scattering is an elastic scattering process triggered by the interaction between the propagating light and the randomly occurring inhomogeneities in the refractive index which are smaller than the wavelength of the propagating light. The inhomogeneities arise from compositional and density fluctuations, which are frozen into the glass under the cooling process, during fabrication. The backscattered Rayleigh signal emerging as a consequence of scattering from frozen imperfections within the fibre, was exploited for distributed optical loss measurements, in the fibre under test. However the distributed strain and temperature probing potential of fibre optics was unleashed when Brillouin scattering was demonstrated to be sensitive to temperature and strain [2, 3] influences.

Under modest pump powers, i.e., without the onset of any optical non linear effects, it is fair to assume that the Rayleigh scattering [4] spectrally resembles the profile of the launched pump beam. However the spontaneous Brillouin scattering [5], which

relies on the existence of phase matching between the incident optical field and the acoustic phonon field, results in a Lorentzian shaped profile. The peak of this Lorentzian shaped resonance spectrum is frequency shifted from the pump wavelength by an amount given by equation 1 [6].

$$v_B = \frac{2nV}{\lambda_p} \qquad (1)$$

Where v_B is the Brillouin frequency shift, n represents the effective refractive index of the propagating mode, V is the acoustic velocity in the fibre and λ_p is the wavelength of pump light launched into the fibre. The dependence of the spontaneous Brillouin shift on the acoustic wave velocity, which is a material property directly influenced by temperature and strain, allows the applied temperature [7] or strain to be ascertained by measuring the shift in the resonance spontaneous Brillouin peak frequency. The FWHM of this Lorentzian profile depends on the decay time of the acoustic phonon field, which translates itself into a 30 – 35MHz natural Brillouin line width [4].

Exploiting the inherent feature of spontaneous Brillouin scattering to be influenced by temperature and strain, both these physical parameters have been probed using the spontaneous Brillouin scattering emerging as a consequence of an optical pulse launched down the optical fibre, recorded as a function of time [8]. This method of Brillouin optical time domain reflectometry (B-OTDR) offered the possibility of using either Brillouin frequency or power [9, 10] for strain and/or temperature sensing. The elegant technique of coherent detection of the spontaneous Brillouin scattering [11, 12] was pioneered that offered both temperature and strain sensing over record lengths [12]. Such a technique, as shown in figure 1, extracted the Brillouin frequency shift by mixing the spontaneous Brillouin backscattered signal from the travelling pulse with the continuous wave (c.w) light from the laser and shining it onto a high bandwidth detector (>11GHz) in order to convert the optical Brillouin signal into electrical domain. This electrical signal was then reduced to a low frequency signal by electrically mixing it with a microwave local oscillator.

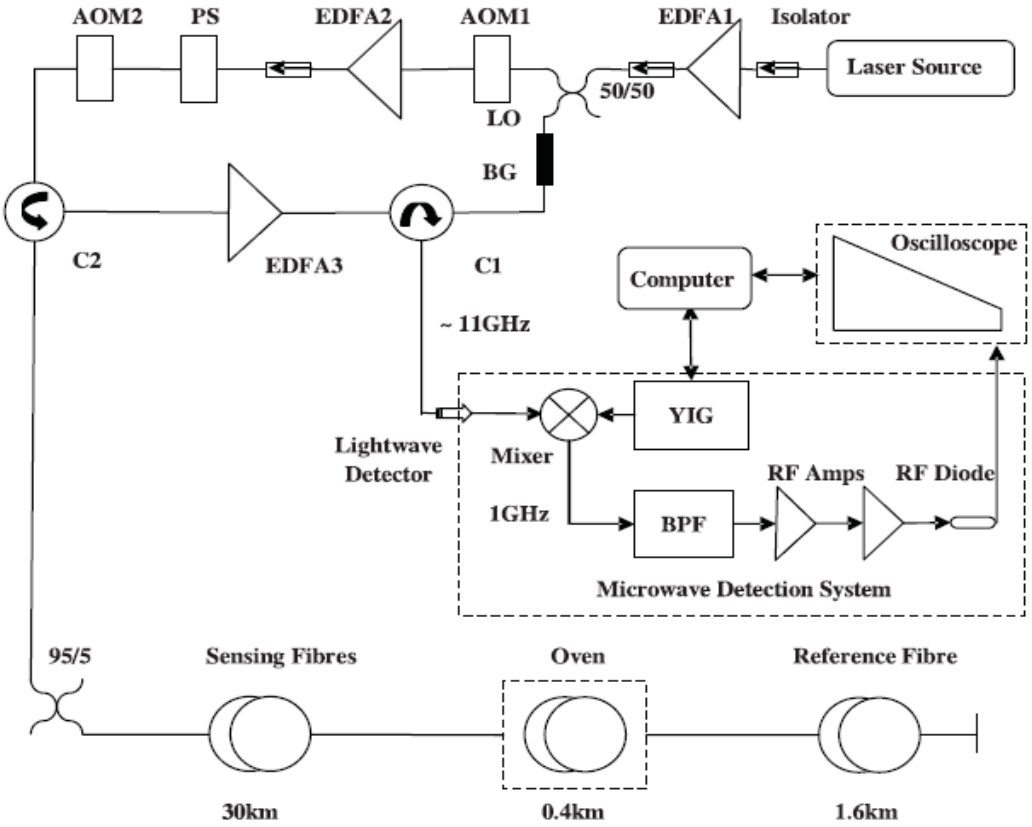

Figure 1. Experimental layout for measuring the Brillouin frequency shift using microwave detection system; exploiting the fundamental B-OTDR technique. Experimental layout comprises EDFA – erbium doped fibre amplifier; AOM – acousto optic modulator; PS - polarization scrambler; LO - local oscillator, BG - Bragg grating; C – circulator; LD - lightwave detector; YIG - YIG synthesizer; BPF – band pass filter) [11]

Reducing the high frequency electrical signal (11GHz) to a low frequency of 1GHz allowed the use of low frequency electronic components (amplifier, detectors etc) resulting in improved signal to noise. The information about temperature or strain was eventually extracted by observing the shift in peak Brillouin frequency spectrum generated by scanning the frequency of the microwave oscillator. The technique was also aimed at achieving reduced intensity noise over long sensing range, and incidentally improvements in intensity measurements automatically yielded improved frequency resolutions too. Moreover, in the light of recent claims highlighting advantages in usage of stimulated Brillouin scattering over spontaneous Brillouin scattering based sensing techniques for short sensing range, it seems

imperative to mention that even though the microwave detection scheme [10-12] was primarily conceived with the objectives of achieving high temperature resolutions over long sensing range (~100kms), as a matter of record it had already proven its capability to offer under a degree temperature resolution capabilities for 20km sensing range [13].

B-OTDR brought with itself the advantage of long range sensing with single ended access, an unarguably valuable feature in long range sensing applications. Since B-OTDR was a pulse based technique, Brillouin frequency measurements made using this technique could not probe measurands with sub-metre spatial resolutions. The explanation was simple and in agreement with fundamentals of Fourier transforms. i.e., a short duration optical pulse bears a broadened spectral image in frequency domain. For sub metre spatial resolution, a pulsed based technique would require < 10ns duration optical pulses. In practise such a requirement increases the error in determining the peak of the broadened Brillouin frequency spectrum, necessary for determining the frequency shift resulting from the application of strain or temperature relative to unstrained-unheated sections of the sensing fibre. The relationship of the uncertainty in the Brillouin frequency spectrum or the peak Brillouin frequency itself $(\delta v_B)$with the Brillouin gain bandwidth (Δv_B) and the electrical signal to noise ratio is given by equation 2 [14]

$$\delta v_B = \frac{\Delta v_B}{(SNR)^{1/4}\sqrt{2}} \qquad (2)$$

So it was well understood that usage of optical pulses less than 10ns would lead to broadening of the Brillouin frequency spectrum far beyond the natural line width value of 35MHz. Such a broadened Brillouin frequency spectrum would result in deterioration of the signal to noise figure required in order to reliably extract the information about strain or temperature hidden in the peak Brillouin frequency shift. Hence reasons emerging from the basic understanding of Fourier transforms, highlighting the limitations on the usability of frequency based spontaneous Brillouin measurements using pulsed based techniques, to probe measurands with sub-metre spatial resolution were well appreciated.

2.2 Brillouin Optical Time Domain Analysis (BOTDA)

Brillouin optical time domain analysis (BOTDA) [15, 16] technique, soon after its inception in the late eighties, was initially exploited for measurement of fibre losses. With its much increased signal levels compared to the OTDR technique and the sensitivity of the Brillouin gain spectrum to strain and temperature, it was soon exploited for distributed strain measurements [17]. The experimental scheme is shown in figure 2.

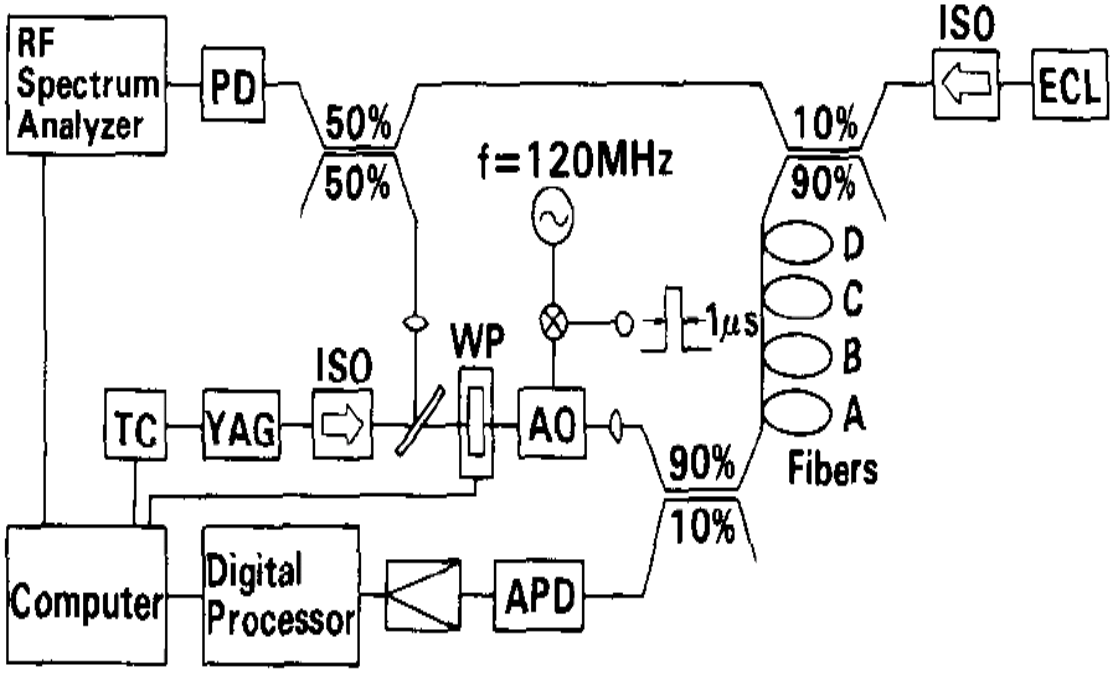

Figure 2. The Brillouin gain based BOTDA arrangement [17]
ISO: isolator, WP: half wave plate, AO: acousto optical modulator, ECL: external cavity semiconductor laser, TC:temperature controller, APD: avalanche photodiode, PD: photodiode.

2.2.1 BOTDA – Brillouin Gain

The Brillouin gain based BOTDA scheme exploited the stimulated Brillouin scattering as against spontaneous Brillouin scattering used in B-OTDR. It used the concept of Brillouin gain witnessed by recording the probe amplitude in the time domain, during a locally interacting intense pump pulse and a weak continuous wave counter-propagating light probe through stimulated Brillouin scattering. The frequency difference between pump and probe was scanned step-by-step and the local amplification of the probe could be retrieved for a given pump-probe frequency difference along with the location of the interaction by simply exploiting the conventional optical time domain reflectometry idea which was already so effectively embedded by virtue of the existing pulsed nature of one of the interacting optical signals. This optimal frequency difference between the interacting pulse and probe resulting in a Brillouin gain curve was affected by strain or temperature, resulting in a shift in the peak frequency corresponding to maximum gain experienced by the probe for a region in the fibre subjected to strain or temperature.

2.2.2 BOTDA – Brillouin Loss

In the conventional experimental scheme of Brillouin gain based BOTDA [17] shown in figure 2, the c.w probe power increases at the expense of a continuously weakened pump pulse due to power transfer to the c.w probe, hence the term Brillouin gain. However, with the weakening of the pump pulse the technique was found unsuitable for longer sensing range. Hence in order to avoid depletion of the pump pulse over longer sensing lengths that the Brillouin loss based BOTDA technique was introduced, experimental layout shown in figure 3 [18].

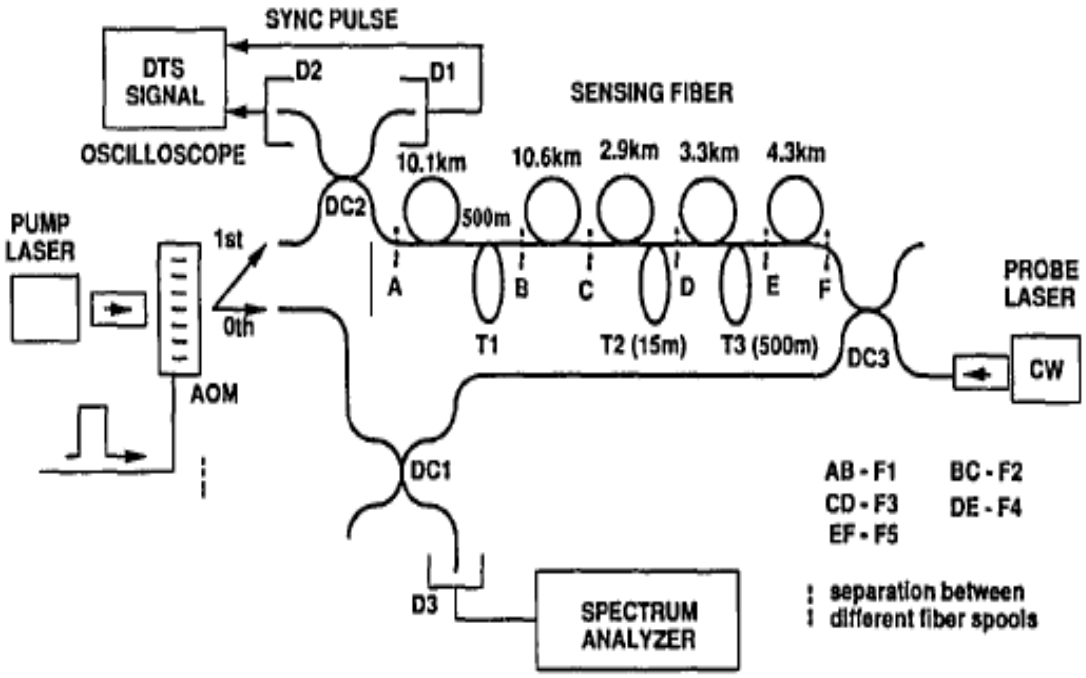

Figure 3. Experimental arrangement for the Brillouin loss based BOTDA technique [18]

In this technique the output of the monitored c.w probe is adjusted such that it is at a higher frequency than the pump pulse. Corresponding to a section of sensing fibre under interrogation, the Brillouin shift between the counter propagating pump and probe signals results in power transfer from the c.w probe to the pump pulse, yielding a stronger pulse as it propagates down the sensing length, resulting in better signal to noise whilst probing measurands over longer distances [18, 19] in situations where substantial lengths of fibre are at the same temperature.

However, closely examining the fundamental features exploited during the BOTDA layouts, it can be identified that the technique is rendered weak due to the induction of systematic errors, which can limit the performance of the sensor based upon such a technique. Especially long range and high-spatial-resolution measurements can lead to inaccurate strain and temperature determinations. The reason for this effect is that the power transfer between pulse and CW light due to Brillouin interaction results in an increase (in the loss method) or decrease (in the gain method) of the pulse power. Such a change in pulse power depends on the Brillouin interaction at every point in the sensing fibre, from the point of entrance of the pulse into the fibre

to the actual measurement point [20]. This results in the distortion of the pulse all the way resulting in localised measurements getting influenced by nonlocal effects, leading to significant errors [21] in identifying the peak Brillouin frequency. Besides this fundamental problem with BOTDA the Brillouin loss mechanism in particular, whilst addressing the issue of long range sensing by amplifying the pulse power, introduces the danger of various non linear effects being triggered due to enhanced pulse powers. Despite the deficiencies identified with the conventional design of the BOTDA techniques (Brillouin gain and Brillouin loss), there still was agreement over the fundamental spatial resolution probing limitation, i.e., below 1m, due to the pulsed nature of the technique, which implied immense broadening of the frequency spectrum for less than 10ns pulses, an understanding which was arrived at as a consequence of the principles of Fourrier transforms. But this understanding was abandoned when the BOTDA arrangement was set for Brillouin loss measurements using < 10ns pulses [22]. The outcome of this experiment was interpreted as a breakthrough made towards providing sub-metre spatial resolution distributed strain or temperature sensing features using Brillouin frequency without compromising the natural Brillouin line width (~35MHz). The set up involved the same Brillouin loss method albeit with less than 10ns pulses. The interpretation of the result was not in agreement with the fundamental concepts of Fourier transforms, i.e., a short duration temporal response carries a broad band profile in frequency domain. In accordance with which one would expect a broadened Brillouin gain spectrum even in a BOTDA experiment where short duration (< 10ns) optical pulses are used. On the contrary Bao's group reported narrowing of Brillouin gain spectrum despite usage of 3ns optical pulses.

Soon the results were experimentally and theoretically reproduced [23] and a more logical explanation emerged. It was identified that due to a finite extinction ratio achieved with the EOM that the c.w Stokes leaking through, interacts with the c.w counter-propagating pump and yields a background signal represented by the natural Brillouin line width profile in the frequency domain. The short pulse interaction, however in line with principles of Fourier transform, results in a broadened Gaussian like profile, which is evident with high extinction ratio EOM output pulses too [23], but less evident for pulses with poor extinction ratio. This is because the gain of the

broadened spectrum produced by the pulse is small compared to the background gain produced by the c.w pedestal leading to the natural Brillouin line width. Although using an EOM with low extinction ratio generates a narrow Brillouin line width, the inherent drawback associated with such methods is the distorted Brillouin gain spectrum. That is the detected Brillouin spectrum is averaged over the fibre length and cannot be used to accurately determine strain or temperature levels with high spatial resolution unless they are hot spots, which are associated with Brillouin frequency shifts greater than the natural Brillouin linewidth. This is a very significant restriction in their applicability.

2.2.2.1 Brillouin Loss - Dark Pulse

It was in line with pushing the sub-metre spatial resolution sensing capability that the Brillouin loss based BOTDA arrangement was tested using the dark pulse scheme, experimental layout shown in figure 4 [24, 25].

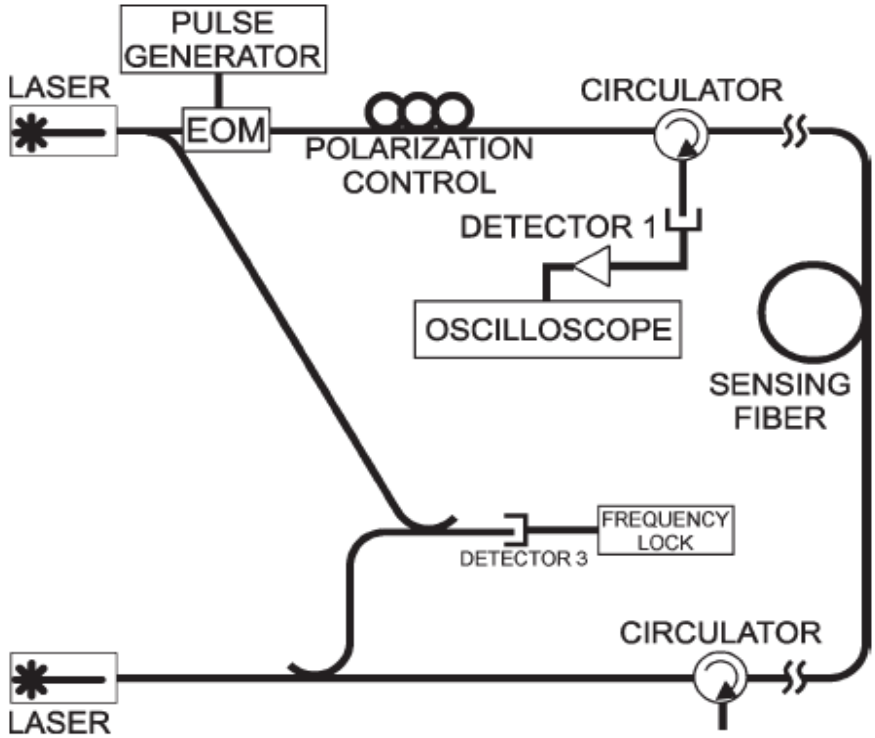

Figure 4. BOTDA sensor configuration for the dark pulse technique [24, 25]

This scheme of BOTDA arrangement comprised complete exploitation of c.w – c.w interaction and instead pump was switched off for a short duration. This implied that instead of using the leakage through the EOM of a finite extinction, a complete c.w – c.w interaction would enhance the signal to noise, which would result in more accurate identification of the peak Brillouin frequency shift, thereby estimating the implied strain or temperature more precisely, while the sub-metre spatial resolution probing of measurand was achieved by switching off the c.w pump for a short time duration, which in other words would imply an absence of pulse or even a dark pulse [19]. This dark pulse was created by gating the optical signal using an electro optic modulator (EOM). And it was this time duration of the off state that corresponded to the required spatial resolution. This technique was presented as an improvement over the bright pulse concept of the BOTDA method. In fact it was identified that with the option of the dark pulse technique which does not suffer the handicap of pulse depletion that Brillouin gain method could still be used. Moreover, since the dark pulse technique in Brillouin loss mode suffers the handicap of c.w pump depletion, over long sensing lengths the Brillouin gain [18] mode appeared all the more beneficial. Interestingly, simulations also suggested [19] that Brillouin gain mode with dark pulse offered a stronger interaction yielding a 2-3 dB increase in signal level. A careful analysis of the experimental findings lead to an obvious conclusion about such techniques, i.e., they were all potentially useful for hot spot detection, which involves imposition of high temperatures or large strains capable of rendering large frequency shifts greater than the natural Brillouin linewidth. However the techniques were inappropriate for general distributed measurements of strain or temperature, where the measurands may not bear significant variations between each other or the rest of the fibre over the entire sensing range.

Despite this very significant restriction to hot spot detection there still has been interest in exploiting the idea of acoustic pre-excitation in the sensing fibre, with a rather misleading notion of applicability to distributed sensing. The reason for this has been the conscious exploitation of the explanation, regarding the c.w leakage due to a finite extinction of the EOM, which instead was given by Lecoeuche et al [23] in order to re-affirm the concepts of Fourier transforms, and to disprove the conclusions drawn by Bao et al [18].

2.3 Brillouin Echo Based Distributed Sensing (BEDS)

Much in line with the acoustic pre excitation concept, the Brillouin echo [26, 27, 28] technique emerged, which essentially exploited a feature similar to the Brillouin loss set up in the dark pulse format, but instead of switching off the pump, the technique capitalised on the ability to destructively interfere the pump with the counter-propagating probe by switching it π out of phase for a short duration, using an electro optic phase modulator, as shown in figure 5 [27].

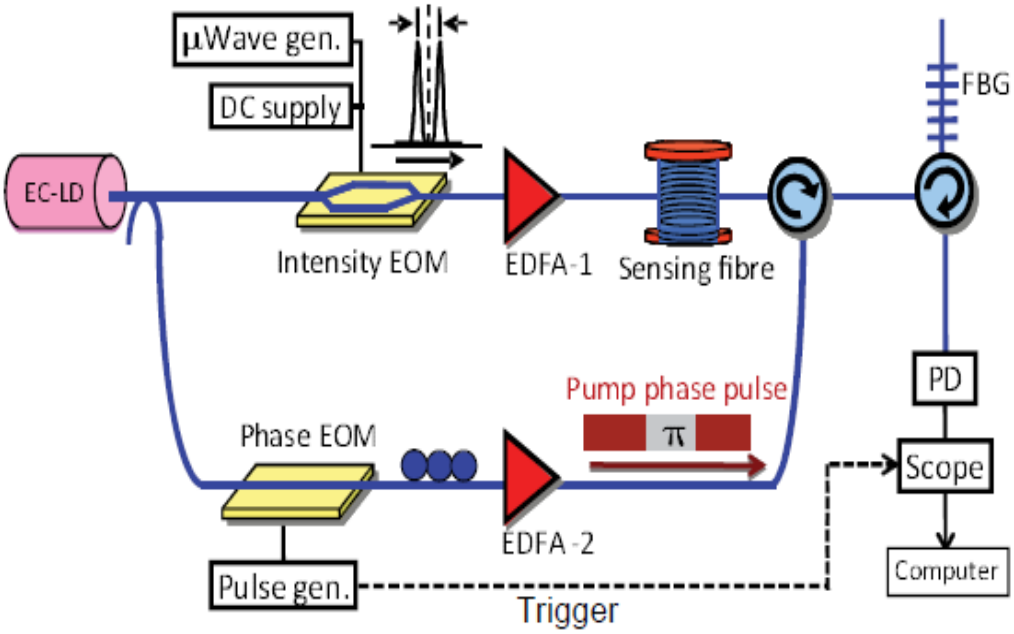

Figure 5. Experimental layout of the Brillouin echo based distributed sensing scheme [27]

The scheme resulted in 3dB improvement of signal to noise figure in comparison to the dark pulse format, however whilst offering improved signal to noise features over the dark pulse format, the scheme introduced a new problem of secondary echoes, i.e., the constructive interferences emerging between the pump and slightly decayed acoustic wave, seen as a consequence of resumption of pump and probe interaction after the operation of the π phase pulse. The post 'π phase pulse' state was sufficient to trigger a false signal from a different part of the fibre, which could easily confuse with the first signal observed during the duration of the 'π phase pulse'. So even if one assumes merit in the usability of the scheme to the class of hot spot detection

systems, based upon the first experimental demonstrations of the technique [26, 27], the issue of secondary echoes detracts from the technique true distributed measurements.

2.4 Differential Pulse Pair Brillouin Optical Time Domain Analysis (DPP-BOTDA)

No sooner did the difficulties in the applicability of the BOTDA schemes, i.e., Brillouin loss based bright and dark pulse or the π phase pulse based Brillouin echo techniques were identified within the distributed sensing domain than Bao's group emerged with another concept of differential Brillouin gain. This technique was based upon the premise that since with 10ns or even shorter pulses there are difficulties achieving a good signal to noise figure, which is effectively due to the broadening of the spectrum in frequency domain that the problem could be solved by using much longer pulses. The race for being the first to pioneer the technique of offering fundamentally non-conflicting capabilities of probing measurands with sub-metre spatial resolutions reached another arguable high with the claims made by this differential pulse width pair Brillouin optical time domain analysis (DPP-BOTDA) technique [29 - 31], shown in figure 6 [29].

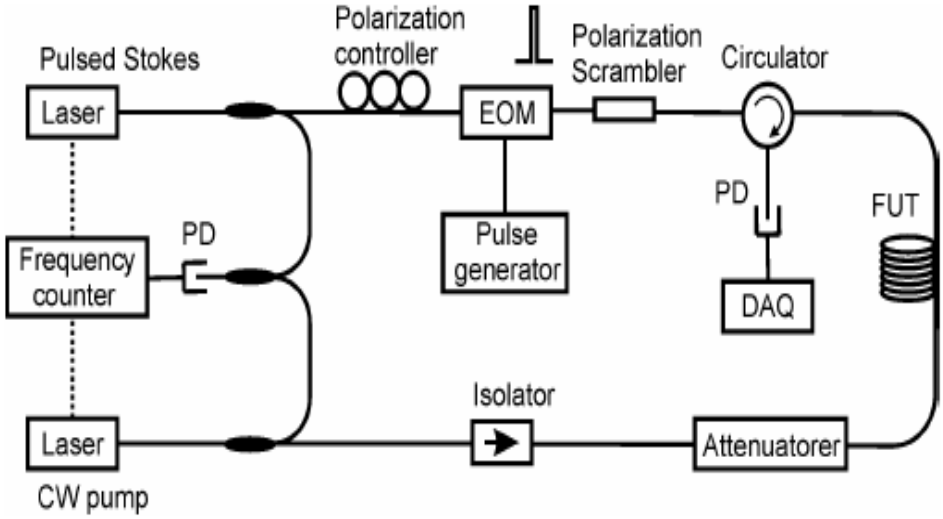

Figure 6. Experimental layout of the DPP-BOTDA technique [29]

The technique addressed the signal to noise issue by using longer pulses in the basic BOTDA set up instead of the conventional use of shorter pulses. The technique also argued that it resulted in a more reliable measure of strain or temperature by subsequently achieving reduced noise on the Brillouin gain curve. It went a step further by claiming that the sub-metre spatial resolution capability was also tackled alongside by simply subtracting the two independent responses to strain or temperature experienced by the 50ns and 40ns duration optical pulses. Although mathematically (i.e. theoretically) one could validate such a treatment under a common or no noise floor situation, under typical experimental environments where the electronic noise contributions are random such a treatment is misleading as the noise contributions are independent hence the subsequent subtraction increases the noise and reduces the signal leading to a much reduced signal to noise ratio.

Furthermore, the treatment proposed in the technique failed to acknowledge the fact that such an experimental procedure simply cannot distinguish any distributed profile of strain or temperature. Interestingly, the demonstration of the spatial resolution [30], i.e., 1m corresponding to the differential pulse of 10ns emerging as a result of a direct subtraction procedure from responses corresponding to 50ns and 40ns long pulses, was not surprising given the fact that the heated region was an extended section much larger than the pulse width itself. Hence the real test for the claims of sub metre spatial probing capability made by the technique based upon the differential concept should be made by using the same pulse widths on a much shorter heated section or perhaps allowing the pulse widths to interrogate a step change in temperature in the existing extended heated section itself, which is smaller than the two pulse widths.

2.5 Brillouin Dynamic Grating Distributed Sensing (BDG-DS)

Whilst it was appearing all the more difficult to appreciate the distributed sensing claims made by the various schemes centred around the BOTDA technique, i.e., Brillouin loss/gain [18, 19, 22, 24, 25], Brillouin echo [26-28] and DPP-BOTDA [29-31], Song et al contributed a rather different perspective to the existing problem

by introducing the concept of Brillouin dynamic gratings (BDG) [32]. It was possibly an attempt to set right the fundamental conflicts associated with the Brillouin loss/gain and Brillouin echo techniques by viewing their manifestation in a different type of fibre, i.e. polarization maintaining (P.M) fibre.

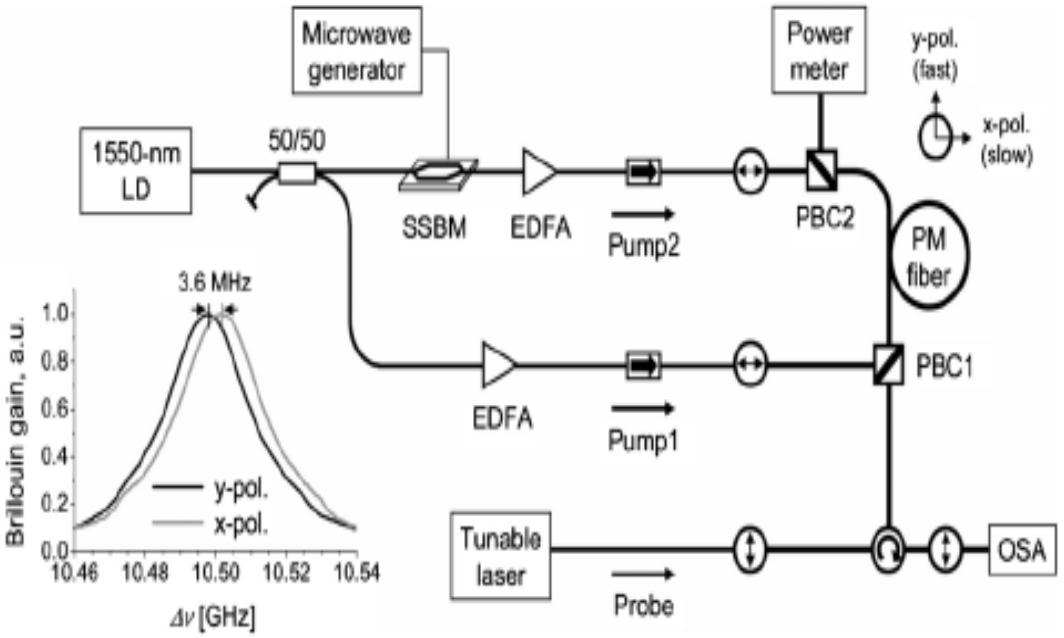

Figure 7. Experimental layout of the Brillouin dynamic grating based sensing scheme using the polarising maintaining fibre [32]

Experimental set up comprises LD - laser diode; SSBM – single sideband modulator; EDFA - Er-doped fiber amplifier; PBC - polarization beam combiner; OSA - optical spectrum analyzer. The inset is the Brillouin gain spectra of the fiber under test in *x* and *y* polarizations.

The technique exploited the Brillouin shifted acoustic wave grating being generated by an optical wave interaction in one axis of the PM fibre, layout shown in figure 7 [32]. Since the acoustic wave was not confined to propagation in one axis, another optical wave sent down the other axis of the PM fibre could still be diffracted from this acoustic wave grating. The diffracted signal could then be used to extract the information about strain or temperature carried in the acoustic wave grating [32]. Following the introduction of the Brillouin dynamic grating idea, it would be fair to attribute the usage of the two axis approach in a PM fibre, with providing means for

a more reliable extraction of information of measurands, i.e., strain or temperature, with an independent axis optical interaction, which was not possible with previous [18, 19, 23-31] methods.

The Brillouin dynamic grating scheme shifted the focus from a conventional single mode standard telecom fibre towards a special fibre, i.e., a PM fibre. In this technique the basic concept of BOTDA was initially limited to one axis of the PM fibre where the pulsed (generated by the electro optic modulator driven by the pulse generator) and c.w (generated by the single side band modulator driven by a microwave generator) counter propagating waves were made to interact in order to generate an acoustic wave grating [32]. The microwave generator driving the single side band modulator was scanned in order to generate the right Brillouin frequency shift influenced by the effective refractive index in that axis. The dynamic Brillouin acoustic grating generated by optical wave interaction in one axis extended over both axes. Moreover any changes in the local birefringence due to strain or temperature application to the fibre would have an influence on the acoustic grating too. Hence it was found that whilst the acoustic grating spreads itself, i.e., begins to share the information it contains about the state of strain or temperature pertaining to the axis in which it was generated, a short optical pulse, comparable to the one used for generation of the acoustic grating could be sent down this other axis where the acoustic grating has begun to penetrate in order to arrange for an interaction between the Brillouin acoustic grating and this short optical pulse [33]. In order to identify the location of interaction between the pulse and the acoustic grating, standard principle of optical time domain reflectometry was applied, as shown in figure 8 [33]. This short pulse was regarded as the read out pulse, since it essentially was used to read the information carried by the acoustic grating. When it comes to usage of specialty fibres, the concept of exploiting the Brillouin dynamic grating (BDG) in PM fibres with spatially resolved measurements achieved by the integration BDG with the principles of B-OTDR and BOCDA, as discussed later, do make the technique reliable, but also complicated.

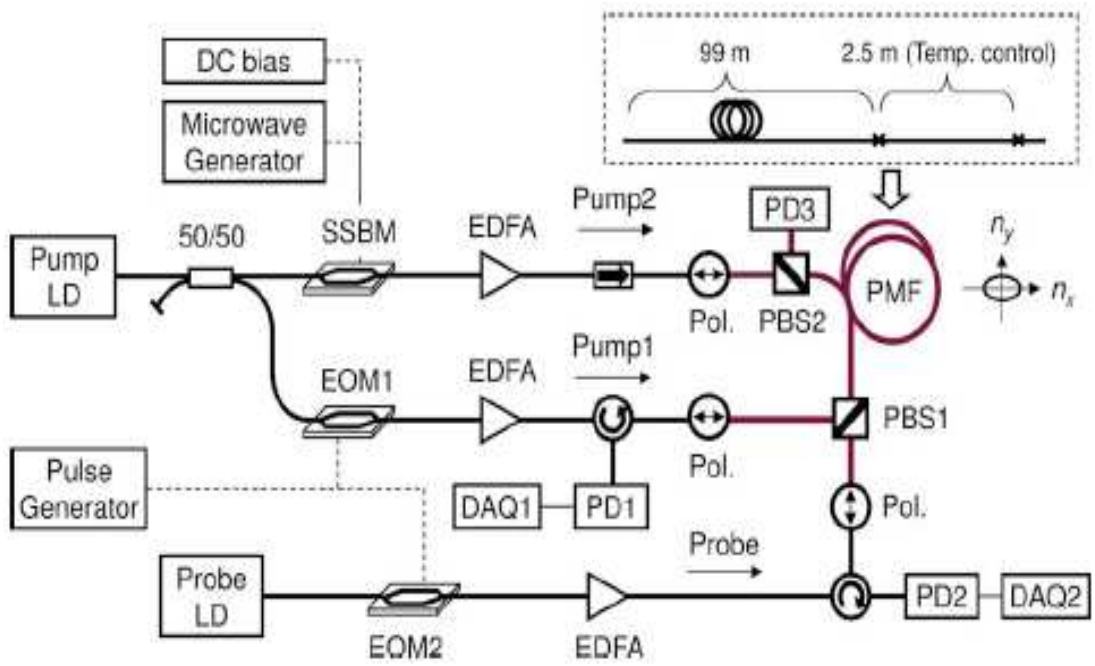

Figure 8. Experimental layout of the optical time domain based measurement of Brillouin dynamic grating spectrum [33]

Experimental setup comprises LD - laser diode; SSBM - single-sideband modulator; EDFA - Er-doped fiber amplifier; PBS -polarization beam splitter; Pol. - polarizer; EOM - electro-optic modulator. The inset shows the structure of the fiber under test.

The technique was further developed by introducing the amalgamation of Brillouin optical correlation domain analysis (BOCDA, discussed in detail later) where the concept of Brillouin acoustic grating generation was localised to a specific region of the sensing fibre due to the underlying feature of BOCDA technique accessing one axis of the PM fibre and the read out optical signal sent down the other axis was also modulated in sync with those responsible for generation of the grating in a certain region of the fibre, shown in figure 9 [34].

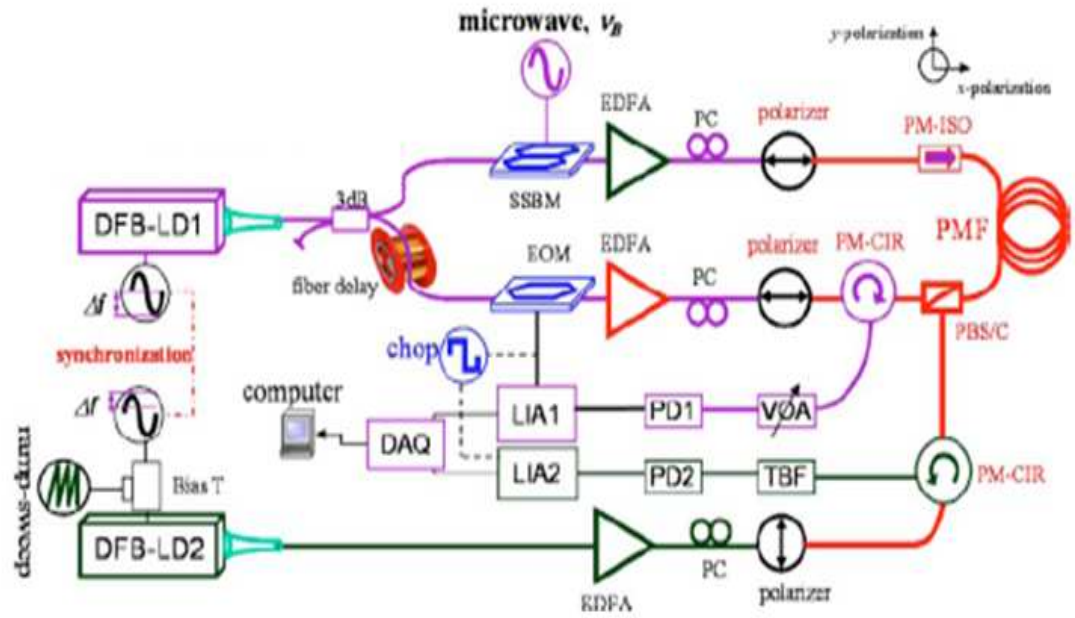

Figure 9. Experimental layout of the correlation based distributed measurement technique of the Brillouin dynamic grating spectrum [34]

This enabled the generation and reading of the acoustic grating in a specific region of the sensing fibre, depending upon the frequency variation produced in the laser frequency due to the injection current modulation of the laser diode. The design of the introductory BDG technique [32] was very similar in its exploitation of c.w - c.w interaction in one axis yielding an acoustic wave grating which was later subjected to a subsequent interrogation by a shorter pulse in another axis, to the previous techniques of Brillouin loss/gain and Brillouin echo where the natural line width was preserved due to the c.w – c.w interaction while high spatial resolution was achieved by looking at the diffracted light emerging from shorter pulse and acoustic wave grating interaction, but the BDG technique soon matured and came up with techniques agreeing fully with the basic understanding of Fourier transforms, i.e., interestingly none of the BDG related techniques [32-34] ever claimed sub-metre spatial resolutions, whilst exploiting optical signals in pulsed regimes.

Overlooking the details in the experimental layout of the BOTDA techniques of Brillouin loss (dark and bright pulse) and Brillouin echo [18, 19, 23-31] one can spot a common ground. Since the measurand interrogation schemes relied on the interaction between the short pulse and the continuously floating dynamic Brillouin

shifted acoustic signal, which is a representation of the combined sensing fibre condition, i.e., a collection of regions under strain or temperature, unstrained and unheated, that such sensing techniques indisputably may have a place for point sensing or qasi distributed measurements, where the region of sensing fibre under interrogation is subject to distinctively different strain or temperature in comparison to the rest of the strain and temperature state of the fibre. Such an imposition of strain or temperature would be capable of sufficiently influencing the Brillouin shifted acoustic wave grating. A short pulse then probing this acoustic wave would be able to extract the information contained in it against the background contribution from the rest of the fibre. In other words the techniques as demonstrated [18, 19, 23-31], worked only under conditions where the measurand imposed a frequency change much larger than the natural Brillouin line width. For any other manner of imposition of temperature or strain the techniques would fail to recognise a distributed pattern of either strain or temperature, instead would record an average value.

2.6 Brillouin Optical Correlation Domain Analysis (BOCDA)

Although various groups, within the distributed sensing family, were making efforts to come forth with a convincing solution towards achieving sub-metre spatial resolution temperature or strain probing capabilities, the maturity and elegance in Hotate's Brillouin optical correlation domain analysis technique, secured a unique place on the race map for high spatial resolution distributed strain sensing, experimental layout shown in figure 10 [35]. This is because the BOCDA technique since its inception in 2000 [35] till date, continues to be the only technique capable of providing distributed strain or temperature probing capabilities with spatial resolutions much below a metre, whilst preserving the natural linewidth of the Brillouin frequency spectrum.

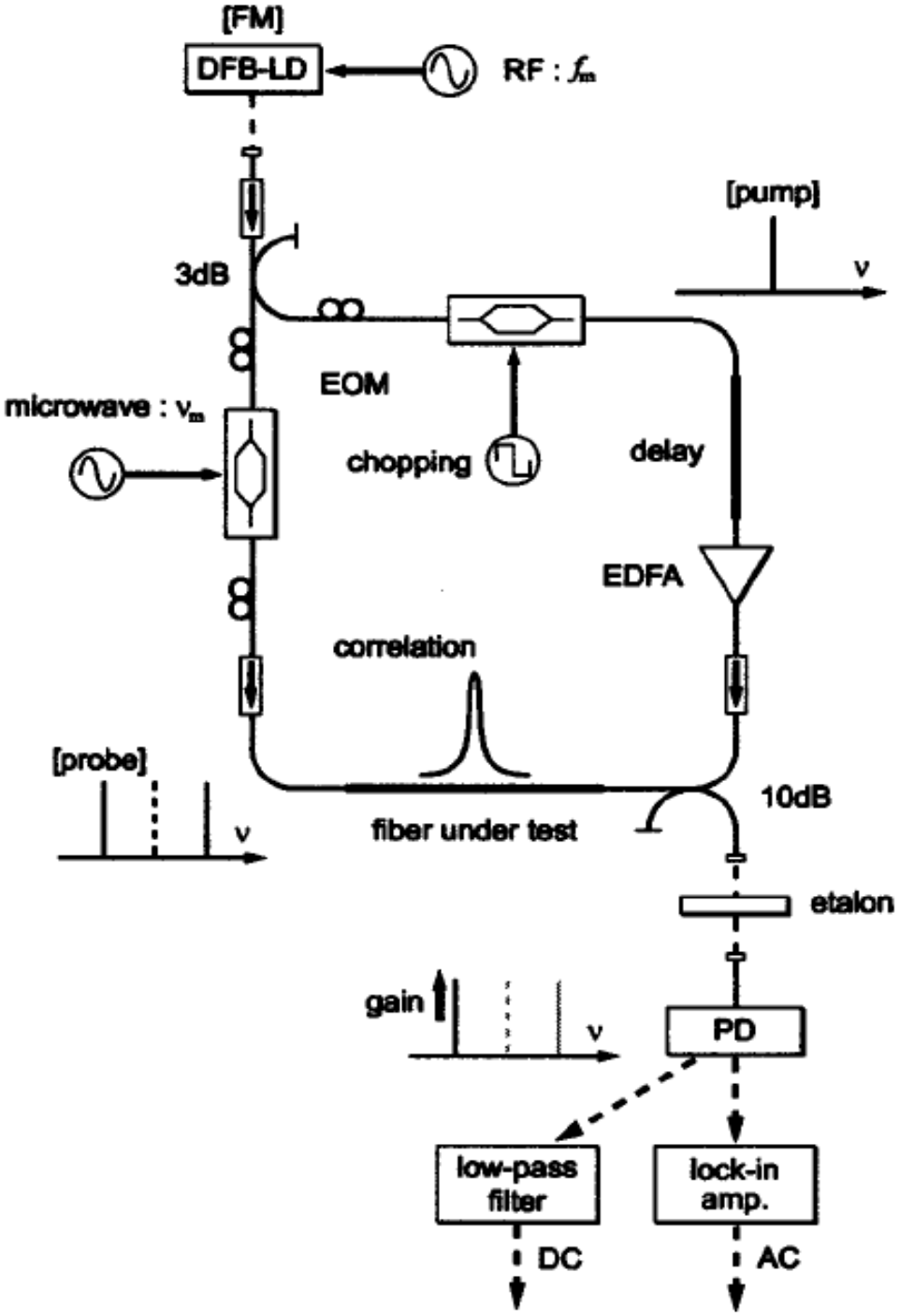

Figure 10. Experimental layout of the distributed strain measuring technique based upon the BOCDA format [35]

The method involves separating a frequency swept laser into two beams of light, one of which is frequency shifted by an amount close to the expected Brillouin frequency shift. Each of the two separated optical beams of light is launched into the opposite ends of the sensing fibre. A strong Brillouin interaction is localized to a region of the

fibre corresponding to zero delay between the counter-propagating beams of light. Scanning the frequency of the frequency shifter allows the peak Brillouin frequency to be determined in this region. This region can then be swept along the fibre by delaying the phase of one beam relative to the other. This is normally achieved by incorporating a delay fibre outside the sensing fibre such that any change in the frequency at which the frequency of the laser is swept translates into a change in phase and hence the sensing position along the sensing fibre. Since its inception, the BOCDA technique has undergone meticulous improvements by the inventors themselves and all efforts have paid off towards it's attainment of rigor and robustness over the contemporary BOTDA techniques namely Brillouin loss/gain, Brillouin Echo, the earlier version of the Brillouin dynamic grating technique and the DPP-BOTDA technique [18, 19, 23-31], despite their authors continuing to sell their achievements as fully distributed strain or temperature measuring sensors, though as discussed previously these techniques are only suited for hot spot detection.

In BOCDA the linear separation distance between correlation points along the sensing fibre is directly proportional to the ratio of velocity of light in fibre and the modulation frequency of the laser. For the ease of extraction of information regarding strain or temperature based upon shifts in peak Brillouin frequency spectrum, it is best to choose the sensing range such that there is only one correlation peak within that sensing fibre. In meeting the requirement of maintaining the presence of a single correlation peak within the sensing fibre, the sensor limits itself with a sensing range governed by the separation between any two correlation peaks. Multiple correlation peaks result in either broadening of the Brillouin spectrum if the imposed temperature or strain values at the various correlation points are close or a Brillouin spectrum with multiple peaks if there is a large variation between the temperature or strain values at those correlation points. The requirement of ensuring a single correlation peak in the sensing fibre, limits the applicability of BOCDA to relatively short range sensing applications (~ at most a kilometre and below) [36]. Moreover the nature of the technique is such that it imposes a subtle relationship between the spatial resolution and the sensing range, i.e., a higher spatial resolution would inherently be attained over a small sensing range [37, 38]. Unlike the other high spatial resolution claiming techniques [18, 19, 22-31], BOCDA probes

distributed strain by demonstrating a clear 10/90% step change [39] in the value of correlation gain whilst moving from region of no strain to region of strain less than the natural Brillouin line width.

2.7 Brillouin Optical Correlation Domain Reflectometry (BOCDR)

The development of BOCDA technique certainly distinguishes itself as an elegant means to probe strain or temperature with high spatial resolutions. Moreover constant improvements in its methodology have also lead to the adoption of the single ended sensing fibre access [40] just as the B-OTDR technique. This feature cunningly uses the reflection from the far end of the sensing fibre that is silver polished, in order to arrange for the counter propagating pump and probe interaction to take place.

Pragmatically viewing the cons associated with the method of reflecting from the far end identifies a need for essentially ensuring high reflectivity is maintained. This problem was solved by the introduction of a mature and improved format of BOCDA, i.e., Brillouin optical correlation domain reflectometry (BOCDR) technique, as shown in figure 11 [41]. BOCDR brought with itself the freedom of avoiding silver polishing treatment on the far end of the sensing fibre.

The technique relies on the Brillouin frequency shifted counter propagating light generated by the sensing fibre in the form of the backscattered Brillouin Stokes. Interaction between the co propagating pump and the counter propagating Stokes results in the formation of the correlation peak in the sensing fibre. The correlation peak is amplified by EDFA2 and later filtered. The filtered signal is self heterodyned using the amplified pump. Usage of the two balanced photodiodes reduces the intensity noise, and the signal is amplified using an electronic amplifier before being fed in to the electrical spectrum analyzer (ESA). Shifts in the peak correlation peak due to strain are monitored on the ESA.

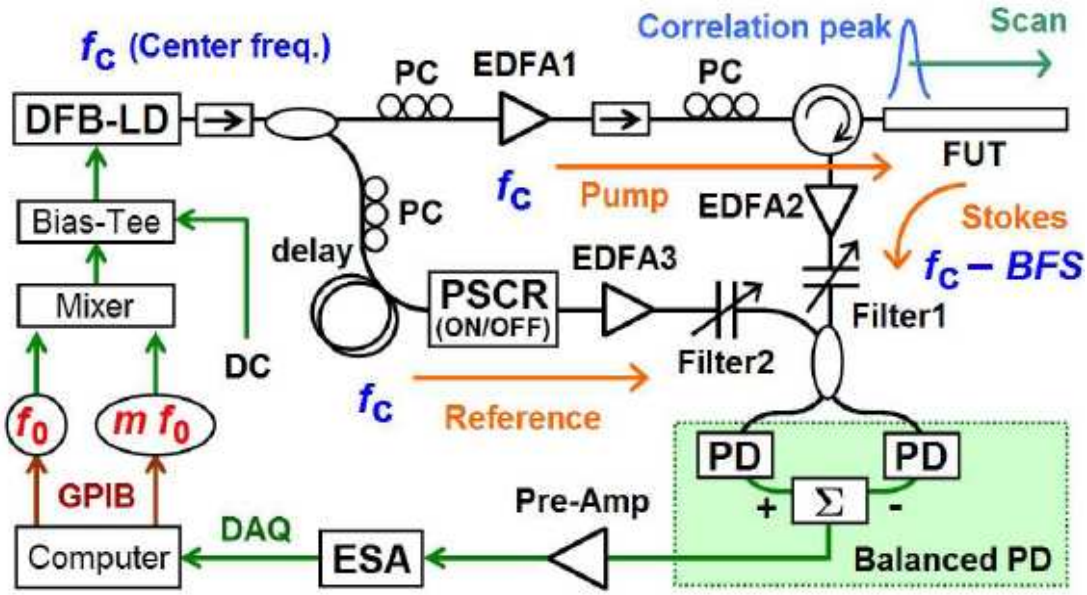

Figure 11. Experimental layout of the distributed strain measuring technique based upon the BOCDR format [41]

The BOCDR technique provided high spatial resolution dynamic strain measurements [42] along with the sensing range enlargement right up to a kilometre [43]. Although the technique provided single ended access to the sensing fibre which was quite an advance from the classical BOTDA but it continues to yearn for much improvement in order to outclass the achievements of BOCDA, especially in the department of high spatial resolution probing of measurand.

Interestingly so, although the handicap of inaccessibility to long range sensing associated with BOCDA was labelled as the obvious downside to the technique, as a consequence of its fundamental working, yet it was soon identified as providing fierce competition to contemporary techniques within the domain of short range Brillouin scattering based sensing providing unrivalled high spatial resolution capabilities.Indisputably its attractiveness for distributed short range high spatial resolution sensing is its elegance of preserving the natural Brillouin line width whilst continuing to exploit the Brillouin frequency for distributed strain measurements. This technique of using the Brillouin frequency in a manner capable of

circumventing the problem of broadening of Brillouin line width for sub metre spatial resolution probing of strain could also encourage utilisation of special fibres with multiple Brillouin peaks, with possibly different strain and temperature coefficients. In this thesis however the approach to sensor design adopts only standard single mode telecom fibres for exploring the capability of offering temperature corrected high spatial resolution distributed strain measurements. Usage of standard fibre also ensures easy integration with other fiberized optoelectronic components under tolerable splice losses.

The following section reviews the attempts made previously towards unambiguously measuring distributed strain i.e. compensated for distributed temperature influences. This review not only highlights the very starting point for the motivation of the central idea of this thesis but also elucidates the various advances made so far. In doing so it identifies the aims of this thesis which have been achieved in chapters 3 and 4 respectively.

2.8 Aims

It would be fair to breakdown the subject of this thesis as a three part problem. That is to say, the design of the sensor essentially must meet three requirements i.e., distributed measurements of strain made simultaneously and independently of distributed temperature measurements with very high spatial resolution capability. It is understood that a simultaneous occurrence of these three features in a sensor, ensures robustness and in turn novelty to the sensor. It is with this view that the following sub-section of the thesis undertakes the task of identifying attempts in the past to combine the three features.

2.8.1 Discussions

Following the success in characterising the temperature [44] and strain [45] dependence of the Brillouin power, combined with the previous knowledge of the Brillouin frequency shift dependence on strain and temperature, the possibility of making simultaneous Brillouin strain and temperature measurement was apparent [46]. The four Brillouin coefficients were subsequently confirmed by Parker et al, using a scanning Fabry-Perot set up [47]. Soon, Kee's [9] work on the cascaded Mach-Zehnder configuration, shown in figure 1, to simultaneously measure both Brillouin intensity and frequency using the double pass Mach Zehnder approach demonstrated a practical means to achieving a distributed sensor capable of unambiguously resolving strain and temperature.

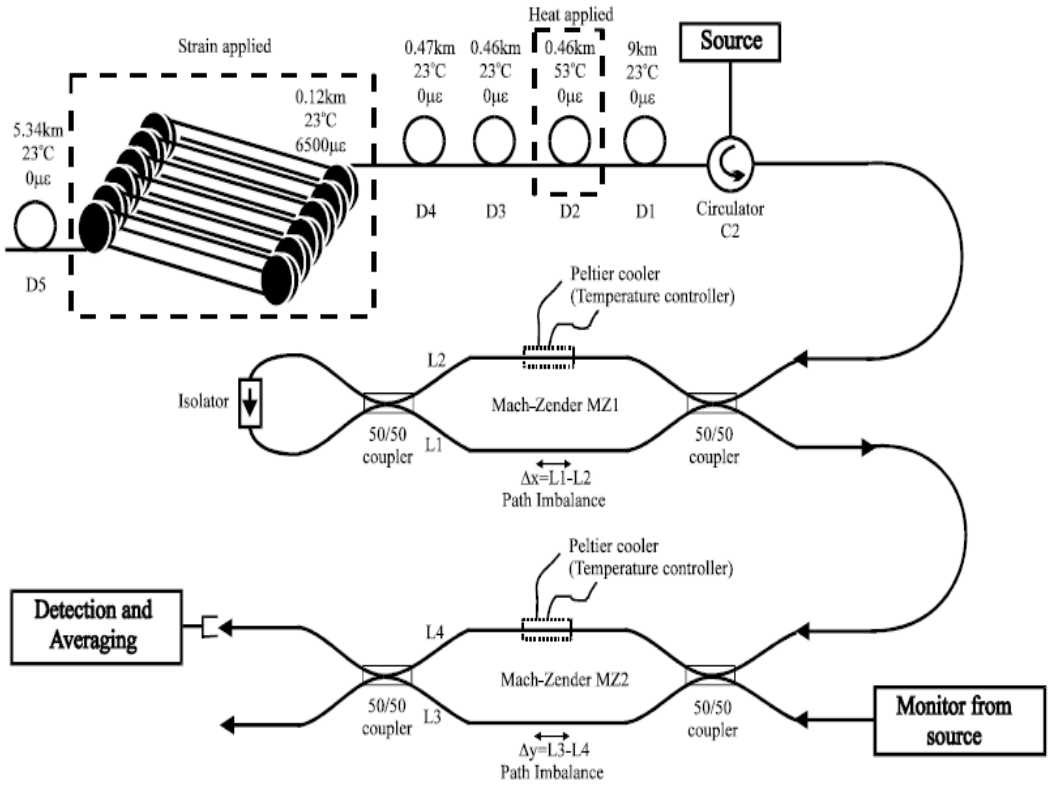

Figure 1. Experimental layout of the sensing fibre and the cascaded Mach Zehnder configuration [9]

The first stage in this cascaded arrangement comprised a double pass Mach Zehnder to filter the Brillouin from the Rayleigh. It resulted in 28dB rejection of Rayleigh. The second stage of the Mach Zehnder involved locking Brillouin frequency at the quadrature point for detection of Brillouin frequency shifts emerging due to temperature changes in a section of sensing fibre. The single ended sensor design proposed by Kee et al [9] was very novel and immensely useful for independent long range distributed measurements of strain and temperature. It achieved 4°C and 290με of temperature and strain resolutions respectively, over a sensing range of 15km with a spatial resolution of 10m.

Despite the achievements of the double pass Mach Zehnder approach, the idea for a more robust commercial solution with improved signal to noise ratio lead to the exploration of the coherent detection scheme [46], explained in section 2.1, figure 1. The scheme proved extremely advantageous and demonstrated an improved simultaneous strain resolution of 100με over a sensing range of 30km with a spatial resolution of 20m, whilst reproducing the temperature resolution previously achieved in Kee's [9] sensing scheme. Additionally this work also contributed towards distributed temperature measurements over 57km, with RMS error in frequency measurement of less than 3MHz for over the entire length and under 0.6MHz for the first 40km. Although the results were an outcome of the very early works in the microwave detection scheme series, yet they stand a unique place in comparison to other long range works to date [48, 49].

Whilst the results from the coherent detection scheme [46, 11, 12, 13] were continually improving, an alternative technique for separating temperature and strain effect was proposed using nonzero dispersion shifted fiber (LEAF) which exhibited two different Briilouin peaks by Lee et al [50]. This approach of measuring the two Brillouin frequencies in a multi compositional fiber core (LEAF) for unambiguously resolving temperature and strain in a distributed sensor [50] was investigated further by Alahbabi et al. [51] who compared its performance with the measurements of intensity and frequency for the single Brillouin peak in a standard single mode

telecommunication fibre. Alahbabi et al. reported that the two Brillouin frequency components of the LEAF exploited to determine the temperature and strain produced almost sevenfold deterioration in the temperature resolution, i.e., from 4.10 °C to 27°C and more than fourfold deterioration in the value of strain resolution compared with that of SMF. It was also inferred, despite the ability of the data collection system to detect peak frequency to a resolution better than a few MHz at the demonstrated range of 22km, the exploitation of dual Brillouin peaks using LEAF imposed more stringent requirements on the accuracy of frequency measurements. That is to say, a differential frequency change exploited to acquire temperature information in the case of LEAF lowered the required frequency change as a function of temperature from 1MHz/°C to 190kHz/°C. Moreover, for a temperature resolution better than 1°C, the requirement for individual frequency resolution was found to be approximately 135kHz, which would in practise be difficult to achieve in the presence of noise for a 35MHz spontaneous Brillouin linewidth.

A few months later, much in line with exploiting different fibres for simultaneous measurements of distributed strain and temperature, Bao's group introduced the possibility of using polarization maintaining (PM) [52] fibres, namely Panda, bow-tie, and tiger, for similar purpose. The reason for using PM fibres was largely centred on exploiting the fact that the otherwise random state of polarization which is due to polarization mode dispersion in standard single mode fibre, would be eliminated by using a PM fibre. Hence any further power fluctuation would then, only be attributed to the laser source. Due to elimination of state of polarization fluctuation in the power measurement with SM fibres, it was hoped that strain and temperature could simultaneously be probed with centimetres of spatial resolution using PM fibres instead, which an SM fibre would otherwise limit to a metre spatial resolution. However, due to nonlinear Brillouin amplification of fluctuation induced by the laser power a higher uncertainty was identified in combining the individual information obtained from the Brillouin power and frequency measurements.

Another attempt towards discriminative strain and temperature sensing was made by Alahbabi et al by combining Billouin frequency and spontaneous anti-Stokes Raman power measurements [53] achieving temperature and strain resolutions of 6°C and

150με respectively with a spatial resolution of 10m for a range of more than 23km. Focus also slightly shifted towards trying new fibres with different orders of acoustic mode interaction with the optical field [54], where F doping resulted in reduction of acoustic modes in the fibre with enlargement of frequency spacing between neighbouring modes and also influencing the effect of the Brillouin frequency shifts with temperature and strain by usage of varying concentration of GeO_2 doping in optical fibres [55]. In both cases [54, 55] the fibre design did not lead to the Brillouin frequency coefficients for temperature varying negatively to the strain, or vice versa, which could provide significant performance improvement in discriminative measurement of strain and temperature. It was in line with using special fibres for discriminatively measuring strain and temperature that Zou et al [56] presented the use of exploiting their newly devised technique of Brillouin dynamic grating (BDG) in PM fibres for a complete discrimination of strain and temperature using Brillouin frequency shift and birefringence measurements. It unearthed the possibility of exploiting the large negatively varying temperature coefficient of $C_f^T = -55.8134 MHz/^\circ C$ and the positively varying strain coefficient of $C_f^\varepsilon = 0.8995 MHz/\mu\varepsilon$ as a consequence of the frequency deviation emerging due to birefringence. Up to this point, the technique lacked the distributed sensing capabilities due to the c.w – c.w interactions in one axis of P.M fibre responsible for BDG creation. However, the technique soon graduated to exploiting the c.w wave and pulse interaction towards creation of the BDG in conjunction with spatial interrogation of the BDG using the optical time domain measurement [57] approach. The technique was further developed furthermore by combining the concept of Brillouin correlation domain analysis technique for both the generation of BDG in one axis and its interrogation in the other [58].

Analysing the contributions involving telecom SM fibres [44, 46, 51, 53], special fibres [50, 52, 54-58 and including the recent possibility of exploiting Brillouin scattering in polymer based optical fibre [59], towards providing distributed discriminative temperature and strain measuring capabilities, there still appeared a major gap in designing a sensor capable of offering high spatial resolution temperature compensated distributed strain measurements. Understanding the need to

fill this void, within distributed sensing, the following section proposes the schemes to be explored in order to demonstrate the working model of such a sensor.

2.8.2 Proposed Schemes

Although the review identified various schemes attempting discriminatory distributed strain and temperature measurements using special fibres, the work in this thesis limits the exploration to standard telecom based single mode fibres. The course we adopted is based on exploiting the high spatial resolution Brillouin frequency based distributed strain measuring capabilities offered by BOCDA technique independently combined with power measurements of spontaneous Raman and spontaneous Brillouin to provide separate distributed measure of temperature.

In the following chapters, the experimental performance of the two sets of combinatory schemes, i.e., BOCDA + Raman anti-Stokes intensity and BOCDA + Brillouin anti-Stokes intensity resulting in discrimination of strain and temperature are independently discussed followed by a theoretical performance comparison using similar sensor parameter of sensing length, spatial resolution etc. The Brillouin coefficients calibration experiment which follows this work is conducted in order to check if any corrections are necessary to the Brillouin frequency and intensity coefficients under a temperature controlled variable strain environment. The need for such a calibration emerged because so far it had been assumed that the Brillouin frequency coefficients for strain remain valid under elevated temperature and vice-versa. Given the fact that the sensing fibre had to be subjected to a combined temperature and strain varying condition that it was mandatory to confirm if changes in Young's moduli, refractive index etc., due to simultaneously varying strain and temperature are sufficiently affecting the coefficients, which would then require a correction factor to the existing values of Brillouin frequency and power coefficient of strain and temperature which to date have been experimentally found at room temperature (strain coefficient) and zero strain (temperature coefficient) only.

2.9 References

[1] M.K. Barnoski and S.M. Jensen, ‘‘Fibre waveguides: a novel technique for investigating attenuation characteristics’’, *Applied Optics*, 15(9), p 408 – 410 (1989)

[2] T. Horiguchi, T. Kurashima and M. Tateda, ‘‘A technique to measure distributed strain in optical fibers’’, IEEE *Photonics Technology Letters*, 2(5), p 352–354 (1990)

[3] T. Kurashima, T. Horiguchi and M. Tateda, ‘‘Distributed-temperature sensing using stimulated Brillouin scattering in optical silica fibers’’, *Optics Letters*, 15(18), p 1038–1040 (1990)

[4] S. M. Maughan, PhD Thesis, University of Southampton (2001)

[5] G. P. Lees, Phd Thesis, University of Southampton (1999)

[6] T. Horiguchi, T. Kurashima and M. Tateda, ‘‘Tensile strain dependence of Brillouin frequency shift in silica optical fibers’’, *IEEE Photonics Technology Letters*, 1(5), p 107–108 (1989)

[7] M. Nikles, L. Thevenaz and P. A. Robert, ‘‘Brillouin gain spectrum characterization in single-mode optical fibers’’, *Journal of Lightwave Technology*, 15(10), p 1842–1851 (1997)

[8] T. Horiguchi, K. Shimizu, T. Kurashima, M. Tateda and Y. Koyamada, ‘‘Development of a distributed sensing technique using Brillouin scattering’’, *Journal of Lightwave Technology*, 13(7), p 1296–1302 (1995)

[9] H. H. Kee, G. P. Lees, and T. P. Newson, ‘‘All-fiber system for simultaneous interrogation of distributed strain and temperature sensing by spontaneous Brillouin scattering’’, *Optics Letters*, 25(10), p 695–697 (2000)

[10] Y. T. Cho, M. N. Alahbabi, M. J. Gunning and T. P. Newson, **‘‘**50 km single-ended spontaneous Brillouin based distributed temperature sensor exploiting pulsed Raman amplification’’, *Optics Letters*, 28(18), p 1651-1653 (2003)

[11] M. N. Alahbabi, N. P. Lawrence, Y. T. Cho and T. P. Newson, ‘‘High spatial resolution microwave detection system for Brillouin-based distributed temperature and strain sensors’’, *Measurement Science and Technology*, 15, p 1539-1543 (2004)

[12] M. N. Alahbabi, Y. T. Cho and T. P. Newson, ‘‘150-km-range distributed temperature sensor based on coherent detection of spontaneous Brillouin backscatter

and in-line Raman amplification'', *Journal of the Optical Society of America B*, 22(6), p 1321–1324 (2005)

[13] M. N. Alahbabi, Y. T. Cho and T. P. Newson, ''100km distributed temperature sensor based on coherent detection of spontaneous Brillouin backscatter'', *Measurement Science and Technology*, 15(8), p1544-1547 (2004)

[14] T. Horiguchi, K. Shimizu, and T. Kurashima, "Development of a distributed sensing technique using Brillouin scattering'', *Journal of Lightwave Technology*, 13 (7), p 1296–1302 (1995)

[15] T. Horiguchi and M. Tateda, ''Optical-fiber-attenuation investigation using stimulated Brillouin scattering between a pulse and a continuous wave'', Optics Letters, 14(8), p 408 – 410 (1989)

[16] T. Horiguchi and M. Tateda ''BOTDA-nondestructive measurement of single-mode optical fibre attenuation characteristics using Brillouin interaction: theory'', *Journal of Lightwave Technology*, 7(8), p 1170–1176 (1989)

[17] T. Horiguchi, T. Kurashima and M. Tateda, ''A technique to measure distributed strain in optical fibres'', *Photonics Technology Letters*, 2(5), p 352 – 354 (1990)

[18] X. Bao, D. J. Webb and D. Jackson, ''A 32-km distributed temperature sensor based on Brillouin loss in an optical fiber'', *Optics Letters*, 18(18), p 1561–1563 (1993)

[19] X. Bao, J. Dhliwayo, N. Heron, D. J. Webb, and D. A. Jackson, ''Experimental and Theoretical Studies on a Distributed Temperature Sensor Based on Brillouin Scattering'', *Journal of Lightwave Technology*, 13 (7), p 1340-1347 (1995)

[20] E. Geinitz, S. Jetschke, U. Ropke, S. Schroter, R. Willsch and H. Bartelt, ''The influence of pulse amplification on distributed fibre-optic Brillouin sensing and a method to compensate for systematic errors'', *Measurement Science and Technology*, 10(8), p 112-116 (1999)

[21] T. Horiguchi, T. Kurashima and Y. Koyamada, ''Measurement of temperature and strain distribution by Brillouin frequency shift in silica optical fibres'', Proc. SPIE 1797, 2 (1993)

[22] X. Bao, A. Brown, M. DeMerchant and J. Smith, ''Characterization of the Brillouin-loss spectrum of single-mode fibres by use of very short (<10-ns) pulses'', *Optics Letters*, 24(8), p 510 -512 (1999)

[23] V. Lecoeuche, D. J. Webb, C. N. Pannell and D. A. Jackson, ‘‘Transient response in high-resolution Brillouin-based distributed sensing using probe pulses shorter than the acoustic relaxation time’’, *Optics Letters*, 25(3), p 156–158 (2000)

[24] A. W. Brown, B. G. Colpitts and K. Brown, ‘‘Distributed Sensor Based on Dark-Pulse Brillouin Scattering’’, *IEEE Photonics Technology Letters*, 17 (7), p 1501-1503 (2005)

[25] A. W. Brown, B. G. Colpitts, and Kellie Brown, ‘‘Dark pulse Brillouin optical time domain sensor with 20-mm spatial resolution’’, *Journal of Lightwave Technology*, 25 (1), p 381-386 (2007)

[26] L. Thevenaz and S. Foaleng-Mafang, ‘‘Distributed fiber sensing using Brillouin echoes’’, *Proceedings of the 19th International Conference on Optical Fibre Sensors (OFS)*, 7004 (70043N), Perth (2008)

[27] S. Foaleng-Mafang, J. C. Beugnot and L. Thevenaz, ‘‘Optimized configuration for high resolution distributed sensing using Brillouin echoes’’, *Proceedings of the 20th International Conference on Optical Fibre Sensors (OFS)*, 7503 (75032C), Edinburgh (2009)

[28] L. Thevenaz and J. C. Beugnot, ‘‘General analytical model for distributed Brillouin sensors with sub-meter spatial resolution’’, *Proceedings of the 20th International Conference on Optical Fibre Sensors (OFS)*, 7503 (75036A), Edinburgh (2009)

[29] W. Li, X. Bao, Y. Li and L. Chen, ‘‘Differential pulse-width pair BOTDA for high spatial resolution sensing’’, *Optics Express*, 16(26), p 21616–21625 (2008)

[30] Y. Dong, X. Bao and W. Li, ‘‘Differential Brillouin gain for improving the temperature accuracy and spatial resolution in a long-distance distributed fiber sensor’’, *Appl. Opt.*, 48, p. 4297–4301 (2009)

[31] H. Liang, W. Li, N. Linze, L. Chen, and X. Bao, ‘‘High-resolution DPP-BOTDA over 50 km LEAF using return-to-zero coded pulses’’, *Optics Letters*, 35(10), p. 1503–1505 (2010)

[32] K. Y. Song, W. Zou, Z. He and K. Hotate, ‘‘All-optical dynamic grating generation based on Brillouin scattering in polarization maintaining fiber’’, *Optics Letters*, 33(9), p. 926–928 (2008)

[33] K. Y. Song, W. Zou, Z. He and K. Hotate, ‘‘Optical time-domain measurement of Brillouin dynamic grating spectrum in a polarization-maintaining fiber’’, *Optics Letters*, 34(9), p. 1381–1383 (2009)

[34] W. Zou, Z. He, K. Y. Song and K. Hotate ‘‘Correlation-based distributed measurement of a dynamic grating spectrum generated in stimulated Brillouin scattering in a polarization-maintaining optical fiber’’, *Optics Letters*, 34(7), p. 1126–1128 (2009)

[35] K. Hotate and T. Hasegawa, ‘‘Measurement of Brillouin gain spectrum distribution along an optical fiber using a correlation-based technique-proposal, experiment and simulation’’, *IEICE Transactions on Electronics*, E83- C (3), p 405–412 (2000)

[36] K. Y. Song, Z. He and K. Hotate, ‘‘Enlargement of measurement range in a Brillouin optical correlation domain analysis system using double lock-in amplifiers and single side band modulators’’, *IEEE Photonics Technology Letters*, 18(3), p 499–501 (2006)

[37] K. Hotate and M. Tanaka, ‘‘Distributed fiber Brillouin strain sensing with 1-cm spatial resolution by correlation-based continuous-wave technique’’, *IEEE Photonics Technology Letters*, 14(2), p 179–181 (2002)

[38] K. Y. Song, Z. He and K. Hotate, “Distributed strain measurement with millimeter-order spatial resolution based on Brillouin optical correlation domain analysis,” *Optics Letters*, 31(17), p. 2526–2528 (2006)

[39] K. Hotate and T. Hasegawa, "Measurement of Brillouin gain spectrum distribution along an optical fiber using a correlation-based technique -Proposal, experiment and simulation," *IEICE Trans. on Electronics*, E83-C (3), p 405-412 (2000)

[40] K.Y. Song and K. Hotate, ‘‘Brillouin optical correlation domain analysis in linear configuration’’, *IEEE Photonics Technology Letters*, 20(24), p 2150-2152 (2008)

[41] Y. Mizuno, W. Zou, Z. He and K. Hotate, “Proposal of Brillouin optical correlation-domain reflectometry (BOCDR),” *Optics Express*, 16(16), p 12148-12153 (2008)

[42] Y. Mizuno, Z. He and K. Hotate, "One-end-access high-speed distributed strain measurement with 13-mm spatial resolution based on Brillouin optical correlation-domain reflectometry," *IEEE Photonics Technology Letters*, 21(7), p 474-476 (2009)
[43] Y. Mizuno, Z. He and K. Hotate, "Measurement range enlargement in Brillouin optical correlation-domain reflectometry based on temporal gating scheme," *Optics Express*, 17(11), p 9040-9046 (2009)
[44] P. C. Wait and T. P. Newson, ''Landau Placzek ratio applied to distributed fibre sensing'', *Optics Communications*, 122, p 141-146 (1996)
[45] K.de Souza, P.C.Wait and T.P.Newson, ''Characterisation of strain dependence of the Landau-Placzek ratio for distributed sensing'', *Electronics Letters*, 33(7), p 615-616 (1997)
[46] S. M. Maughan, H. H. Kee and T. P. Newson**, ''**Simultaneous distributed fibre temperature and strain sensor using microwave coherent detection of spontaneous Brillouin backscatter'', *Measurement Science and Technology*, 12, p. 834-842 (2001)
[47] T. R. Parker, M. Farhadiroushan, V. A. Handerek, and A. J. Rogers, ''A fully distributed simultaneous strain and temperature sensor using spontaneous Brillouin backscatter'', *Photonics Technology Letters*, 9 (7), p 979 - 981(1997)

[48] M. A. Soto, G. Bolognin and F. Di Pasquale, ''Enhanced simultaneous distributed strain and temperature fiber sensor employing spontaneous Brillouin scattering and optical pulse coding'', *Photonics Technology Letters*, 21 (7), p. 450-452 (2009)
[49] M. A. Soto, G. Bolognini, F. Di Pasquale and L. Thévenaz, ''Simplex-coded BOTDA fiber sensor with 1 m spatial resolution over a 50 km range'', *Optics Letters*, 35 (2), p. 259-261 (2010)
[50] C. C. Lee, P. W. Chiang, and S. Chi, ''Utilization of a dispersion-shifted fiber for simultaneous measurement of distributed strain and temperature through
Brillouin frequency shift'', *Photonics Technology Letters*, 13(10), p. 1094-1096 (2001)
[51] M. Alahbabi, Y. T. Cho, and T. P. Newson, ''Comparison of the methods for discriminating temperature and strain in spontaneous Brillouin-based distributed sensors'', *Optics Letters*, 29(1), p. 26-28 (2004)

[52] X. Bao, Q. Yu and L. Chen, ‘‘Simultaneous strain and temperature measurements with polarization-maintaining fibers and their error analysis by use of a distributed Brillouin loss system’’, *Optics Letters*, 29(12), p. 1342-1344 (2004)

[53] M. Alahbabi, Y. T. Cho, and T. P. Newson, ‘‘Simultaneous temperature and strain measurement with combined spontaneous Raman and Brillouin scattering’’, *Optics Letters*, 30(11), p. 1276-1278 (2005)

[54] W. Zou, Z. He, M. Kishi, and K. Hotate, ‘‘Stimulated Brillouin scattering and its dependences on strain and temperature in a high-delta optical fiber with F-doped depressed inner cladding’’, *Optics Letters*, 32(6), p. 600-602 (2007)

[55] W. Zou, Z. He, and Kazuo Hotate, ‘‘Investigation of strain and temperature dependences of Brillouin frequency shifts in GeO2 doped optical fibers’’, *Journal of Lightwave Technology*, 26(13), p. 1854-1861 (2008)

[56] W. Zou, Z. He, and K. Hotate**, ‘‘**Complete discrimination of strain and temperature using Brillouin frequency shift and birefringence in a polarization-maintaining fiber’’, *Optics Express*, 17(3), p. 1248-1255 (2009)

[57] K. Y. Song, W. Zou, Z. He and Kazuo Hotate, ‘‘Optical time-domain measurement of Brillouin dynamic grating spectrum in a polarization-maintaining fiber’’, *Optics Letters*, 34(9), p. 1381–1383 (2009)

[58] W. Zou, Z. He, K. Y. Song and K. Hotate, ‘‘Correlation-based distributed measurement of a dynamic grating spectrum generated in a polarization maintaining optical fibre’’, *Optics Letters*, 34(9), p. 1126–1128 (2009)

[59] Y. Mizuno and K. Nakamura, ‘‘Potential of Brillouin scattering in polymer optical fiber for strain-insensitive high-accuracy temperature sensing’’, *Optics Letters*, 35(23), p. 3985–3987 (2010)

Chapter 3

3. Raman intensity assisted temperature compensation for a sub-metre spatial resolution distributed strain sensor

3.1 Introduction

For long-range sensing, it has been demonstrated that measurements of spontaneous Brillouin power [1] and frequency [2] along with spontaneous Raman measurements, can be used to separately resolve temperature and strain albeit with a low spatial resolution of 10m [3]. At long sensing ranges, the challenge is to achieve an adequate signal to noise in order to acquire the desired measurand resolution. A number of techniques have been investigated, in trying to improve the simultaneous strain and temperature measuring capability along with enhancement in the sensing range. The more robust coherent detection [2, 6] followed the direct detection [4, 5] schemes, which not only improved the simultaneous strain and temperature resolution measurements but also enhanced the sensing range. However the ultimate sensing range of 150km was achieved for distributed temperature measurements only by combining the Brillouin coherent detection with in-line Raman amplification [7]. An alternative technique for separately resolving temperature and strain by exploiting the differential frequency shift in fibres exhibiting multiple Brillouin peaks [8, 9] was also explored. In such fibres, the Brillouin frequency shifts of the first and second peaks were found different for temperature, but similar for strain. So by measuring the Brillouin frequency shifts of both peaks, it was possible to separate the temperature and strain. However, as a consequence of the relatively small differential change in the frequency of the two peaks with temperature, the technique has not yet

proven advantageous over the power and frequency approach for long-range sensing [8].

At short sensing ranges, requiring sub-metre spatial resolution, spectral broadening of the pulse limits the achievable accuracy of Brillouin frequency measurements. This is because the resultant Brillouin spectrum is a convolution of the pulse bandwidth and Brillouin natural linewidth. As discussed previously, an elegant technique which overcomes this problem and achieves high spatial resolution of the order of millimetres is Brillouin Optical Correlation Domain Analysis (BOCDA) [9] (figure 10, chapter 2) technique. A frequency swept laser output is split using a fibre coupler. One of the output light beams is frequency shifted by an amount close to the expected Brillouin frequency shift using an electro optic intensity modulator (EOM), driven by a high frequency (~ 9GHz – 11GHz) synthesizer, the other is fed through a delay fibre followed by another EOM, driven by a low frequency (~kHz) square wave input from a standard signal generator. The output of the signal generator is split such that a simultaneous input can also be provided to the lock-in amplifier. These two beams of light are then launched into the opposite ends of the sensing fibre.

Strong Brillouin interaction is localized to a region of the sensing fibre corresponding to zero delay and hence constant frequency difference between the counter-propagating beams of light. Scanning the high frequency synthesizer driving the EOM, allows for the Brillouin frequency gain spectrum to be generated. A Lorentzian function is fitted to this Brillouin frequency gain spectrum in order to identify the peak Brillouin frequency corresponding to the region under interrogation. The position of this region under interrogation can then be swept along the sensing fibre by delaying the phase of one beam relative to the other. This phase delay between the counter propagating beams of light is achieved by incorporating a delay fibre outside the sensing fibre such that any change in the frequency at which the frequency of the laser is swept translates into a change in phase and hence a change in the sensing position along the sensing fibre.

For the BOCDA-based measurements, the spatial resolution (*z*) and the measurement range corresponding to the interval between correlation peaks (*d*) are given by the following equations [9, 10]:

$$z = \frac{d \times {}^{Br}\Delta v_{LW}}{\pi \times \Delta f} \qquad (1)$$

$$d = \frac{V_g}{2 f_m} \qquad (2)$$

where f_m is the modulation frequency, Δf is the frequency variation achieved when the laser wavelength is swept at frequency f_m, ${}^{Br}\Delta v_{LW}$ is the linewidth of the Brillouin spectrum and V_g is the velocity of light in the fibre. The above equations indicate that in this mode of operation, the ratio of spatial resolution to sensing length is determined by the ratio of the Brillouin gain linewidth to the modulation depth.

Despite BOCDA's ability to offer Brillouin frequency measurements with indisputably high spatial resolution, when used on a standard single mode fibre (SMF) it is unable to disentangle the temperature influences during strain induced frequency measurements. Hence so far it's applicability in SMF is limited to situations where the temperature is well defined. This chapter describes the combination of BOCDA with an independent measurement of temperature based on the determination of the intensity of the anti-Stokes Raman scattering (R-OTDR) with very much higher spatial resolution than previously reported [3], in order to produce a fully temperature compensated strain sensor with high spatial resolution.

3.2 Theory

This section briefly describes the theoretical basis for the R-OTDR technique.

3.2.1. Raman Optical Time Domain Reflectometry

In Raman scattering, the probability for anti-Stokes transition increases with increase in temperature, and the Bose–Einstein factor for the anti-Stokes line [11] is given as

$$R_{A.S} = \frac{e^{-\left(\frac{\Delta E}{kT}\right)}}{1\text{-}e^{-\left(\frac{\Delta E}{kT}\right)}} \qquad (3)$$

where $R_{A.S}$ is the Raman anti-Stokes probability, ΔE is the energy difference between two vibrational states, k is the Boltzmann's constant and T is the temperature in Kelvin. From this equation, the temperature sensitivity of the intensity of spontaneous anti-Stokes Raman scattering is found to be ~ 0.8%/°**C** [12, 13], at room temperatures.

The threshold for stimulated Raman scattering can be calculated using equation 4 [14]. In the case of Stimulated Raman scattering, the Raman Stokes signal which experiences gain along the fibre length propagates in the pump direction, while the anti-Stokes Raman signal counter propagates to the pump direction. This way it becomes easier to filter out the Raman anti Stokes signal.

$$P_{Th.}^{SRS} = \frac{16 \times A_{eff}}{L_{eff} \times g_R} \qquad (4)$$

Where $P_{Th.}^{SRS}$ is the threshold power beyond which stimulated Raman effect is dominant, leading to pump depletion, A_{eff} is $80\mu m^2$ for the fibre used in the experiments, L_{eff} is the length given by equation 5 [14], while g_R is the Raman gain coefficient, which for the pump wavelength of 1550nm is $7\times10^{-14}\,m/W$ [14]. The value of the loss parameter $\alpha = 0.046/km$ and the value of dispersion at operating wavelength of 1550nm is, D=17ps/nm.km [14].

$$L_{eff} = \frac{[1-\exp(-\alpha L)]}{\alpha} \qquad (5)$$

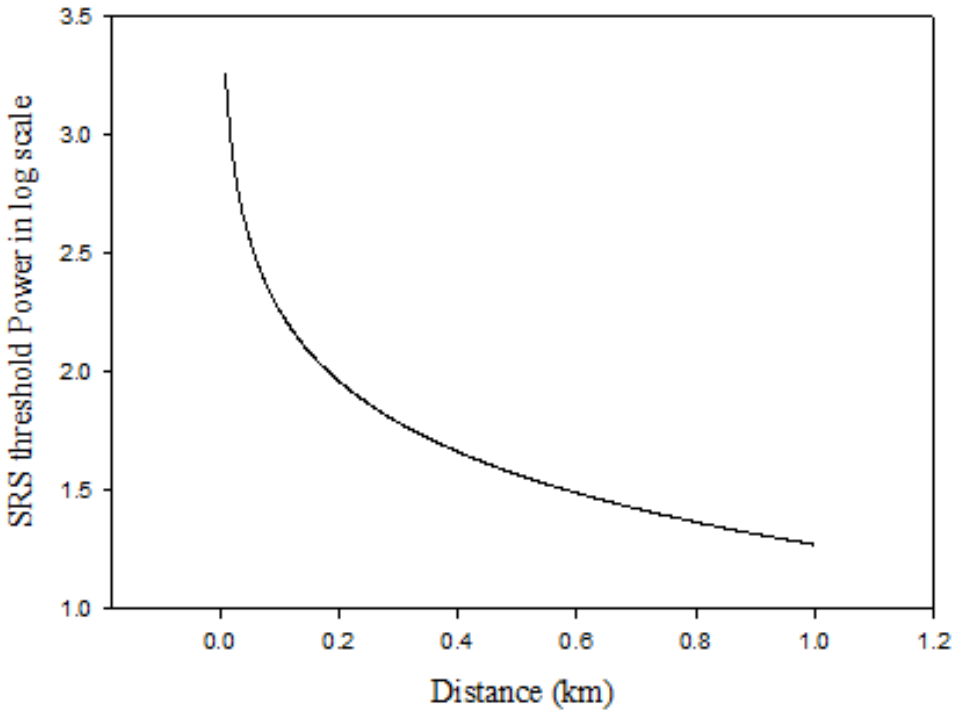

Figure 1. Theoretically calculated SRS thresholds using equation 4, presented in log scale

Figure 1 shows the plot of equation 4. The plot reveals, at short sensing lengths, the threshold for stimulated Raman scattering is relatively high, so the R-OTDR measurement can be obtained with short high peak power pulses which allow high spatial resolution interrogation along the sensing length, whilst maintaining the required signal to noise.

The R-OTDR measurements require normalisation in order to eliminate features such as the splice and transmission losses which are gathered by the distributed Raman anti-Stokes measurements. Commercial Raman-based distributed temperature sensors used the Rayleigh signal at the Raman shifted wavelength to account for the distributed splice and transmission losses over the sensing length. However, for the purpose of demonstration of the combinatory technique used in this chapter, we used the distributed Raman measurement for the unheated fibre as the reference measurement and used it to normalize the measured trace corresponding to the situation when a section of the fibre is heated. The temperature profile is given by equation 6.

$$\Delta T_R(L) = \frac{\left(\Delta I_{R_{A.S}}(L) / I_{R_{A.S}}(L)\right) \times 100}{C_{RI}^T} \tag{6}$$

where L is the distance along the fibre, $\left(\Delta I_{R_{A.S}}(L) / I_{R_{A.S}}(L)\right) \times 100$ is the percentage change in Raman anti-Stokes intensity normalised with the room temperature measurements of the anti-Stokes Raman and C_{RI}^T is the coefficient of the Raman intensity change with temperature. The temperature resolution can be found using equation 7.

$$\delta\Delta T_R(L) = \frac{\left(\delta\left(\Delta I_{R_{A.S}}(L)\right) / I_{R_{A.S}}(L)\right) \times 100}{C_{RI}^T} \tag{7}$$

where $\delta \Delta T_R(L)$ is the temperature resolution and $\left(\delta\left(\Delta I_{R_{A.S}}(L)\right)/I_{R_{A.S}}(L)\right)\times 100$ is the percentage normalised intensity resolution achieved on the Raman anti-Stokes backscattered signal .

3.2.3. Temperature and strain discrimination

The change in the Brillouin frequency shift from BOCDA and intensity from R-OTDR can be represented by the following matrix equation [2]:

$$\begin{bmatrix} \Delta \nu_B \\ \Delta I_{R_{A.S}} \end{bmatrix} = \begin{bmatrix} C^{\varepsilon}_{B\nu} & C^{T}_{B\nu} \\ C^{T}_{RI} & C^{\varepsilon}_{RI} \end{bmatrix} \begin{bmatrix} \Delta \varepsilon \\ \Delta T \end{bmatrix} \qquad (8)$$

where $C^{\varepsilon}_{B\nu}$ and $C^{T}_{B\nu}$ are the coefficients for the Brillouin frequency shift due to strain and temperature respectively and C^{T}_{RI} is the coefficient for the Raman anti-Stokes intensity change with temperature. The coefficient for the Raman anti-Stokes intensity is insensitive to strain, hence C^{ε}_{RI} = 0. $\Delta \nu_B$ and $\Delta I_{R_{A.S}}$ are the Brillouin frequency shift and the anti-Stokes Raman intensity change respectively. The inverse of equation (8) yields:

$$\begin{bmatrix} \Delta \varepsilon \\ \Delta T \end{bmatrix} = \frac{1}{\left| C^{\varepsilon}_{B\nu} C^{T}_{RI} \right|} \times \begin{bmatrix} 0 & -C^{T}_{B\nu} \\ -C^{T}_{RI} & C^{\varepsilon}_{B\nu} \end{bmatrix} \begin{bmatrix} \Delta \nu_B \\ \Delta I_{R_{A.S}} \end{bmatrix} \qquad (9)$$

Where $\Delta \varepsilon$ is the change in applied strain, while ΔT is the change in temperature.

The corresponding error in the temperature-compensated strain measurement is given by [2] equation 10,

$$\left|\delta\varepsilon\right| = \frac{\left|C_{RI}^{T}\right|\left\|\delta\nu_{B}\right| + \left|C_{B\nu}^{T}\right|\left\|\delta I_{R_{A.S}}\right|}{\left|C_{B\nu}^{\varepsilon} C_{RI}^{T}\right|} \qquad (10)$$

where $\delta\nu_B$ and $\delta I_{R_{A.S}}$ are the RMS errors in the Brillouin frequency shift and the Raman anti-Stokes intensity change measurements.

3.3 Experimental setup and procedure

3.3.1. Experimental setup

The experimental setup for the short range distributed strain measurement with temperature compensation is shown in figure 2(*a*). The detailed layout of the sensing fibre is depicted in figure 2(b).

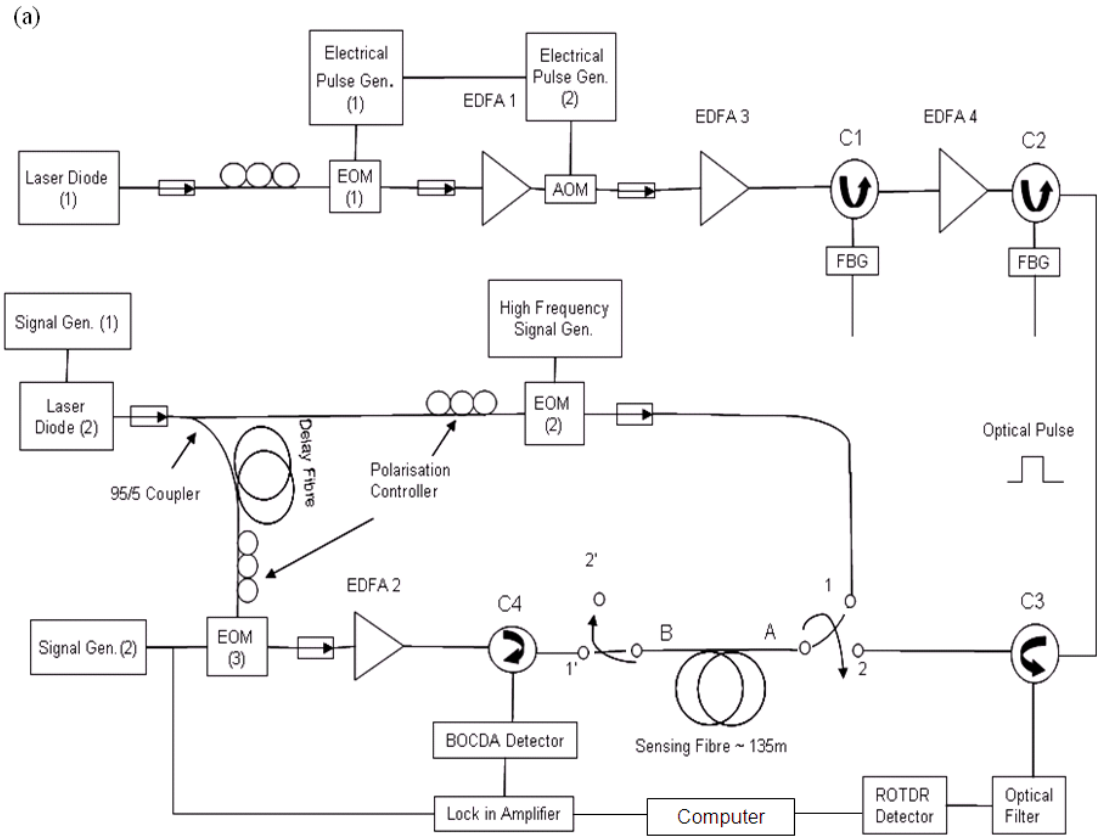

Figure 2a. Proposed scheme for the temperature-compensated distributed strain sensor system

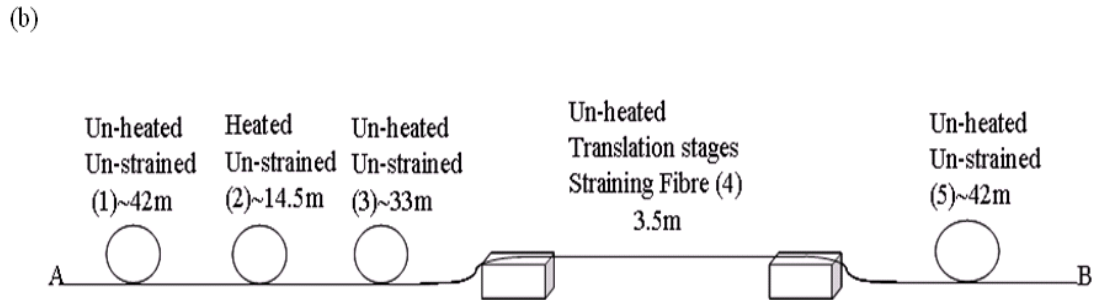

Figure 2b. Detailed layout of the 135m sensing fibre.

The details of the scheme presented in figure 2(a) can be more easily understood by examining the experimental layout of the individual techniques i.e., R-OTDR and BOCDA that have been combined in order to demonstrate the temperature

compensation feature during a sub-metre spatial resolution distributed strain measurement.

The R-OTDR setup comprised a continuous wave (CW) laser diode (1) operating at 1550nm (linewidth ~ 5MHz) with an output power of 20mW, followed by an optical isolator, preventing back reflections from damaging the diode. A polarization controller was used to align the azimuth of the linear light to the electro optic intensity modulator (EOM (1)). EOM1 with an insertion loss of 3dB and an extinction ratio of 18dB, was used to gate the CW optical output from the laser diode 1 using a pulse generator (PICOSECOND PULSE LABS, model no. 2600 B) operating at 1ns pulse width at a repetition rate of 10kHz. This combination of the pulse width and repetition rate rendered a duty cycle of 10^{-5}. An isolator was used immediately after the EOM1 in order to suppress the backward amplified spontaneous emission (ASE) from the erbium doped fibre amplifier (EDFA (1)) with a 30dB optical gain, potentially capable of damaging the EOM (1). An acousto optic modulator (AOM) with an insertion loss of 4dB and extinction ratio of 40dB was used immediately after the EDFA (1) to suppress any inter-pulse ASE component from the first 30dB gain EDFA (1). The pulse after the AOM was amplified to a peak power of 240W using two stages of EDFA 3 & EDFA 4, each with a gain of 9dB, combined with two ASE filtering stages using circulators C1 and C2 and fibre Bragg gratings, FBG (1) and FBG (2), both centred at 1550nm with 3dB bandwidth of 3nm and side band suppression of 30dB. The purpose of the ASE filtering stages was to get rid of the ASE which was capable of clipping the gain in the subsequent amplifier stages, preventing signal amplification. The amplified pulse with peak power of 240W was launched into the sensing fibre via the circulator C3, which was also responsible for channelling the backscattered signal onto the detector.

The spontaneous Raman anti-Stokes backscattered signal was separated from the Rayleigh and Brillouin signals by an optical filter series, comprising a 5nm (3dB bandwidth) broad band fibre Brag grating centred at 1550nm with 30dB side band suppression, used in transmission along with two 20dB edge filters with cut off

wavelength at 1500nm. The filtered optical signal was detected using a 600MHz APD with gain of 30,000V/W and a noise equivalent optical power of $1.3 pW/\sqrt{Hz}$. The output voltage was further amplified using a 350MHz voltage amplifier with a 30dB gain and input shorted noise of $2 nV/\sqrt{Hz}$. A 300MHz oscilloscope was used to observe the amplified signal voltage.

In the BOCDA setup, laser diode (2) operating at 1550nm (linewidth ~ 5MHz) was used. The sinusoidal sweep rates (f_m) for the signal generator (1) were chosen using equation 2 so as to allow for a single correlation peak to be swept through the sensing fibre length (d), which is also the separation between the correlation peaks. The injection current of the laser diode was modulated to achieve a frequency variation (Δf) of 7.7GHz with two sets of sinusoidal sweep rates (f_m), i.e., 649.2kHz – 649.7kHz and 671.6kHz – 672.2kHz (frequency step of 0.02kHz). The frequency variation emerging as a consequence of modulating the injection current of the distributed feedback (DFB) laser diode was measured using a Mach Zehnder interferometer with a free spectral range of 0.25nm. In this arrangement the d.c bias of the DFB laser output was matched to the quadrature point of the Mach Zehnder interferometer. The extent of movement on either side of the quadrature point as a consequence of sinusoidal modulation in the injection current over the d.c bais unfolded the change in wavelength experienced by the laser. Erbium amplifier in gain saturation mode was used between the Mach Zehnder interferometer and the DFB laser output, to suppress the optical power fluctuations emerging as a result of injection current modulation. The wavelength change due to the injection current modulation was used in equation 12 in order to estimate the variation in laser frequency.

$$\Delta f = -\frac{c/n}{\lambda^2}\Delta\lambda \qquad (12)$$

The frequency span (f_m) of 649.2kHz – 649.7kHz restricted the scanning of the correlation peak from section 1 to section 2 while an (f_m) range of 671.6kHz – 672.2kHz resulted in the scanning of the correlation peak between sections 3 and section 4 only. EOM (2) was driven by the high-frequency signal generator to generate side bands corresponding to the Brillouin frequency shift of 10GHz – 12GHz. During the course of the BOCDA experiment described in this chapter, the high frequency side band generated by EOM (2) was not filtered, though it should typically be removed in order to increase the signal to noise ratio. This is because for values of frequency variation (Δf) comparable or greater than the Brillouin separation, there is a counterbalancing of the Brillouin gain and loss by the two sidebands from the EOM which results in reduction of the Brillouin gain at the correlation point [15]. But in this experiment since the frequency variation (Δf ~ 7.7GHz) was less than the Brillouin shift of 10.8GHz there was no drop in the signal to noise ratio which would have otherwise imposed difficulties in identifying the peak Brillouin shift due to heat or strain. The signal generator (2) was used to provide a 30kHz (square wave) signal to the intensity (EOM (3)) and also to provide a reference signal to the lock-in amplifier (EG&G BROOKDEAL) with a bandwidth of 100kHz. The 30kHz square wave modulation input to EOM3, coded the high frequency counter propagating pump. Transfer of power to the low frequency probe rendered gain to the probe bearing a 30kHz modulation signature. With the lock in amplifier locked to the 30kHz modulation signal, the gain of the probe was easily recovered. The Brillouin signal was detected using a 1GHz detector with a responsitivity of 0.95A/W.

As shown in figure 2(b), the 135m sensing fibre comprised five sections of SMF (effective area ~ 80μm^2, loss ~ 0.20dB km^{-1} and dispersion ~ 17ps km^{-1} nm^{-1} at 1550nm). Optical fibres in sections 1, 3 and 5 were unstrained and kept at room temperature. The lengths of optical fibres in sections 1, 3 and 5 were 42m, 33m and 42m, respectively. The length of the optical fibre in section 2 was 14.5m and it was loosely coiled and maintained at an elevated temperature on a hot plate, with a temperature stability of ±1°C. Temperature of the hot plate was monitored using a

thermistor probe with an accuracy of ±0.1°C. A 3.5m length of unheated optical fibre was strained between translation stages, this formed section4. Table1 summarizes the details of each section of the sensing fibre.

Data from the frequency based Brillouin optical correlation domain analysis experiments and the intensity based anti-Stokes Raman optical time domain reflectometry experiments were collected and analysed by a personal computer.

Table1:

Sections	1	2	3	4	5
Length (m)	42	14.5	33	3.5	42
Strained	No	No	No	Yes	No
Heated	No	Yes	No	No	No

Table1. Detail of the five sections of the 135m sensing fibre.

3.3.2. Experimental procedure

During the experiment, section 2 of the sensing fibre was loosely coiled and heated to 52°C on a hot plate. Section 4 of the sensing fibre was strained to 571.4με and its temperature was maintained at 25°C. For the BOCDA measurement, the input port of the circulator (C4) was spliced to optical path 1' and the front end (A) of the sensing fibre spliced to optical path 1, allowing for the counter-propagating laser diode (2) light to interact in the sensing fibre. The corresponding correlation peak resulting from the interaction was swept from section 1 to section 2 and section 3 to section 4 respectively. The sweeping of the correlation peak between section 1 and section 2 was achieved by the frequency span $(f_m)$of 649.2kHz – 649.7kHz, while the span

between 671.6kHz – 672.2kHz was responsible for moving of the correlation peak between sections 3 and section 4 of the sensing fibre.

During the R-OTDR measurements, the front end (A) of the sensing fibre was spliced to circulator (C3) via optical path 2, while the splice between circulator (C4) and far end (B) of sensing fibre was broken and terminated in a knot depicted by point 2'. This allowed 1ns pulses with 240W peak power to be launched into the 135 m sensing fibre, with the knot on the far end preventing any strong back reflections. Section 2 was heated to five different temperatures: 31.7°C, 41°C, 52°C, 62°C and 71.5°C. At a particular temperature each R-OTDR trace comprised 1000 points averaged 65536 times on the 300MHz oscilloscope. 50 such traces were stored onto the computer and subsequently averaged on it. This entire process took 40 minutes.

The process of splicing between measurements was adopted only as means to demonstrate the working of this combinatory sensing technique however in principle an optical switch can be used instead.

3.4 Results

3.4.1 Brillouin Optical Correlation Domain Analysis of the heated section

Figure 3 shows the Brillouin frequency results extracted from the heated section using the Brillouin optical correlation domain analysis technique.

Figure 3a, shows the plot of the Brillouin gain distribution for the fibre kept at room temperature at 25°C in section 1 and the fibre heated to 52°C in section 2.

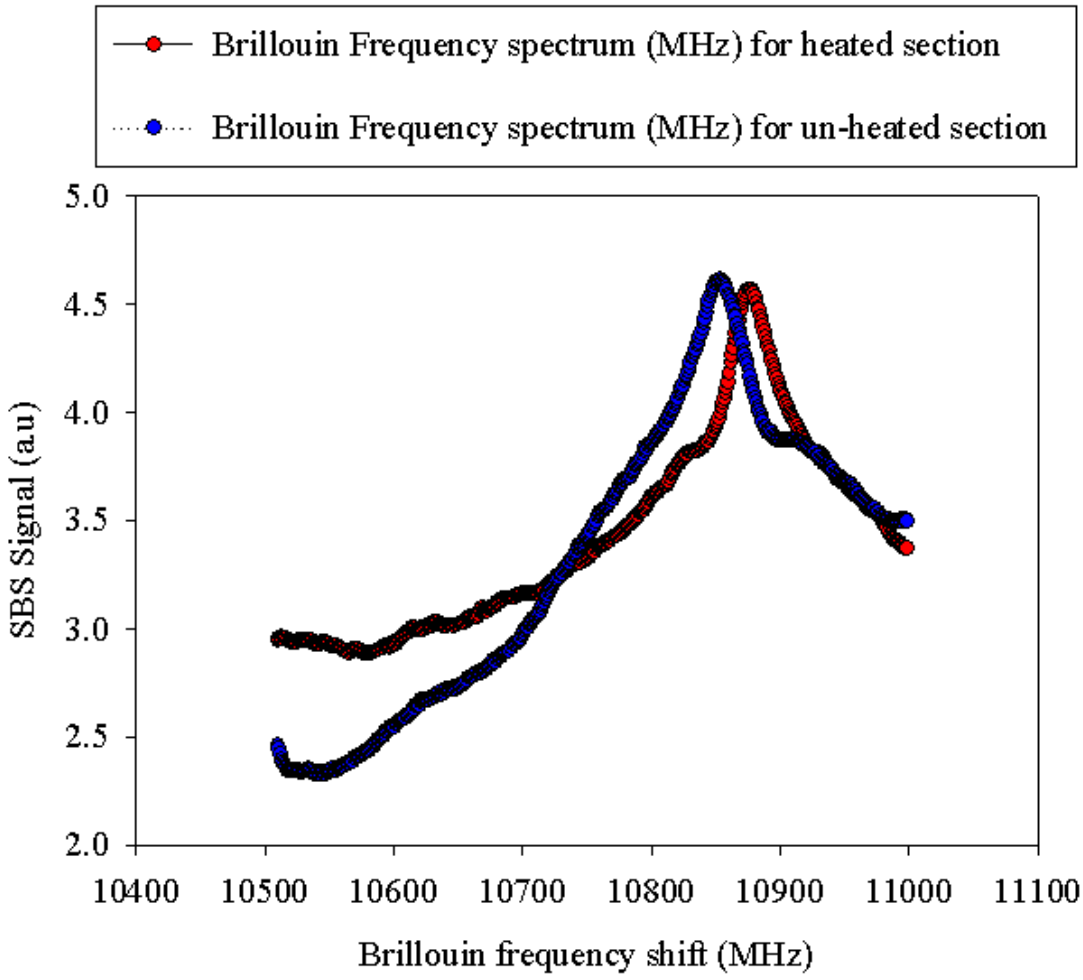

Figure 3a. The Brillouin peaks corresponding to the fibre kept at 25°C and heated to 52°C

The plot in figure 3b shows the shift in the peak Brillouin frequency, arising as a consequence of moving the correlation peak from section 1 to section 2. While the plots in figure 3c show the Brillouin gain distribution across sections 1 and 2, at peak Brillouin frequency of the unheated (10853MHz) and heated (10881MHz) regions. A spatial resolution of 19cm was calculated using a 10/90% step response from figure 3c.

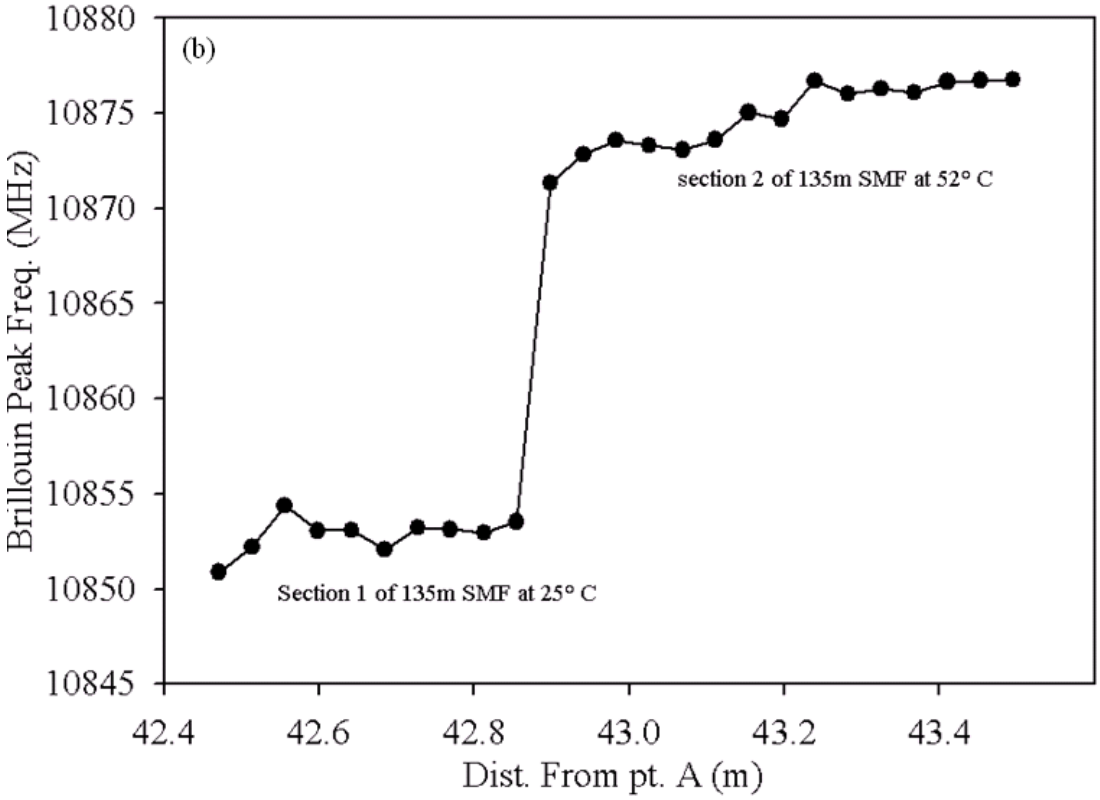

Figure 3b. Step change in the Brillouin peak frequency when scanning the correlation peak from the unheated to heated region.

The change in the Brillouin frequency shift was measured to be 28MHz, which corresponded to a coefficient for the change of the Brillouin shift with temperature of 1.04MHz/°C. A 5MHz (~ 5°C) drift in the heated section was attributed to a temperature gradient present on the hot plate.

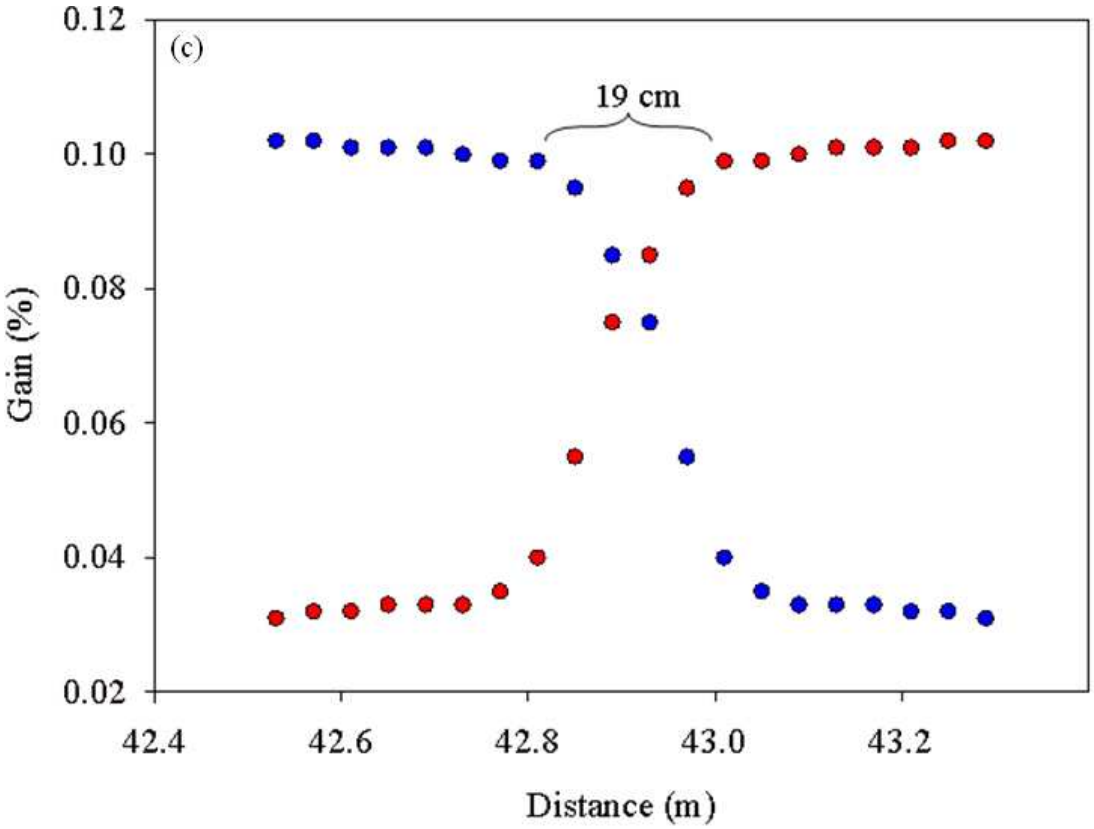

Figure 3c. The Brillouin gain distribution at peak Brillouin frequency of the un-heated (10853MHz – blue trace) and heated (10881MHz - red trace) regions

3.4.2. Brillouin Optical Correlation Domain Analysis of the strained section

Figure 4 shows the Brillouin frequency results extracted from the strained section using the Brillouin optical correlation domain analysis technique.

Figure 4a, shows the plot of the Brillouin gain distribution for the loosely coiled fibre kept at room temperature at 25°C in section 3 and the fibre strained to 571.4$\mu\varepsilon$ in section 4.

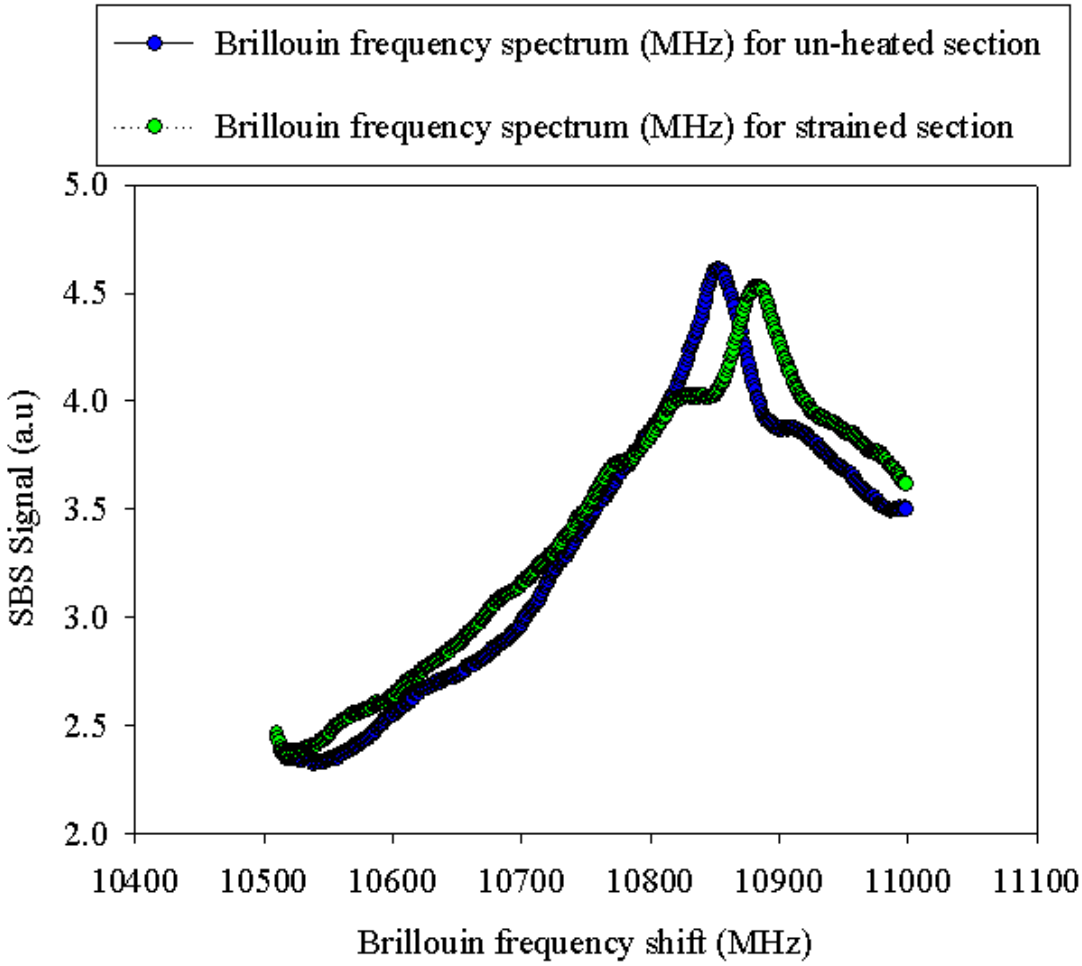

Figure 4a. The Brillouin peaks corresponding to the unstrained fibre and strained fibre sections.

The plot in figure 4b shows the shift in the peak Brillouin frequency, arising as a consequence of moving the correlation peak from section 3 to section 4. While the plots in figure 4c show the Brillouin gain distribution across sections 3 and 4, at peak Brillouin frequency of the unheated/unstrained (10853MHz) and strained (10879MHz) regions. A spatial resolution of 18cm was calculated using a 10/90% step response from figure 4c.

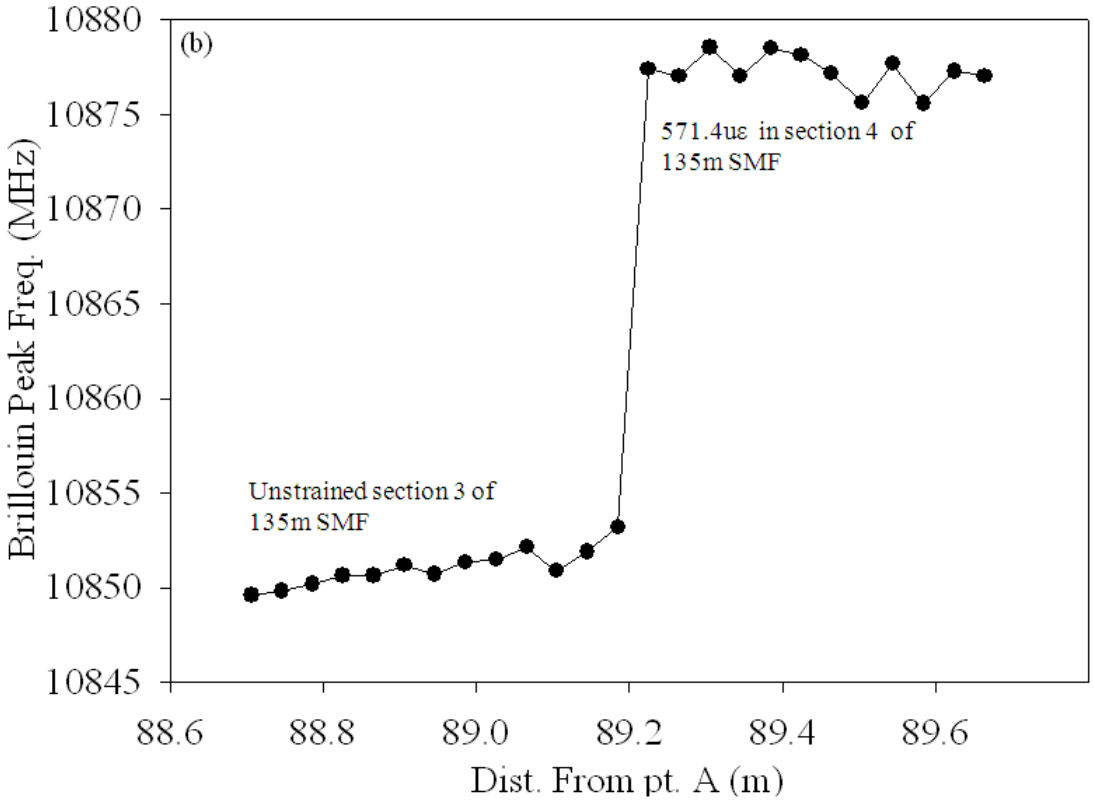

Figure 4b. Step change in the Brillouin peak frequency when scanning the correlation peak from the unstrained to strained region.

The change in the Brillouin peak frequency of the fibre strained to 571.4$\mu\varepsilon$ with respect to the fibre at zero strain was measured to be 26MHz, and this corresponded to a coefficient of the Brillouin frequency shift of 4.5 MHz/100$\mu\varepsilon$.

The temperature in both sections of fibre was kept at 25 °C. The RMS frequency error $\delta\nu_B$ was measured to be 1.7MHz. The value of RMS frequency error is representation of the variation in the Brillouin peak frequency along the sensing fibre. However an error of 0.1MHz was found whilst fitting a Lorentzian function to the Brillouin frequency spectrums shown above.

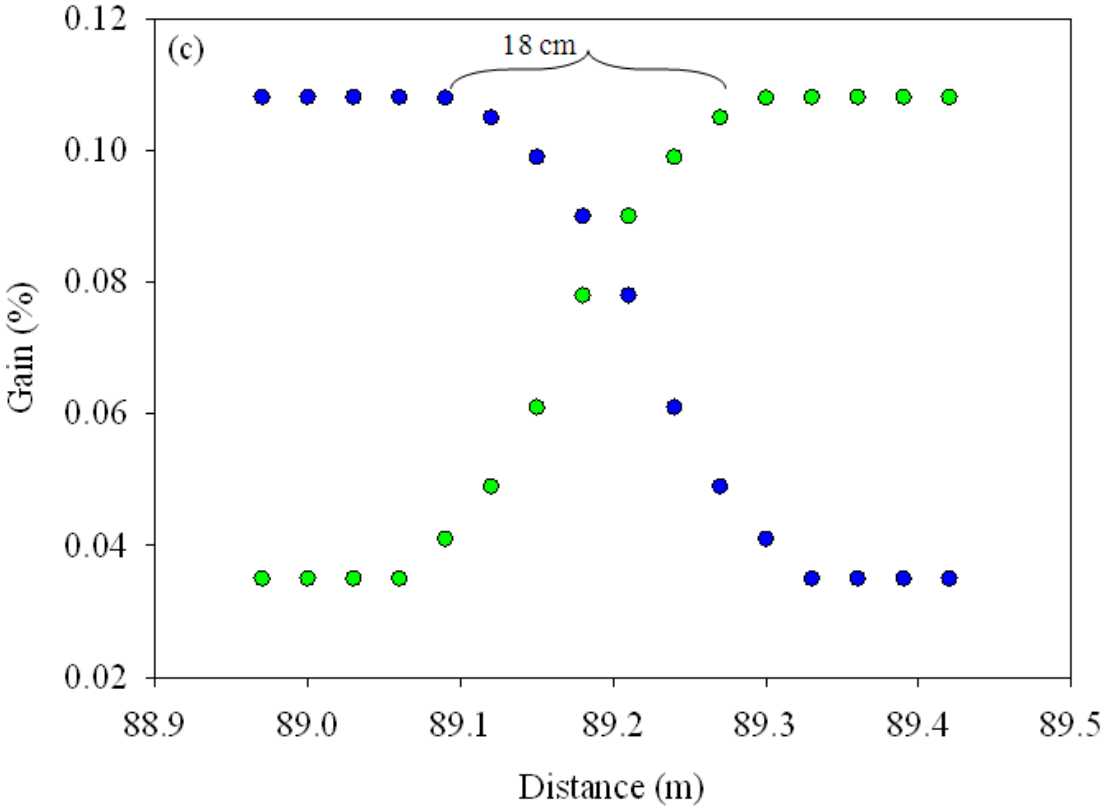

Figure 4c. The Brillouin gain distribution at peak Brillouin frequency of the un-strained (10853MHz – blue trace) and strained (10879MHz - green trace) regions

3.4.3. Raman Optical Time Domain Reflectometry of the heated section

Figure 5 shows the anti-Stokes Raman intensity results of the 135m length of sensing fibre, collected using the Raman optical time domain reflectometry technique.

Figure 5*a* shows the spatially resolved backscattered Raman anti-Stokes signal generated by pulses of 240W peak pulse power and width of 1ns in the 135m sensing fibre. The black plot was obtained with fibre kept at 23.8°C, and the red trace was obtained when fibres in section 2 was heated to 52°C.

The difference in offsets seen before and after the sensing fibre is attributed to the use of an ac coupled APD detector together with pump depletion effects.

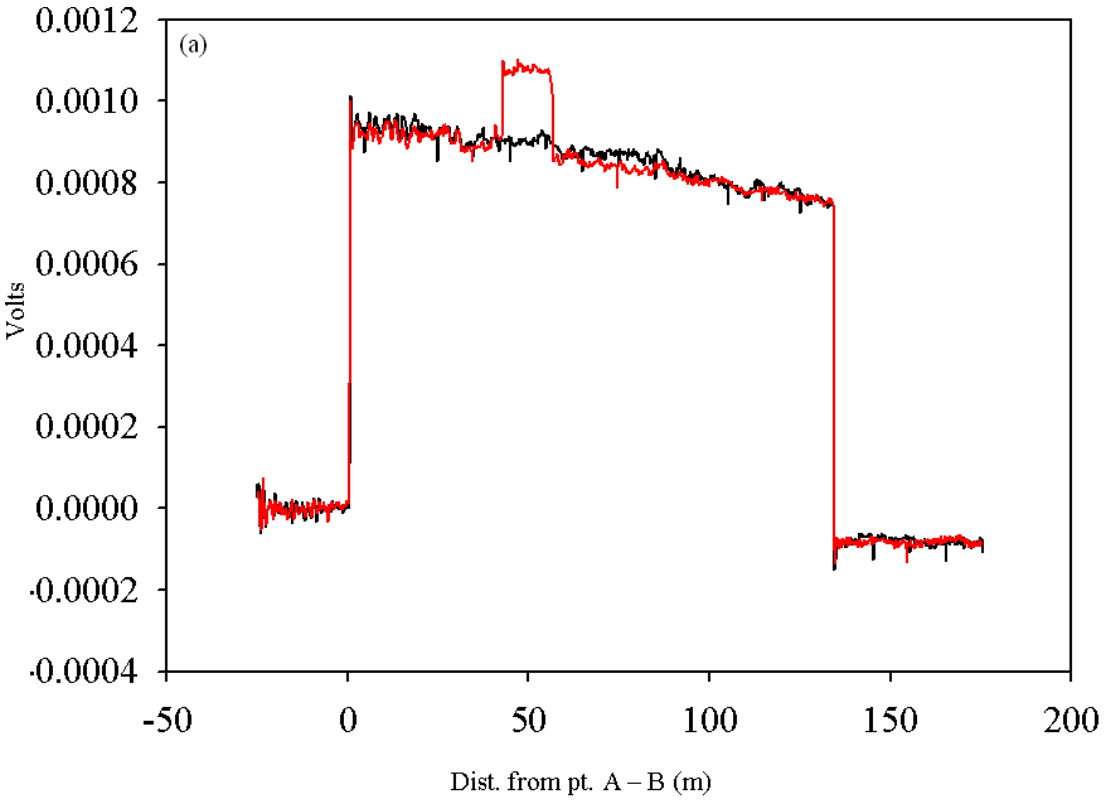

Figure 5a. Black plot - R-OTDR trace of the fibre in section 2 kept at 23.8°C, Red plot - R-OTDR trace of the fibre in section 2 heated to 52°C.

Figure 5 b shows the backscattered traces for the heated portion of the sensing fibre subjected to temperatures of 52.0°C (indicated by a red line), 62.0°C (indicated by a green line) and 71.5°C (represented by a blue line) and normalized by the trace obtained at room temperature of 23.8°C.

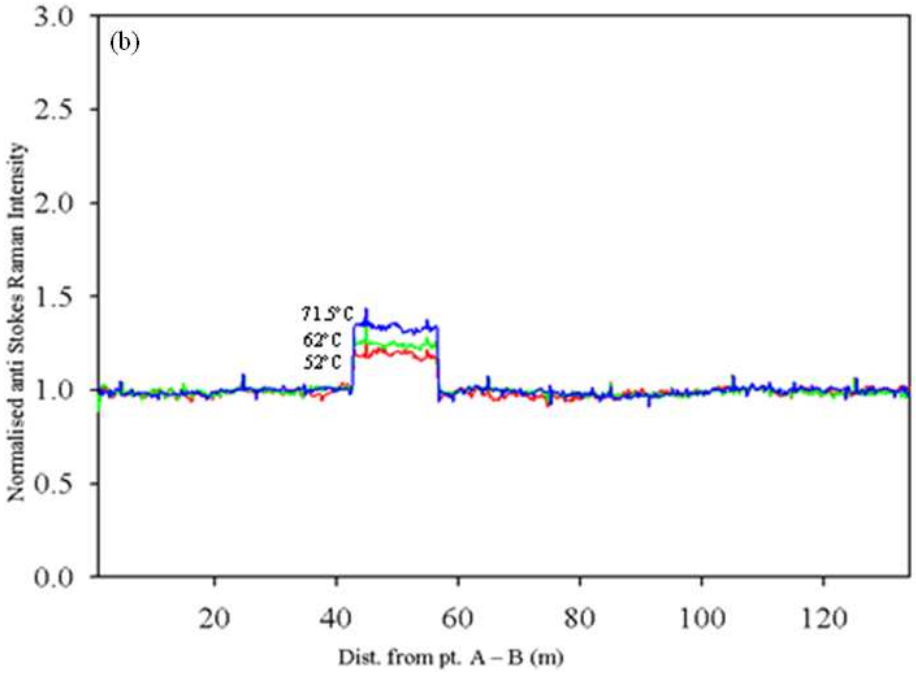

Figure 5b. The normalized R-OTDR plots of the fibre in section 2 heated to different temperatures.

The intensity change for the five different temperatures is plotted in figure 6.

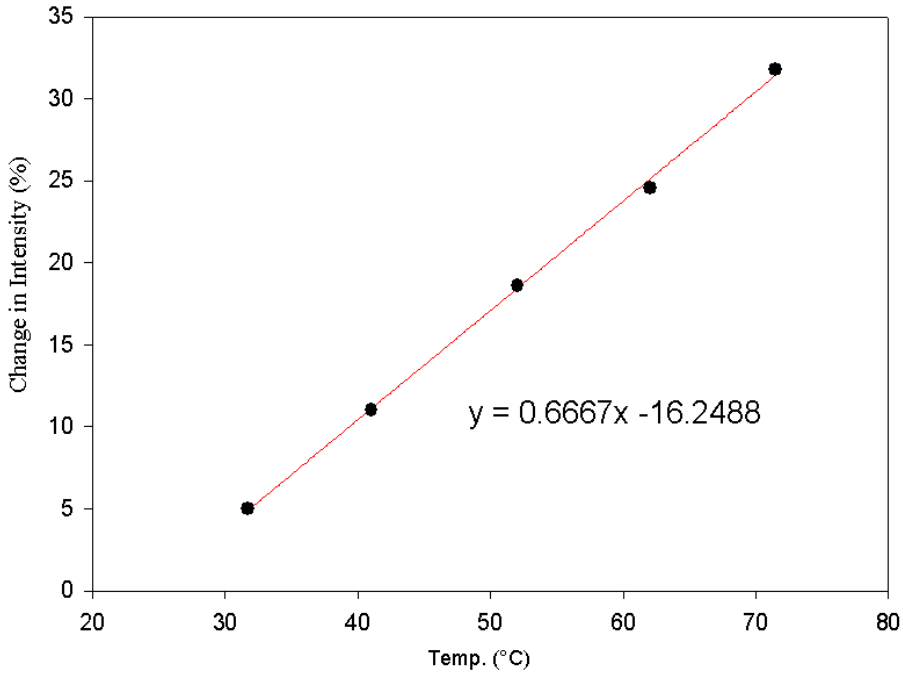

Figure 6. The % intensity change of the Raman anti-Stokes signal versus temperature.

A linear relationship of change in Raman anti-Stokes intensity with temperature is indicated in figure 6. The slope corresponding to the coefficient of intensity change with temperature extracted from the equation of a linear fit was 0.66% /°C.

Figure 7 shows the normalized plot of 100-point running median of the normalized data (figure 5(*a*), red plot). A spatial resolution of 24cm was calculated using the 10⁄90% step response corresponding to the temperature change between fibres of sections 1 and 2. The effective electronic bandwidth of the data acquisition system limited the spatial resolution to 24cms.

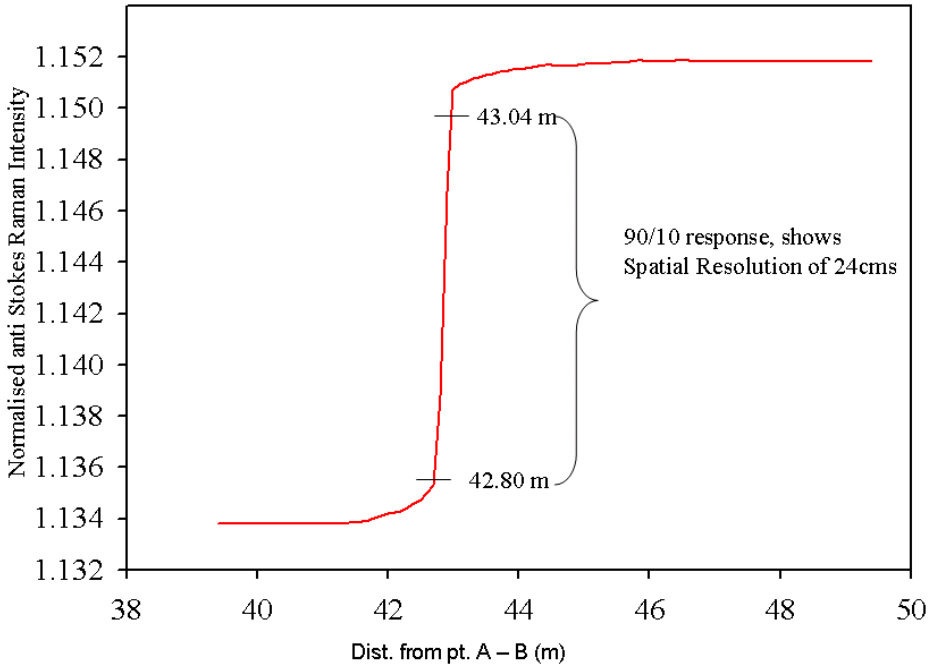

Figure 7. Normalized 10⁄90% step response for the transition from the un-heated (1) to heated (2) fibre section.

3.5 Discussions

The correlation peak observed in the BOCDA measurements is a representation of the net Brillouin gain observed at the phase matched interaction point between the counter propagating optical waves. However whilst attempting to move this correlation peak from section 1 to section 2, or between sections 3 and 4, there is emergence of another Brillouin peak at the cross over region. This results in sharing of the net Brillouin gain in a proportion decided by the percentage of correlation point sitting in one region relative to the other. For instance the data shown in figure 3b or figure 4b represents the peak Brillouin value corresponding to those positions in the sensing fibre where at least 70% of the correlation region is present in any one section relative to the other. The data shown in figure 3c is the increase (or decrease) in the Brillouin gain percentage for the peak Brillouin frequency corresponding to heated (or unheated and unstrained) region of the sensing fibre and similarly the data shown in figure 4c is the increase (or decrease) in the Brillouin gain percentage for the peak Brillouin frequency corresponding to strained (or unstrained and unheated) region of the sensing fibre.

Brillouin frequency based distributed temperature and strain measurements with a spatial resolution of 19cm and 18cm were obtained using the BOCDA technique (sections 3.1 and 3.2). These experimental values were in close agreement with theoretical estimates of 19.1cm for the heated section and 18.5cm for the strain section were using equation 1. The parameters used in the calculation were Δf ~ 7.7GHz and $\left(f_m\right)$~ 649.2kHz – 649.7kHz and 671.6kHz – 672.2kHz, respectively. Equation 2 reveals that the increase in value of $\left(f_m\right)$not only results in moving the correlation peak across the fibre but also influences the spatial resolution, i.e., the spatial resolution improves for a higher value of $\left(f_m\right)$, which explains the slight improvement in the spatial resolution value in the strain region as compared to the heated region. The resolution in the Brillouin frequency shift along the sensing fibre

obtained using the BOCDA technique was measured to be 1.7MHz, which corresponded to a strain resolution of 38με in the absence of temperature uncertainty.

The R-OTDR measurements used very high peak power (240W) pulses. Such high peak powers were achieved with a cascaded erbium amplifier arrangement. However, such an arrangement could have also witnessed stimulated Brillouin scattering effects within the amplifier, which would have affected the overall performance of the amplifiers and could have also resulted in distorted pulse. But the usage of short pulses of the order of 1ns, in order to meet the high spatial resolution requirement, suppressed the phenomenon of SBS in amplifiers. This was largely due to the inability of such short pulses to contribute towards any significant acoustic wave build up leading to SBS [14].

The detection system essentially required capturing of the backscattered anti-Stokes Raman signal. It is useful to have some idea about the peak powers that can be launched before detrimental effects from SRS begin to influence the distributed temperature measurements. Although a rough estimate of the SRS threshold was obtained using equation 4, i.e., 135W, there is value in launching peak powers in excess of this value in order to increase the signal to noise ratio, before pump depletion begins to deteriorate the same. The process of stimulated Raman scattering was modelled for 240W peak power pulses. The model comprised solving of the coupled differential equations shown in equation 13 and 14 [14].

$$\frac{d\left(P_s / A_{eff}\right)}{dz} = g_R \frac{P_p}{A_{eff}} \frac{P_s}{A_{eff}} - \alpha_s \frac{P_s}{A_{eff}} \tag{13}$$

$$\frac{d\left(P_p / A_{eff}\right)}{dz} = -\frac{\omega_p}{\omega_s} g_R \frac{P_p}{A_{eff}} \frac{P_s}{A_{eff}} - \alpha_p \frac{P_p}{A_{eff}} \tag{14}$$

Where A_{eff} ,is the effective area of the fibre, P_s is the stokes power, P_p is the pump power, g_R is the Raman gain coefficient for the pump wavelength of 1.55µm, ω_p/ω_s is the ratio of pump to stokes frequencies, while α_p and α_s are the fibre losses for the pump and stokes wavelengths. Outcome of the model is shown as plots in figure 8, depicting the power levels of the first order Raman Stokes and the pump as a function of sensing length. The outcome of the simulation predicts a 10% depletion of the pump power, over 135m of sensing length.

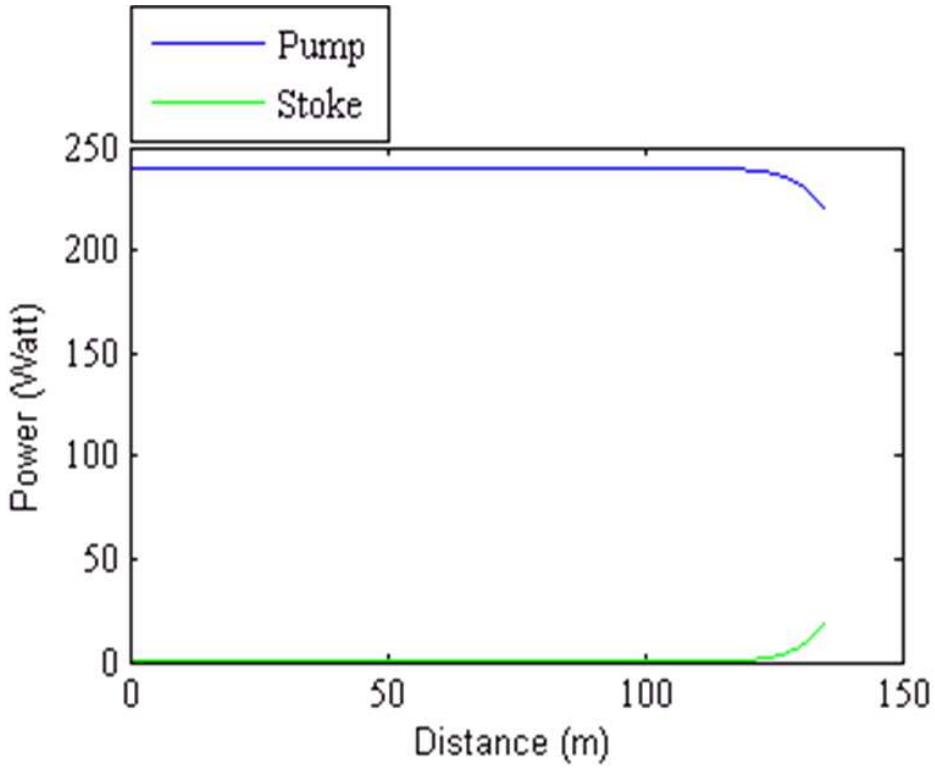

Figure 8. Outcome of the simulation predicting the pump and stokes power levels as a function of 135m of sensing length for launched peak powers of 240W

In order to compare the theoretical prediction of 10% pump depletion with experimental observation, plots of figure 5a are revisited. It is seen that there is a 22.4% drop in the anti-Stokes Raman backscattered signals between the front end and the far end of the 135m sensing fibre. In order to explain the remaining 12.4%, we have to consider the effect due to the ac coupled APD with bandwidth of 15kHz –

600MHz,used for detecting the anti-Stokes Raman backscattered signal. To a first approximation a detector with such characteristics, could be assumed to behave as a high pass RC filter. Knowing the transfer function of such a filter would enable to ascertain the circuit response to frequency, i.e., would explain the remaining difference in offsets. The transfer function across the capacitor is given by equation 15, where $Z_R = R$ and $Z_C = 1/j\omega C$. R and C are the resistance and capacitance of the circuit. he lowest frequency (f) of 15kHz value when used in equation 15, predicts a 12% drop in signal level at the far end of sensing fibre in comparison to the front end.

$$H_C(j\omega) = \frac{1}{1 + RCj\omega} \tag{15}$$

In order to derive the time domain behavior of the transfer function, the Laplace transforms of the expression for V_C is used, which is given by equation 16. This transforms $j\omega \rightarrow s$.

$$V_C(s) = \frac{1}{1 + RCs} V_{in}(s) \tag{16}$$

Assuming a step input (i.e. $V_{in} = 0$ before $t = 0$ and then $V_{in} = V$ afterwards) together with expression $V_{in}(s) = V\frac{1}{s}$ in equation 16 transforms equation 16 as shown in equation 17.

$$V_C(s) = V\frac{1}{1 + RCs}\frac{1}{s} \tag{17}$$

Using partial fractions expansion and inverse Laplace transform in equation 17 results in the expression given by equation 18,

$$V_C(t) = V\left(1 - e^{-t/RC}\right) \quad (18)$$

Where $RC = \frac{1}{2\pi f}$. Using equation 18, the fractional drop in voltage over 135m sensing fibre can be calculated as shown in the expression below

$$\left(1 - \frac{1}{e^{\left(\frac{L \times 2\pi \times f}{V_g}\right)}}\right) \times 100$$

Where, V_g is the velocity of light in fibre, i.e., $2 \times 10^8 m/s$ and L is the sensing length of 135m. Using the above expression results in a 6.16% drop in voltage over 135m, due to ac coupling. This drop in voltage due to ac coupling together with 10% drop in voltage due to SRS predicts a total expected drop of 16%, which is in the right order of magnitude experimentally observed, i.e., 22.4% in the signal level at the far end in comparison to the front end, as shown in figure 5a. The slight discrepancy in the theoretically estimated and experimentally observed values can be explained as a consequence of a simple high pass RC circuit model assumed for the APD detector, which would other in reality comprise a much more complicated circuit. Also that the low frequency of 15kHz as quoted in the data sheet of the APD lacked any details about tolerances and the details on the frequency roll offs, something which put together should be able to provide a more accurate value of voltage drop off. The undershoot in the signal below the zero voltage level at the far end of sensing fibre, as shown in figure 5a, recovers back to the zero voltage level after 100µsec, which is equivalent to the repetition rate of the pulses.

The traces of the normalised anti-Stokes Raman intensities in figure 5b were achieved by normalising the higher temperature based R-OTDR measurements with

the room temperature based R-OTDR measurements. Such a treatment ensured that the effect of pump depletion and hence drop in the back scattered signal level as a function of sensing length does not influence the normalised distributed temperature measurements. The experimental value of the RMS intensity noise was calculated by finding the ratio of the standard deviation to the mean of the heated section of the blue trace in figure 5b. On converting this ratio into a percentage it yielded a temperature error of 1.7%. With the experimentally calculated Raman intensity coefficient value of 0.66%/°C the 1.7% error yielded a temperature error of 2.5 °C. Equation 7 is used to calculate a theoretical estimate of the temperature error. The theoretical noise equivalent voltage (NEV) of 0.012×10^{-3} V for the 600MHz detector and the 350MHz voltage amplifier with N averages is calculated using equation 19.

$$NEV = \frac{\sqrt{\left[\left(\left(NEP_{\text{det.}}\times G_{\text{det.}}\times\sqrt{B_{\text{det.}}}\right)\times G_{amp.}\right)^2+\left(NEV_{amp.}\times\sqrt{B_{amp.}}\right)^2\right]}}{\sqrt{N}} \qquad (19)$$

Where, $NEP_{\text{det.}} = 1.3 pW/\sqrt{Hz}$ is the noise equivalent optical power of the photo receiver, $G_{\text{det.}} = 30{,}000 V/W$, $G_{amp.} = 30 dB$ is the gain of the photo receiver and amplifier respectively, $B_{\text{det.}} = 600 MHz$ is the photo receiver bandwidth, $NEV_{amp.} = 2 nV/\sqrt{Hz}$ is the noise equivalent output voltage of the amplifier, $B_{amp.} = 350 MHz$ is the bandwidth of the voltage amplifier and $N = 50\times65536$ are the 65536 averages taken 50 times.

The anti-Stokes Raman signal was estimated by assuming that Raman signal was 30dB smaller than the Rayleigh signal. A 1ns broad pulse with peak power of 240W results in a 1nW Raman signal. This was amplified by the detector with gain of $G_{\text{det.}} = 30{,}000 V/W$ followed by the voltage amplifier gain of $G_{amp.} = 30 dB$, yielding a

signal equivalent voltage *(SEV)* of $9\times10^{-4}V$ corresponding to the unheated region. Equation 20 [12, 16] describes the intensity of the anti-Stokes Raman signal as a function of temperature and equation 21 which is derived from equation 20 is used to determine the theoretical change in the normalised anti-Stokes Raman signal with temperature.

$$I_{RA}\alpha\left[\frac{1}{\exp\left(\frac{hcv}{KT}\right)-1}+\text{Constant}\right] \tag{20}$$

$$\frac{dI_{RA}/dT}{I_{RA}}=\frac{\frac{hcv}{KT^2}\exp\left(\frac{hcv}{KT}\right)}{\exp\left(\frac{hcv}{KT}\right)-1} \tag{21}$$

Where I_{RA} is the anti-Stokes Raman intensity, $v=44000m^{-1}$ is the wave number corresponding to the anti-Stokes Raman wavelength, $K=1.38\times10^{-23}Kgm^2/s^2K$ is the Boltzman constant, $h=6.62\times10^{-34}Kgm^2/s$ is the Planck's constant, $T=344.65K$ is the equivalent temperature in Kelvin for a temperature of $71.5°C$. Using these values in equation 21, yields a normalised change in anti-Stokes Raman intensity with temperature, i.e., $\frac{dI_{RA}/dT}{I_{RA}}=6.3\times10^{-3}/°C$. Using this coefficient, the value of SEV is calculated to be $1.16\times10^{-3}V$ for the region experiencing a temperature of $71.5°C$. The value of $NEV=0.012\times10^{-3}V$ contributes to a 1% error. Using the value of the normalised change in the anti-Stokes Raman intensity with temperature calculated in equation 21, this 1% error in the signal due to electronic noise from the photo receiver and voltage amplifier corresponds to a temperature error of 1.5°C on the

distributed temperature measurements made at 71.5°C using the anti-Stokes Raman intensity signal. The experimentally calculated error of 1.7% from figure 5b corresponds to a temperature error of 2.5°C. The reason for an increased temperature error is due to the electronic noise peaks on the anti-Stokes Raman backscattered traces shown in figure 5 b. Emergence of the noise peaks was attributed to the non shielded GPIB cable used to communicate the PC with the oscilloscope. However, the error from the region of the data where these electronic peaks are absent is estimated to be 1.3%, which translated into a temperature error of 2°C.

The combined experimental errors of the Brillouin frequency measurement $\left(\delta\nu_B = 1.7MHz\right)$ and Raman intensity measurement $\left(\delta I_{R_{A.S}} = 1.3\%\right)$ are used together with the experimentally estimated Brillouin coefficients in sections 3.4.1 and 3.4.2 $\left(C_{B\nu}^{T} = 1MHz/°C;\ C_{B\nu}^{\varepsilon} = 0.045MHz/\mu\varepsilon\right)$ and Raman coefficient in section 3.4.3 $\left(C_{RI}^{T} = 0.66\%/°C\right)$ in equation 10, as shown below, to produce a temperature-compensated strain resolution of 82με.

$$\delta\varepsilon_{Exp.} = \frac{\left(0.66\%/°C \times\ 1.7MHz\right) + \left(1MHz/°C \times 1.3\%\right)}{\left(0.045MHz/\mu\varepsilon \times 0.66\%/°C\right)}$$

$$\delta\varepsilon_{Exp.} = 82\mu\varepsilon$$

The value of 1.7MHz used for the error in the Brillouin frequency measurements is in fact the drift in the peak Brillouin frequency in any section of unstrained-unheated or strained or heated region along the sensing fibre. Using this value of Brillouin frequency error is actually the worst case scenario. Alternatively if we consider the Brillouin frequency error as the error in the Lorentzian fit to the Brillouin gain spectrums shown in figures 3a and 4a, then the value of error estimated from the fit

was 0.1MHz. Using this value in the calculation above results in an experimentally estimated temperature compensated strain measure of 46με. Whilst, using the larger Brillouin frequency error of 1.7MHz takes into account the non-uniformities along the length of the fibre. To best assess the performance of this experimental technique it is more appropriate to use the error in the fit of the Lorentzian to the Brillouin gain curve or the correlation peak. Theoretically a temperature error of 1% together with the Brillouin frequency error of 0.1MHz, would result in a temperature compensated strain resolution of 36με.

3.6 Conclusions

BOCDA has proven to be a useful technique for achieving an extremely high spatial resolution of the peak Brillouin gain measurement of a sensing fibre. Information regarding temperature or strain can be obtained from measurements of peak Brilluoin gain measurements using this technique. However, the technique by itself is unable to distinguish between strain and temperature because the technique relies only on Brillouin frequency measurements. In order to ascertain high spatial resolution temperature compensated distributed strain measurements, the frequency based BOCDA measurements was combined with the Raman anti-Stokes intensity measurements.

The Raman anti-Stokes measurements were used to determine the temperature of the sensing fibre and this information when combined with the BOCDA allowed the pure strain to be determined. The distributed strain measurements were made exploiting the high spatial resolution capability of the BOCDA. Likewise the high powered pulses generated using cascaded erbium-doped fibre amplifiers not only allowed for the signal-to-noise of the distributed temperature measurements to be adequately maintained during backscattered anti-Stokes Raman intensity measurements using nano second pulses, but also maintained the high spatial resolution measuring capability with the distributed temperature measurements.

Using R-OTDR, we have demonstrated a spatial resolution of 24cm and temperature resolution of 2°C. When combined with the Brillouin frequency measurement using BOCDA, the resolution of the temperature-compensated strain sensor of 46με was achieved over the 135m sensing range. However in order to increase the sensing range whilst trying to maintain the spatial resolution, the frequency variation Δf has to increase by the same factor as the increase in sensing length, whilst reducing the value of f_m by the same factor. If the value of Δf is comparable or greater than Brillouin shift of 10.8GHz then the up shifted frequency sideband generated from EOM (2) in figure 1(*a*) would have to be suppressed in order to avoid cancellation of the Brillouin gain and loss by the two sidebands [17] at the correlation point.

3.7 References

[1] T. Kurashima, T. Horiguchi and M. Tateda, ‘‘Distributed temperature sensing using stimulated Brillouin scattering in optical silica fibers’’, *Journal of Lightwave Technology,* 7, p. 1170–1173 (1989)

[2] S. M. Maughan, H. H. Kee and T. P. Newson, ‘‘Simultaneous distributed fibre temperature and strain sensor using microwave coherent detection of spontaneous Brillouin backscatter’’, *Measurement Science and Technology,* 12, p. 834-842 (2001)

[3] M. N. Alahbabi, Y. T. Cho and T. P. Newson, ‘‘Simultaneous temperature and strain measurement with combined spontaneous Raman and Brillouin scattering’’, *Optics Letters,* 30, p 1276-1278 (2005)

[4] K. De Souza and T. P. Newson, ‘‘Signal to noise and range enhancement of a Brillouin intensity based temperature sensor’’, *Optics Express* 12**,** p. 2656–2661 (2004)

[5] H. H. Kee, G. P. Lees, and T. P. Newson, ‘‘All-fiber system for simultaneous interrogation of distributed strain and temperature sensing by spontaneous Brillouin scattering’’, *Optics Letters,* 25(10), p 695–697 (2000)

[6] M. N. Alahbabi, N. P. Lawrence, Y. T. Cho and T. P. Newson, ‘‘High spatial resolution microwave detection system for Brillouin-based distributed temperature and strain sensors’’, *Measurement Science and Technology,* 15**,** p. 1539–1543 (2004)

[7] M. N. Alahbabi, Y. T. Cho, and T. P. Newson, ‘‘150km range distributed temperature sensor based on coherent detection of spontaneous Brillouin backscatter and in line Raman amplification’’, *JOSA B,* 22, p. 1321–1324 (2005)

[8] M. N. Alahbabi, Y. T. Cho and T. P. Newson, ‘‘Comparison of the methods for discriminating temperature and strain in spontaneous Brillouin based distributed sensors’’, *Optics Letters,* 29**,** p. 26–28 (2004)

[9] W. Zou, Z. He, M. Kishi and K. Hotate, ‘‘Stimulated Brillouin scattering and its dependences on strain and temperature in a high-delta optical fiber with F-doped depressed inner cladding’’, *Optics Letters,* 32**,** p. 600–602 (2007)

[10] K. Hotate and M. Tanaka, ‘‘Distributed fiber Brillouin strain sensing with 1cm spatial resolution by correlation-based continuous-wave technique’’, *IEEE Photonics Technology Letters*, 14, p. 179–181 (2002)

[11] Long D A 1977 *Raman Spectroscopy* (New York: McGraw-Hill)

[12] A. H. Hartog, A. P. Leach and M. P. Gold, ‘‘Distributed temperature sensing in solid-core fibres’’, *Electronic Letters*, 21, p. 1061–1062 (1985)

[13] H. H. Kee, G. P. Lees and T. P. Newson, ‘‘1.65μm Raman based distributed temperature sensor’’, *Electronic Letters*, 35**,** p. 1869-1871 (1999)

[14] G. P. Agrawal, ‘‘Non linear fibre optics’’, Third Edition, *Academic Press*, ISBN 0-12-045143-3 (2001)

[15] S. M. Maughan, PhD Thesis, University of Southampton (2001)

[16] T. Wakami and S. Tanaka, ‘‘1.55μm long span fibre ptic distributed temperature sensor’’, *10th International Conference on OFS*, p. 134 – 137 (1994)

[17] K. Y. Song, Z. He and K. Hotate, ‘‘Enlargement of measurement range in a Brillouin optical correlation domain analysis system using double lock-in amplifiers and single side band modulators’’, *IEEE Photonics Technology Letters*, 18, p. 499–501 (2006)

Chapter 4

4. Brillouin intensity based temperature compensation for a high spatial resolution distributed strain sensor

4.1 Introduction

The previous chapter introduced the idea of using the spontaneous anti-Stokes Raman scattering in conjunction with BOCDA for disentangling temperature and strain. Despite using high peak pulse powers, the spatial resolution achieved was limited to 24cms even with averaging times of 40min, due to the very weak nature of the spontaneous Raman scattering. In order to more fully exploit the high spatial resolution capability of the BOCDA, this chapter investigates the possible benefit of combining the much stronger Brillouin anti-Stokes signal with the Brillouin frequency based BOCDA technique. The known temperature dependence of $0.36\%/^{\circ}C$ [1] and small strain dependence of $-9\times10^{-4}\%/\mu\varepsilon$ [2], of the Brillouin anti-Stokes intensity is used to allow for temperature corrected distributed strain to be determined from the B-OTDR and BOCDA information. The spontaneous Brillouin power is typically 15dB stronger than the spontaneous Raman power, and if the pump wavelength is chosen to be within the erbium gain bandwidth then there is an additional advantage of the ability to amplify the Brillouin signal. However, the disadvantage of using Brillouin power for distributed temperature measurements as against Raman power is its intensity coefficient for temperature, i.e., $0.36\%/^{\circ}C$ is nearly half that of the Raman intensity coefficient, $0.72\%/^{\circ}C$. Also due to the small separation in optical frequency of 11GHz between the Brillouin and the Rayleigh backscattered signal, there is always a threat of Rayleigh contamination due to

inappropriate optical filtering of the Brillouin signal, whereas such a condition does not arise with Raman signals because of its much large separation, i.e., 13THz from the Rayleigh signal. The purpose of this chapter is to identify whether temperature compensation is best achieved with Brillouin or Raman intensity measurements.

4.2 Theory

This section briefly describes the theoretical basis for the B-OTDR technique.

4.2.1. Brillouin Optical Time Domain Reflectometry

When a pulse of light is sent down an optical fibre, it is scattered either elastically resulting in Rayleigh scattering or in-elastically leading to Brillouin and Raman scattering. Brillouin scattering was first observed in bulk silica in 1950 [3]. Since then it has been shown [4–7] that the Brillouin backscattered power exhibits both strain and temperature dependence.

Spontaneous Brillouin scattering results when a small fraction of the incident light is in-elastically scattered by thermally excited acoustic waves (acoustic phonons) in the optical fibre. The strength of the Brillouin back scattered light resulting from a light pulse travelling down the fibre is measured and integrated as a function of time, and is represented as a function of fibre length commonly known as B-OTDR.

4.2.2. Temperature and strain discrimination

The change in the Brillouin frequency shift from BOCDA and intensity from B-OTDR can be represented by the following matrix equation [1]:

$$\begin{bmatrix} \Delta\nu_B \\ \Delta I_{BI} \end{bmatrix} = \begin{bmatrix} C^{\varepsilon}_{B\nu} & C^{T}_{B\nu} \\ C^{\varepsilon}_{BI} & C^{T}_{BI} \end{bmatrix} \begin{bmatrix} \Delta\varepsilon \\ \Delta T \end{bmatrix} \tag{4}$$

where $C^{\varepsilon}_{B\nu}$ and $C^{T}_{B\nu}$ are the coefficients for the Brillouin frequency shift due to strain and temperature while C^{ε}_{BI} and C^{T}_{BI} are the coefficients for the Brillouin anti-Stokes intensity change with strain and temperature respectively. The inverse of equation (4) yields:

$$\begin{bmatrix} \Delta\varepsilon \\ \Delta T \end{bmatrix} = \frac{1}{\left| C^{\varepsilon}_{B\nu} C^{T}_{BI} - C^{\varepsilon}_{BI} C^{T}_{B\nu} \right|} \times \begin{bmatrix} C^{T}_{BI} & -C^{T}_{BI} \\ -C^{\varepsilon}_{BI} & C^{\varepsilon}_{B\nu} \end{bmatrix} \begin{bmatrix} \Delta\nu_B \\ \Delta I_{B_{A.S}} \end{bmatrix} \tag{5}$$

The corresponding error in the temperature-compensated strain measurement is given by equation 6 [1]

$$\left|\delta\varepsilon\right| = \frac{\left|C^{T}_{BI}\right|\left|\delta\nu_B\right| + \left|C^{T}_{B\nu}\right|\left|\delta I_{B_{A.S}}\right|}{\left|C^{\varepsilon}_{B\nu} C^{T}_{BI} - C^{\varepsilon}_{BI} C^{T}_{B\nu}\right|} \tag{6}$$

Where $\delta\nu_B$ and $\delta I_{B_{A.S}}$ are the RMS errors in the Brillouin frequency shift and Brillouin anti-Stokes intensity change measurements.

4.3 Experimental setup and procedure

4.3.1. Experimental setup

The experimental setup for the short range distributed strain measurement with temperature compensation is shown in figure 1(a). The detailed layout of the sensing fibre is depicted in figure 1(b).

The details of the scheme presented in figure 1(a) can be best understood by individually examining the experimental layout of the two techniques i.e., B-OTDR and BOCDA that have been combined in order to demonstrate temperature compensation during of spatial resolution distributed strain measurements.

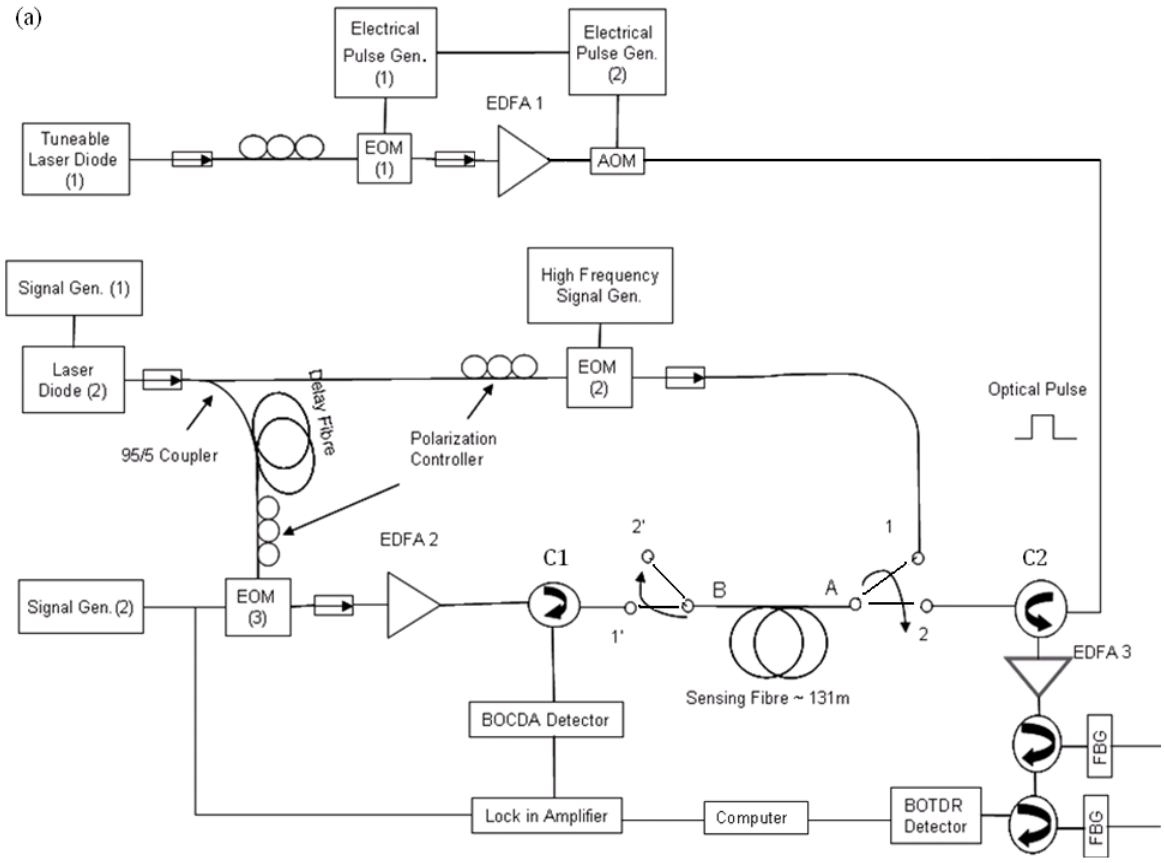

Figure 1a. Proposed scheme for the temperature-compensated distributed strain sensor system

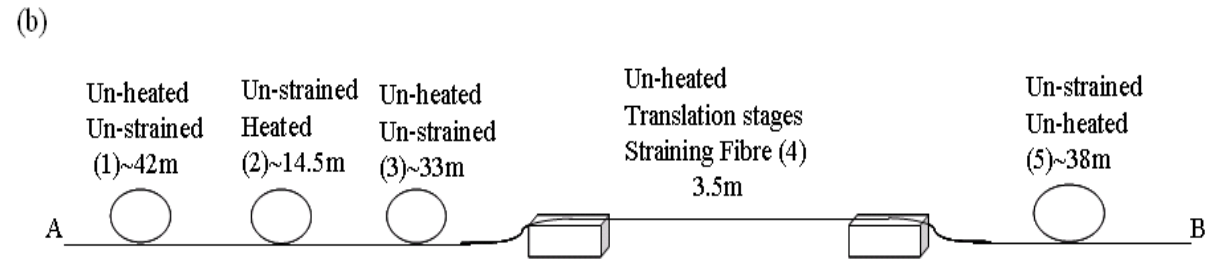

Figure 1b. Detailed layout of the 131 m sensing fibre

The R-OTDR set up was modified in order to meet the requirements for the B-OTDR setup. These changes comprised:

1) Replacing the distributed feedback laser diode operating at 1550nm by a tuneable laser (1) operating at 1533.9nm (linewidth ~ 100kHz). Use of the tuneable laser allowed for the aligning of the narrow linewidth (~35MHz) Brillouin signal with the fibre Bragg gratings used during the filtering of the Brillouin backscattered signal.

2) Removing the two stages of pulse amplification and ASE cleaning using the fibre Bragg gratings. The two stages of pulse amplification were used in the case of R-OTDR for high peak power pulses. However in the case of B-OTDR much lower peak power was required, i.e., 1W – 2W, which was achieved with a single amplification stage sandwiched between the EOM and AOM, as shown in figure 1(a).

3) Adding a 30dB erbium amplifier stage for the amplification of backscattered signal together with a cascaded tuneable fibre Bragg grating arrangement initially centred at 1533.8nm with a 3dB bandwidth of 3.5GHz and side band suppression in excess of 30dB. The Brillouin backscattered signal overlapped with the erbium gain bandwidth and hence the erbium amplifier was used to increase the signal level. Cascaded fibre Bragg gratings were used in order to reduce the ASE noise and to ensure that whilst filtering Brillouin the

Rayleigh backscattered signal is suppressed 30dB from each grating, ensuring negligible contamination of the Brillouin signal.

4) Removing the 350MHz amplifier from the previous electronic detection system and replacing the 300MHz oscilloscope by a 3GHz oscilloscope. The bias voltage of the APD was adjusted to a nominal bandwidth of 650MHz, with a gain of 30,000V/W. The 650MHz APD was considered capable of spatially resolving a step change in temperature with a spatial resolution below 10cms.

5) Reducing the pulse widths to 500ps – 600ps but produced at the same repetition rate of 10kHz. In order to spatially probe the temperature step with under 10cms spatial resolution capability the optical pulses had to be reduced accordingly.

Equations 1 and 2 in chapter 3 showed that increase in frequency variation together with increased sinusoidal sweep rates result in enhancing the spatial resolution probing capability of the BOCDA technique. This lead to minor changes in the BOCDA set up:

1) Increased frequency variation (f) of 8.8GHz from previously used value of 7.7GHz.

2) Increased sinusoidal sweep rates (f_m) of 1.07252MHz – 1.07330MHz, corresponding to scanning of correlation peak from section 2 to section 3, and 1.10922MHz – 1.11000MHz (frequency step of 0.03kHz) enabling scanning of the correlation peak from section 3 to section 4.

Data from the frequency based Brillouin optical correlation domain analysis experiments and the intensity based anti-Stokes Brillouin optical time domain reflectometry experiments was collected and analysed by the personal computer.

Figure 1(b) shows the same sensing fibre with the same set up as used previously, with some minor changes to the layout. These changes comprised:

1) Removing 4m of fibre from the previously used 42m of section (5), thereby reducing its length to 38m, and the total sensing length to 131m. With 135m of sensing length, increased sinusoidal sweep rates as mentioned above resulted in more than one correlation peak within the sensing length. So in order to limit to a single correlation despite increased sweep rates the sensing length had to be reduced by 4m.

2) Increasing the strain on section 4 of sensing fibre from the previously used value of 571.4με to 1044.4με. In the previous chapter the shift in the Brillouin frequency observed from the heated and strained regions during the BOCDA experiments was nearly similar. For safety reasons the temperature of the heated section could not be raised any higher but the strain could easily be increased. Hence the strain value was chosen to be almost twice the previously used value in order to impose dissimilar impact of strain and temperature on the Brillouin frequency shift.

Table 1 summarizes the details of each section of the sensing fibre.

Table 1:

Sections	1	2	3	4	5
Length (m)	42	14.5	33	3.5	38
Strained	No	No	No	Yes	No
Heated	No	Yes	No	No	No

Table 1. Detail of five sections of the 131m sensing fibre.

4.3.2. Experimental procedure

The procedure followed for both BOCDA and B-OTDR experiments is similar to that reported previously. But for a particular temperature, each B-OTDR trace comprised 16,000 points averaged 65536 times on the 3GHz oscilloscope. 10 such traces were stored onto the computer and subsequently averaged. This process took a little over a minute.

4.4 Results

4.4.1 Brillouin Optical Correlation Domain Analysis of the heated section

Figures 2a, 2b, 2c show the Brillouin frequency results extracted from the heated section using the Brillouin optical correlation domain analysis technique.

Figure 2a, shows the plot of the Brillouin gain distribution for the fibre kept at room temperature at 25°C in section 1 and the fibre heated to 52°C in section 2.

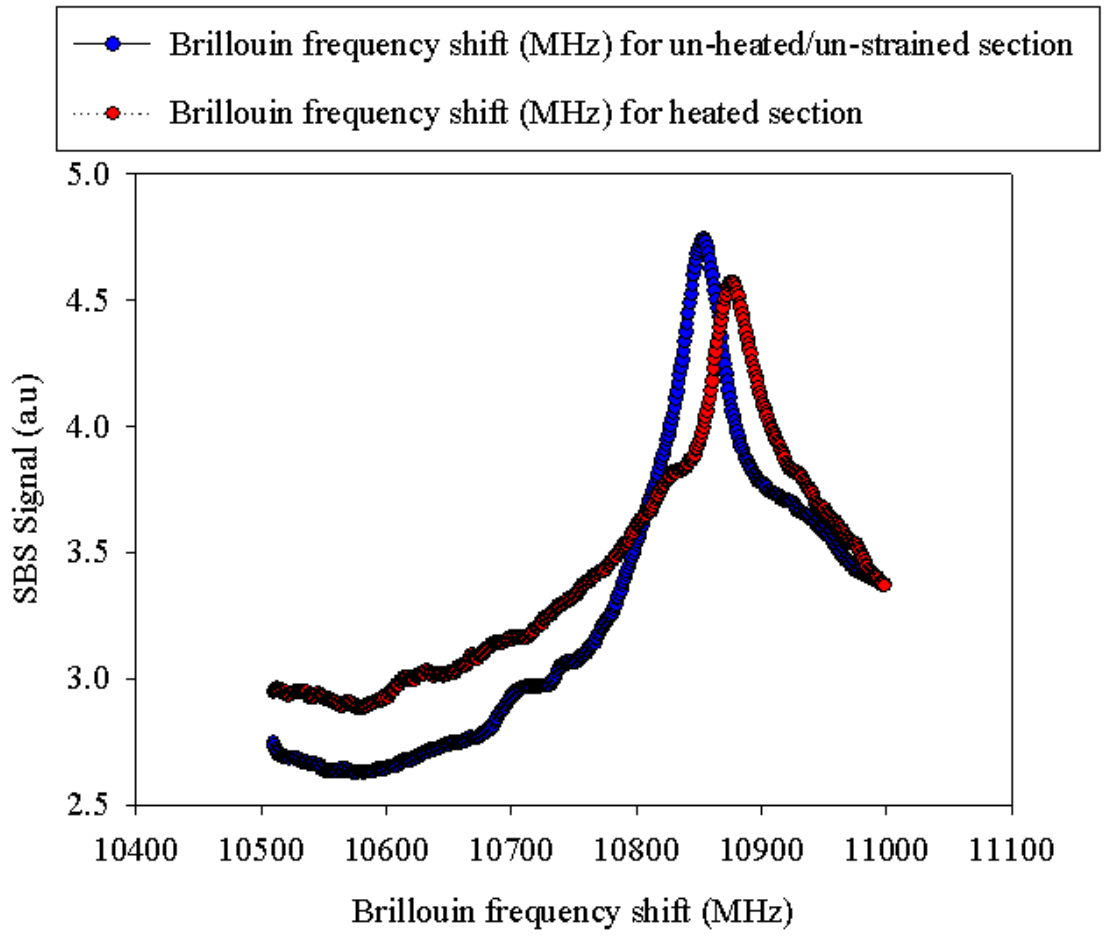

Figure 2a. The Brillouin peaks corresponding to the fibre kept at 25°C and heated to 52°C

The plot in figure 2b shows the shift in the peak Brillouin frequency, arising as a consequence of moving the correlation peak from section 1 to section 2.

The change in the Brillouin frequency shift was measured to be 28MHz, which corresponded to a coefficient for the change of the Brillouin shift with temperature of 1.04MHz/°C. A 4MHz (~ 4°C) drift in the heated section was attributed to a temperature gradient present on the hot plate.

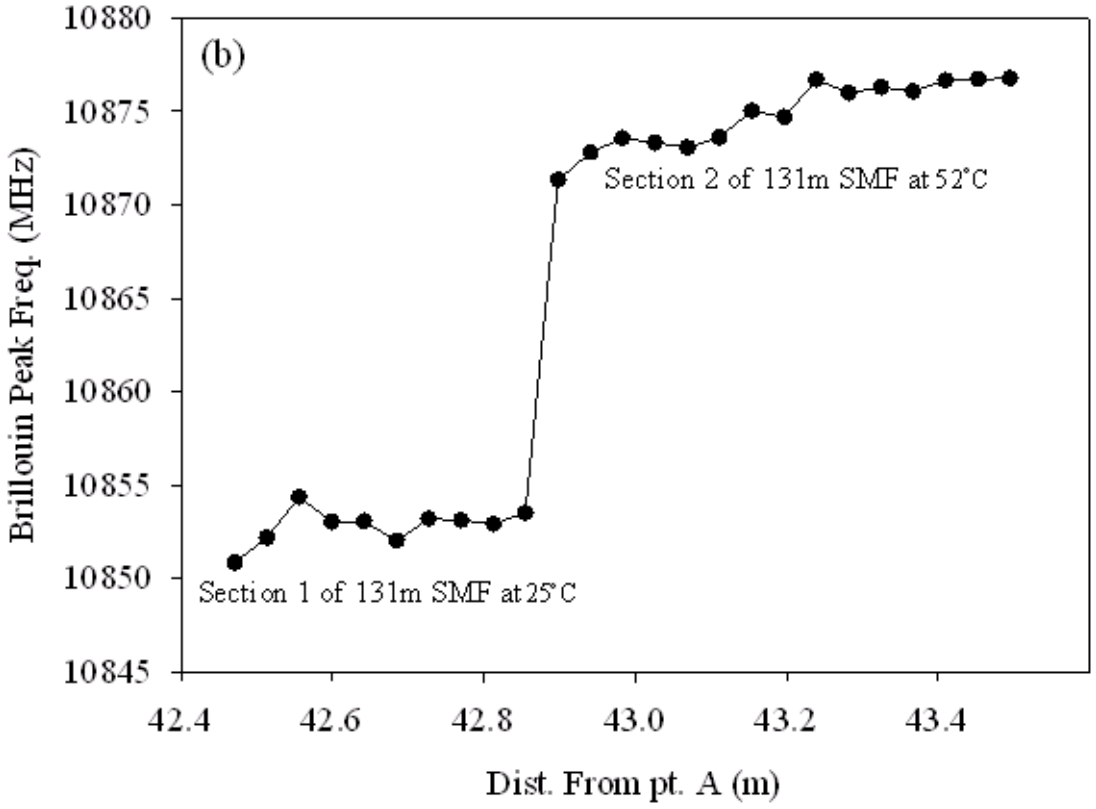

Figure 2b. Step change in the Brillouin peak frequency when scanning the correlation peak from the unheated to heated region.

Plots in figure 2 c show the Brillouin gain distribution across sections 1 and 2, at peak Brillouin frequency of the unheated (10853MHz) and heated (10881MHz) regions. A spatial resolution of 10cm was calculated with a 10/90% step response from figure 2(c).

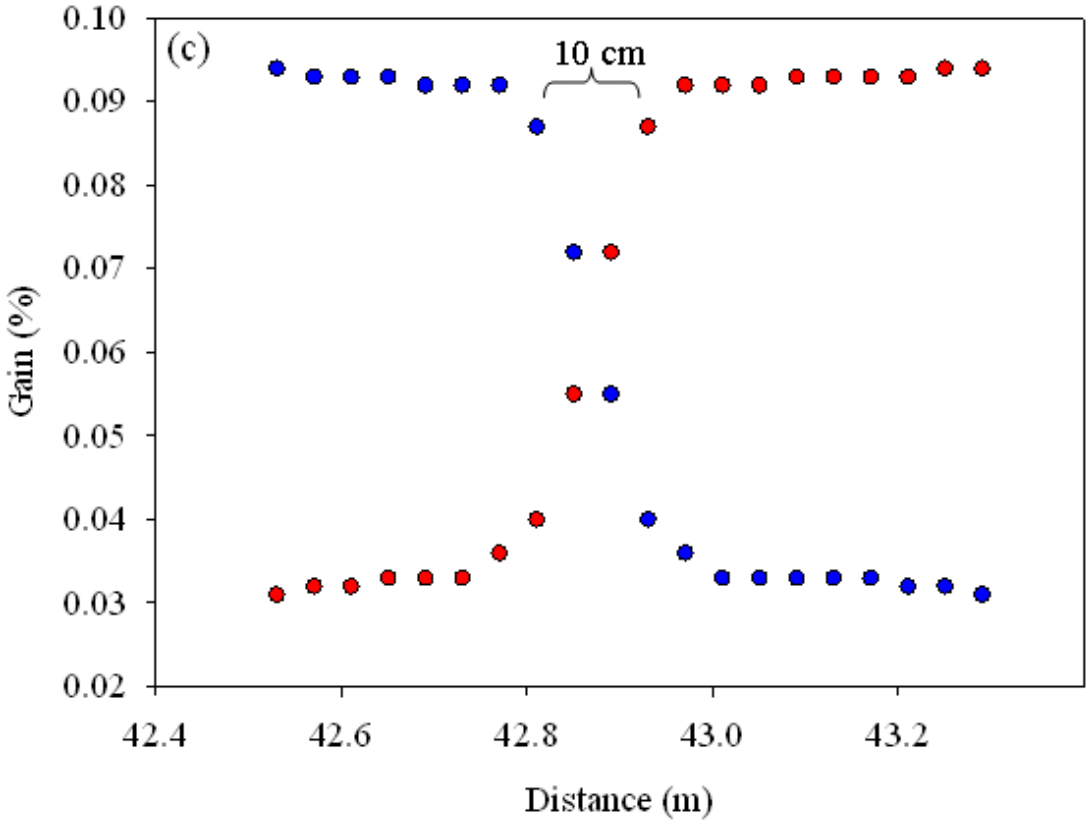

Figure 2c. The Brillouin gain distribution at peak Brillouin frequency of the un-heated (10853MHz – blue trace) and heated (10881MHz - red trace) regions

4.4.2 Brillouin Optical Correlation Domain Analysis of the strained section

Figures 3a, 3b, 3c show the Brillouin frequency results extracted from the strained section using the Brillouin optical correlation domain analysis technique.

Figure 3a, shows the plot of the Brillouin gain distribution for the loosely coiled fibre kept at room temperature at 25°C in section 3 and the fibre strained to 1044.4$\mu\varepsilon$ in section 4.

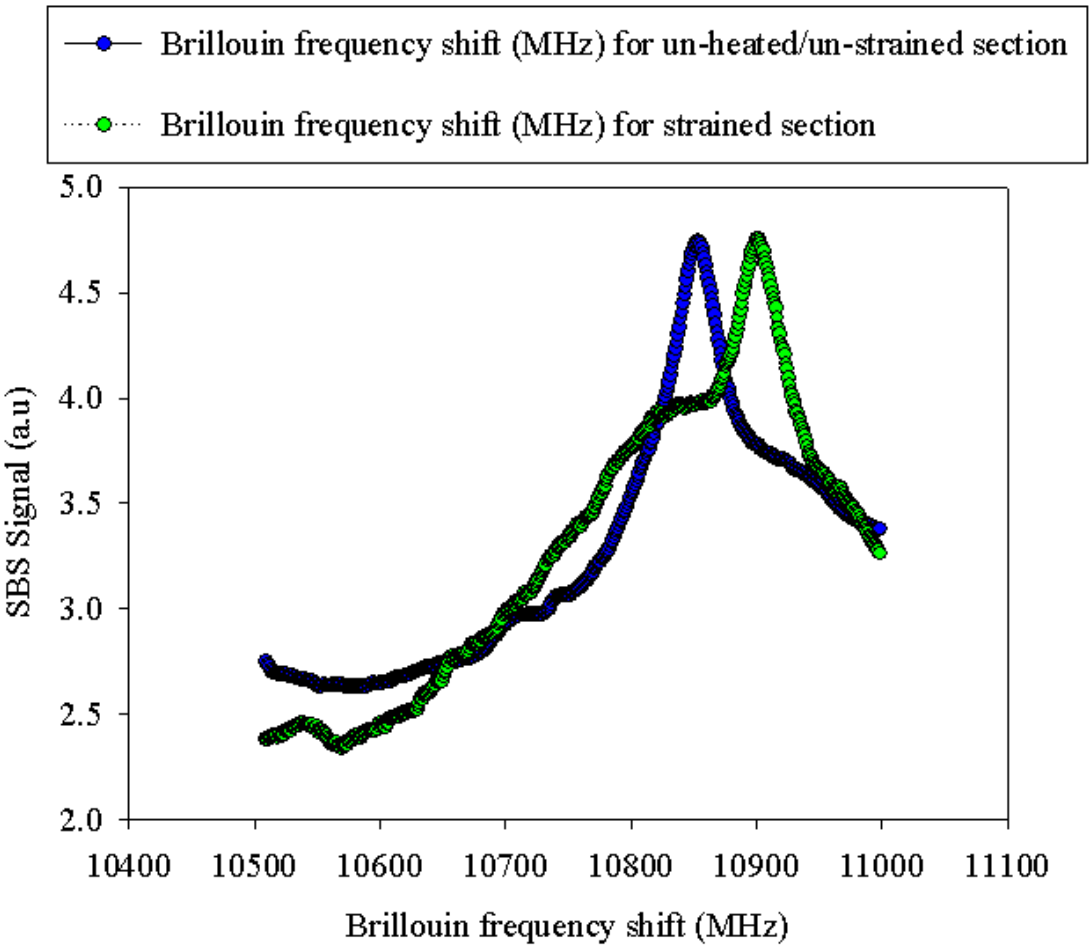

Figure 3a. The Brillouin peaks corresponding to the unstrained fibre and strained fibre sections.

The plot in figure 3b shows the shift in the peak Brillouin frequency, arising as a consequence of moving the correlation peak from section 3 to section 4. The change in the Brillouin peak frequency of the fibre strained to 1044.4$\mu\varepsilon$ was measured to be 47MHz, and this corresponded to a coefficient of the Brillouin frequency shift of 4.5MHz/100$\mu\varepsilon$.

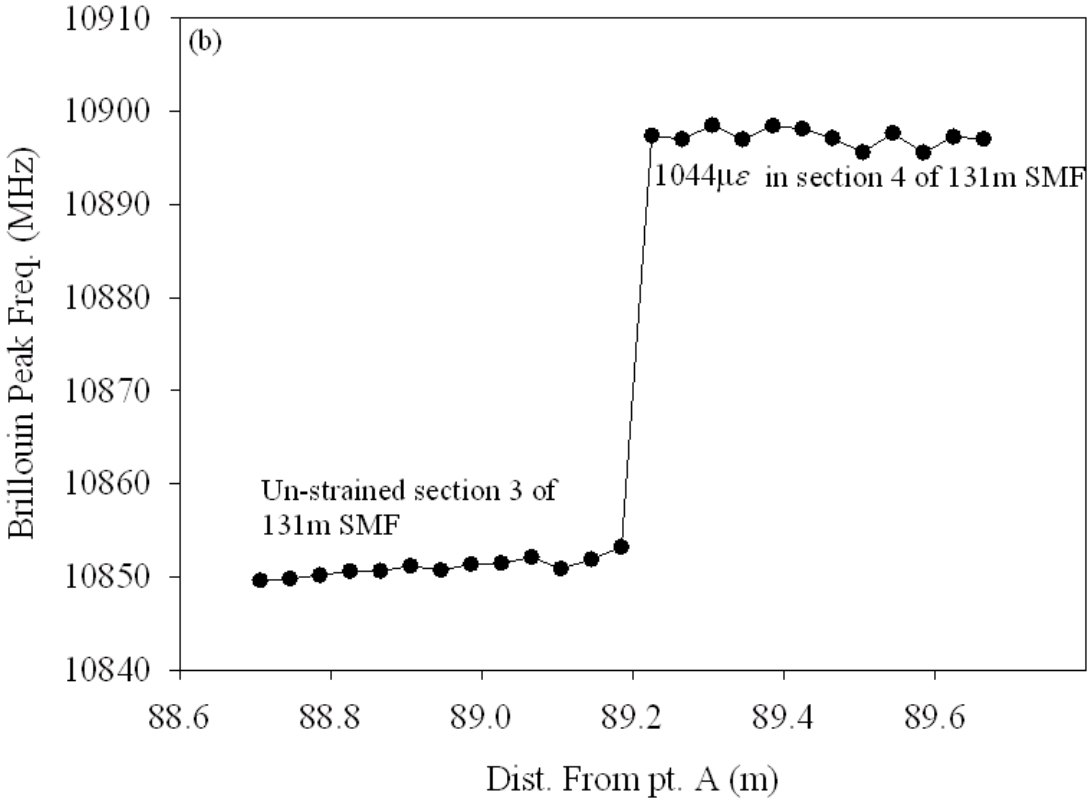

Figure 3b. Step change in the Brillouin peak frequency when scanning the correlation peak from the unstrained to strained region.

The RMS frequency error $\delta\nu_B$ was measured to be 1.7MHz in section 3 and 4. This is the variation in Brillouin peak frequency along the sensing fibre for the unheated-unstrained and unheated-strained regions. However the error in the Lorentzian fit to the Brillouin gain spectra of the two regions was 0.1MHz.

The plots in figure 3c show the Brillouin gain distribution across sections 3 and 4, at peak Brillouin frequency of the unheated-unstrained (10853MHz) and strained (10900MHz) regions. A spatial resolution of 9cm was calculated using a 10/90% step response from figure 3c.

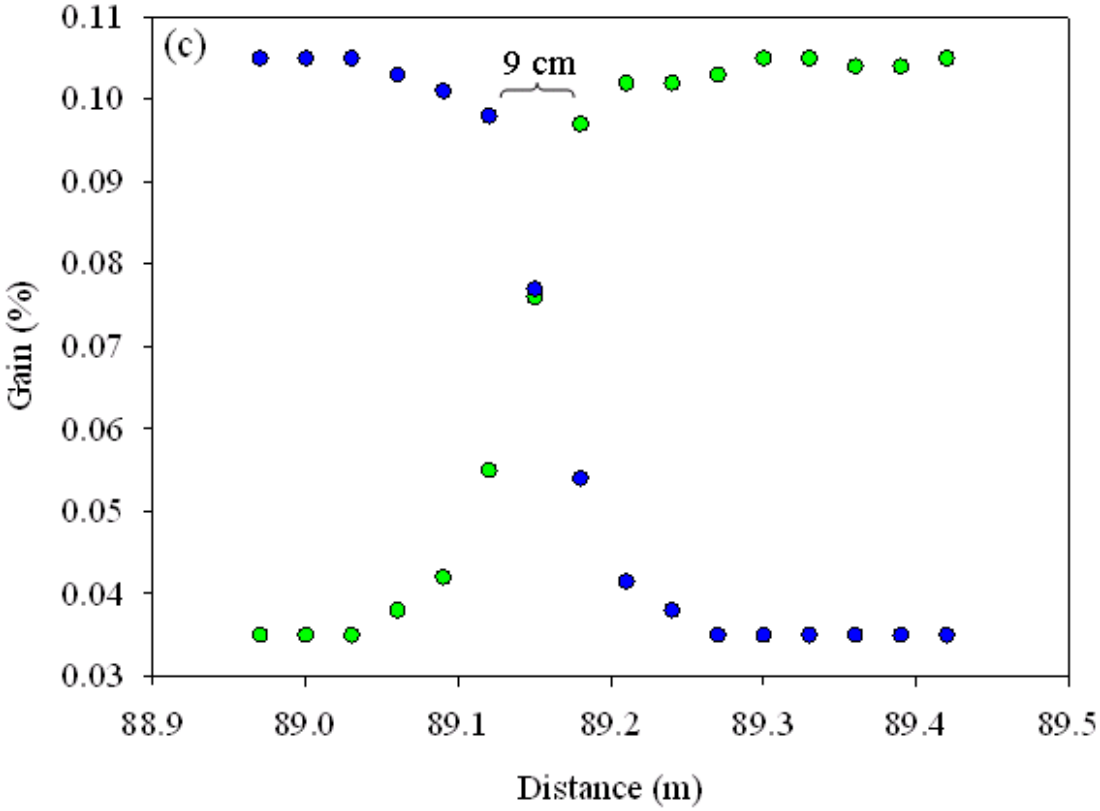

Figure 3c. The Brillouin gain distribution at peak Brillouin frequency of the un-heated and un-strained (10853MHz – blue trace) and strained (10900MHz - green trace) regions

4.4.3 Brillouin Optical Time Domain Reflectometry of the heated section

Figure 4(a) shows the spatially resolved backscattered Brillouin anti-Stokes signal generated by 2W peak power pulses with 0.5ns – 0.6ns pulse widths in the 131m sensing fibre. The black plot was obtained with fibre kept at 23.8°C, and the red trace was obtained when fibre in section 2 was heated to 52°C.

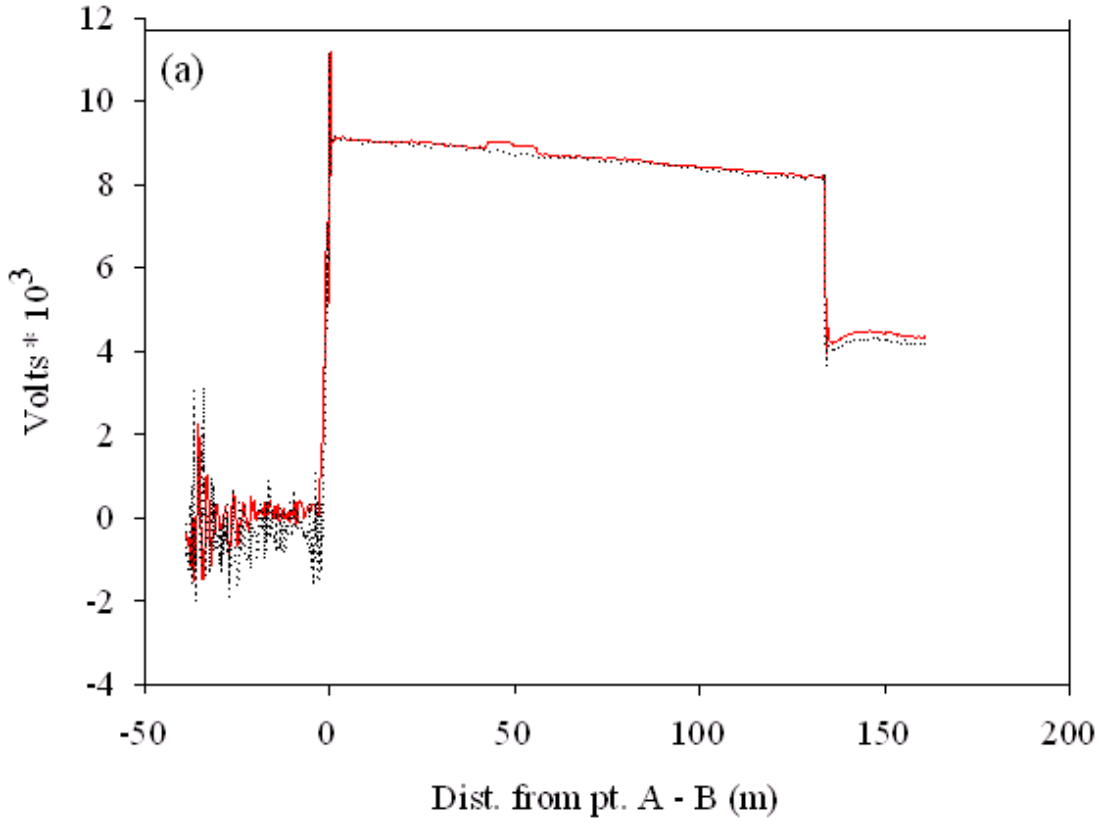

Figure 4a. Black plot - B-OTDR trace of the fibre in section 2 kept at 23.8°C, Red plot - B-OTDR trace of the fibre in section 2 heated to 52°C

The slope in figure 4a is attributed to the ac coupling of the APD. No satisfactory explanation has yet been found for the difference in the offsets.

Figure 4b shows the backscattered traces for the section 2 of the fibre heated to 52.0°C (indicated by red plot), 62.0°C (indicated by green plot) and 71.5°C (represented by blue plot), normalized by the trace obtained at room temperature of 23.8°C. The RMS intensity noise measured on the trace with 14.5m fibre heated to 52°C (red plot) was 0.34%, which yielded a temperature resolution of 0.95°C.

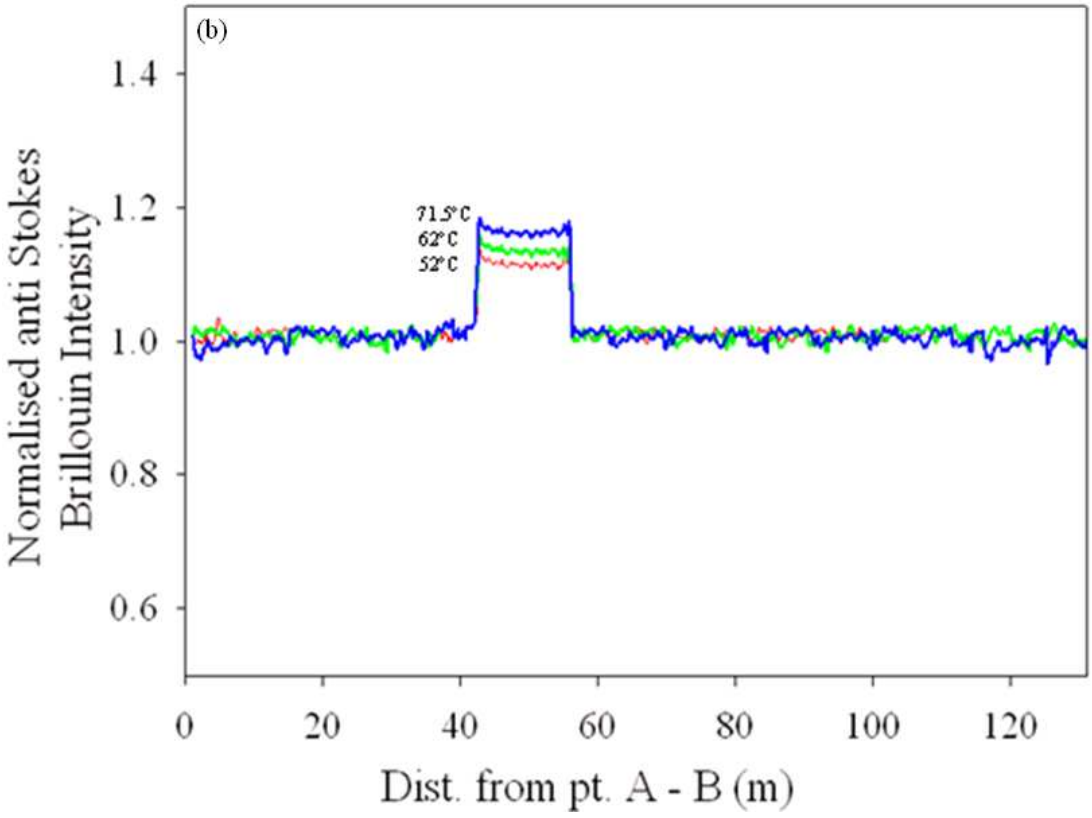

Figure 4b. The normalized B-OTDR plots of the fibre in section 2 heated to different temperatures.

The intensity change for the five different temperatures is plotted in figure 5. The data points are fitted with a straight line with the value of R^2 =0.99.

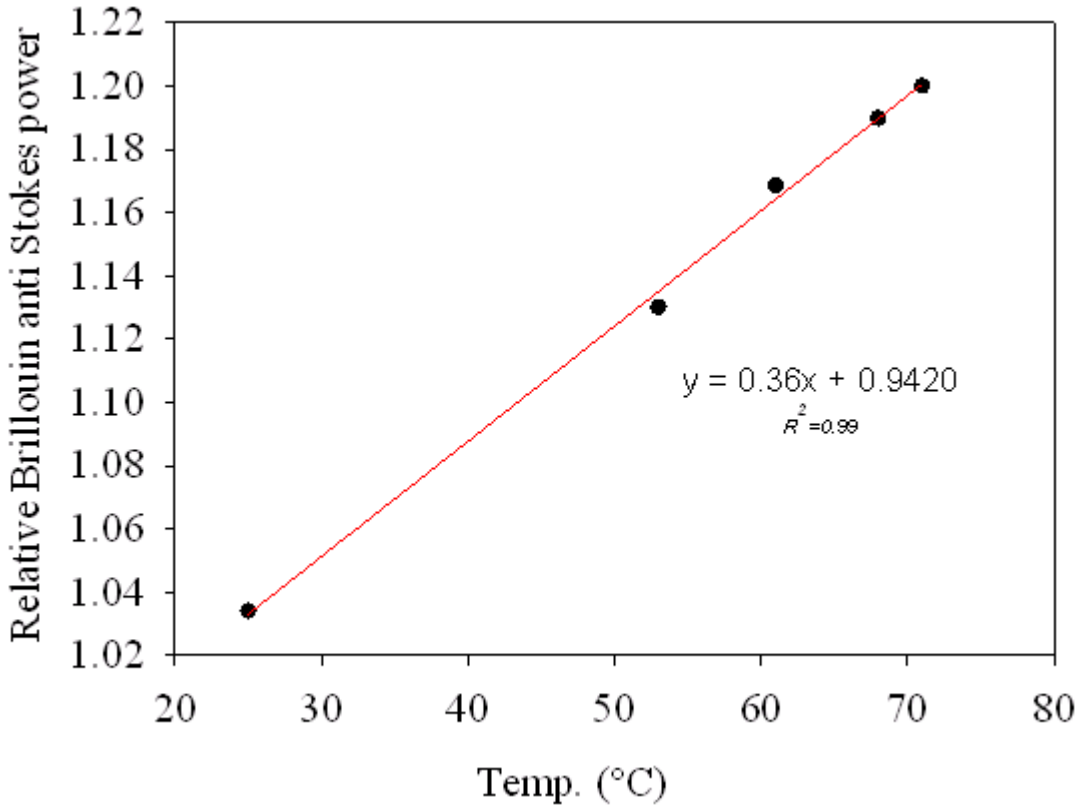

Figure 5. The percentage intensity change of the Brillouin anti-Stokes signal versus temperature

The slope corresponding to the coefficient of intensity change with temperature extracted from the equation of a linear fit to the plot in figure 5 was 0.36%/°C, which is in agreement with the previously reported value [1].

Figure 6 shows the normalized plot of anti-Stokes Brillouin intensity as a function of sensing length corresponding to the transition region between the un-heated section 1 and heated section 2 of the 131m sensing fibre.

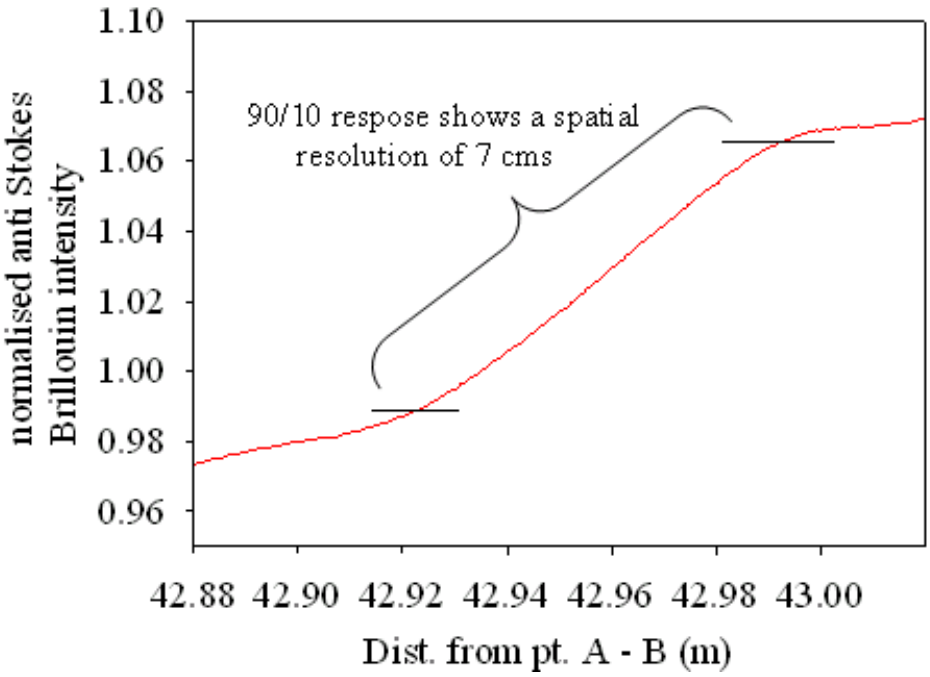

Figure 6. Normalized 10/90% step response for the transition from the un-heated (section 1) to heated (section 2) of the fibre sections

A spatial resolution of 7cm was calculated using the 10/90% step response corresponding to a temperature change between the fibre of sections 1 and 2 respectively.

4.5 Discussion

The slope and difference in offsets seen before and after the sensing fibre in figure 4a (B-OTDR) differs from that of figure 3a (R-OTDR) of the previous chapter. Due to the absence of pump depletion in the case of B-OTDR, there is only a 12% drop in the slope of figure 4a (B-OTDR), as compared to the 22% in the case of figure 3a (R-OTDR). The 12% drop in the slope of figure 4a (B-OTDR) is explained due to the lowest detectable frequency of 15kHz on the ac coupled APD detector. Section 3.5 of the previous chapter discusses this aspect in detail. The narrow linewidth fibre Bragg gratings were used to reduce the ASE-ASE beat noise generated due to the optical

amplifier used for amplifying the backscattered signal. The difference in the offsets seen before and after the sensing fibre is rather unusual and is presently unexplained.

Distributed temperature and strain measurements with a spatial resolution of 10 cm and 9cm were obtained using the Brillouin frequency based BOCDA technique. These experimentally found values of spatial resolution for the heated and strained regions agreed with the theoretically calculated values of 10.1cm for the heated section and 9.7cm for the strain section using equation 2. The parameters used in the calculation comprised the frequency variation f ~ 8.8GHz and modulation frequency f_m ~ 1.07252MHz – 1.07330MHz and 1.10922MHz – 1.11000MHz, corresponding to sections 1 – 2 and section 3 – 4 respectively. The value of the frequency variation f was estimated using the 21GHz Mach Zehnder as described in chapter 3.

The error in locating the peak Brillouin frequency during a Lorentzian fit in the BOCDA technique was found to be 0.1MHz. However the variation in Brillouin frequency along the sensing fibre was estimated to be 1.7MHz. In the absence of temperature uncertainty the error of 0.1MHz in identifying the peak Brillouin frequency corresponded to a strain resolution of 2.2με. Moreover, the reproducibility of the BOCDA technique is demonstrated by figure 7, where the variation in the peak Brillouin frequency over the time period between building and testing of the two temperature compensated distributed strain sensing schemes is computed by taking the difference in the peak Brillouin frequencies for the unheated region (section 1) and heated region (section 2) between plots in figure 3(b) of chapter 3 and Figure 2(b) of chapter 4.

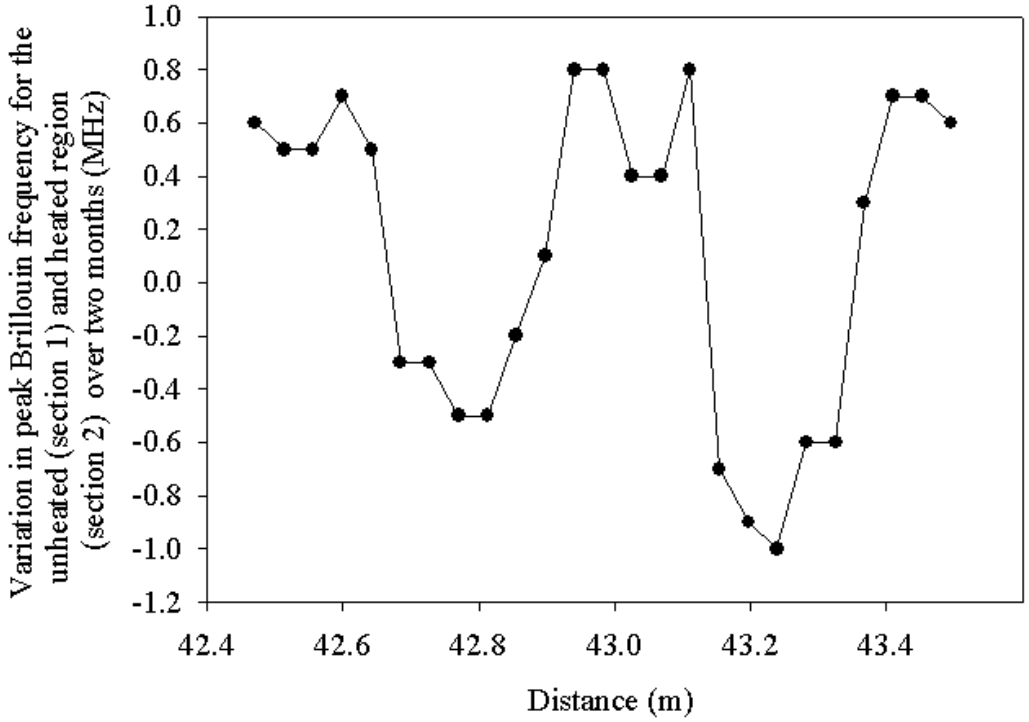

Figure 7. Shows the variation in the peak Brillouin frequency for the section 1 and 2 of the sensing fibre over the two sensing schemes

B-OTDR yielded a spatial resolution of 7cm and temperature resolution of 0.95°C over the 131m length of sensing fibre. Using the combined experimental errors of the Brillouin frequency measurement, 0.1MHz and Brillouin intensity measurement, 0.34%, together with the Brillouin coefficients of frequency and intensity, i.e., $C_{B\nu}^{\varepsilon} = 0.45MHz/^{\circ}C$; $C_{BI}^{T} = 0.36\%/^{\circ}C$; $C_{BI}^{\varepsilon} = -9\times10^{-4}\%/\mu\varepsilon$; $C_{B\nu}^{T} = 1MHz/^{\circ}C$ in equation 6, we ascertain a temperature-compensated strain resolution of 22με, as shown below.

$$\delta\varepsilon_{Exp.} = \frac{\left(0.36\%/°C\times\ 0.1MHz\right)+\left(1MHz/°C\times 0.34\%\right)}{\left[\left(0.045MHz/\mu\varepsilon\times 0.36\%/°C\right)-\left(-9\times10^{-4}\%/\mu\varepsilon\times 1MHz/°C\right)\right]} = 22\mu\varepsilon$$

4.6 Conclusions

The Brillouin intensity measurements together with the Brillouin frequency based BOCDA have provided temperature compensated distributed strain measurements with an improved spatial resolution of 7cms compared to the 24cms demonstrated in the previous chapter. The temperature compensated strain resolution also improved from 46με to 22με. The urge to improve upon the spatial resolution probing capability together with reduced temperature error motivated this investigation of the B-OTDR technique which provides a stronger backscattered signal.

The following chapter theoretically analyses the performance of the two techniques under certain fixed sensor parameters of sensing length, spatial resolution, temperature error, detection time etc.

4.7 References

[1] S. M. Maughan, H. H. Kee, and T. P. Newson, "Simultaneous distributed fibre temperature and strain sensor using microwave coherent detection of spontaneous Brillouin backscatter," *Measurement Science and Technology*, 12, p. 834–842 (2001)

[2] K. De Souza, P. C. Wait, and T. P. Newson, "Characterisation of the strain dependence of the Landau Placzek ratio for distributed sensing," *Electronics Letters*, 33(7), p. 615–616 (1997)

[3] K. Y. Song, Z. He, and K. Hotate, "Distributed strain measurement with millimeter-order spatial resolution based on Brillouin optical correlation domain analysis," *Optics Letters*, 31, p. 2526–2528 (2006)

[4] Krishnan R S 1950 Fine structure of the Rayleigh line in amorphous substances *Nature* 165 933–4

[5] Smith J, Brown A, DeMerchant M and Bao X 1999 Simultaneous distributed strain and temperature measurement *Appl. Opt.* **38** 5372–7

[6] Horiguchi T, Kurashima T and Tateda M 1989 Tensile strain dependence of Brillouin frequency shift in silica optical fibres *IEEE Photon. Technol. Lett.* **1** 107–8

[7] Culverhouse D, Farahi F, Pannell C N and Jackson D A 1989 Potential of stimulated Brillouin scattering as a sensing mechanism for distributed temperature sensors *Electron.Lett.* **25** 913–15

[8] De Souza K, Wait P C and Newson T P 1997 Characterisation of strain dependence of the Landau–Placzek ratio for distributed sensing *Electron. Lett.* **33** 615–16

Chapter 5

5. Theoretical performance comparison between R-OTDR and B-OTDR techniques

5.1 Introduction

Chapters 3 and 4 have independently highlighted the performance of the combinatory techniques of Brillouin frequency based BOCDA with either Raman intensity based R-OTDR or Brillouin intensity based B-OTDR. An improved spatial resolution was experimentally proven for the B-OTDR. However, apart from requiring different optical filters, a number of improvements were also made to the detection of the backscattered signals. This raised the question as to whether B-OTDR+BOCDA, was fundamentally a better technique compared to R-OTDR+BOCDA, or the improved results were simply a consequence of improvements to the detection system. To resolve this issue, this chapter examines the theoretical performance of the two techniques, i.e., R-OTDR and B-OTDR.

5.2 Analysis

In order to judge the performance of the two techniques, the signal to noise ratio of each is calculated for a 1ns pulse at a wavelength of 1.55µm launched to probe a sensing length of 100m, with 2^{20} times averaging of the backscattered signal. A sensing fibre with an effective area of 80µm^2 and a zero dispersion wavelength of 1.55µm is considered. The electronic detection system comprises a 600MHz APD

(noise floor 1.3 $pW/\sqrt{Hz}$, gain 30,000V/W) together with a 300MHz oscilloscope, yielding a $NEV_{\text{det.}}$ of $1.3\times10^{-12}\times\sqrt{300\times10^{6}}\times30{,}000=6.75\times10^{-4}V$.

5.2.1 R-OTDR

In order to theoretically estimate the signal to noise ratios during the R-OTDR measurements, the maximum pulse peak powers that can be used without setting up non linear effects, which may contaminate the R-OTDR measurements, have to be calculated. Since the operating wavelength is the same as the zero dispersion wavelength of the sensing fibre, group velocity dispersion (GVD) effects and Rayleigh broadening due to modulation instability (MI) can be neglected [1]. Acoustic phonon lifetime for spontaneous Brillouin scattering is typically of the order of 8ns [1]. Hence, use of pulses smaller than 8ns limits the growth of the acoustic phonon population necessary to seed the SBS process [1]. So for 1ns pulse widths SBS can also be neglected.

Due to the broadband spectral profile of the Raman signal, the R-OTDR measurements can also be performed using spectrally broadband sources. Although self phase modulation (SPM) may lead to spectral broadening of the backscattered Rayleigh signal, a 100nm separation between the Rayleigh and the Raman signals not only prevents any contamination from the Rayleigh but also facilitates optical filtering of the Raman signal. This however is true only as long as SPM is not accompanied with other non linear processes such as stimulates Raman scattering (SRS) or four wave mixing (FWM), where the broadened spectrum can extend over 100 THz or more, leading to a supercontinuum [1]. In order to avoid such a situation and also to avoid excessive pump depletion, it is necessary to operate with peak powers below the SRS threshold. Using equation 1 [1], the threshold pulse peak power for SRS, over 100m of sensing length is calculated to be 183W. This value of the SRS defines the peak pulse power beyond which significant power transfer from the pump to the Raman Stokes begins to take place.

$$P_{Th.}^{SRS} = \frac{16 \times A_{eff}}{L_{eff} \times g_R} \qquad (1)$$

Where, $g_R = 7 \times 10^{-14}\, m/W$ is the Raman gain coefficient value for the pump wavelength at 1.55µm [1], $A_{eff} = 80 \mu m^2$ is the effective area of the sensing fibre and L_{eff} is the effective sensing length, which in this case is 100m.

The strength of the spontaneous Raman backscattered signal is known to be 30dB weaker compared to the Rayleigh backscattered signal [2]. Using this knowledge, equation 2 [2] can be used to calculate the Raman backscattered signal power for launched pulse peak powers of 183W over a sensing length of 100m.

$$P_{Raman} = \frac{P_{Rayleigh}}{1000} = \frac{\frac{1}{2} \times P_{pk.} S \gamma_R W_p V_g \exp(-2\alpha L)}{1000} = 987\ pW \qquad (2)$$

Where $S = \frac{(NA)^2}{4n}$ is the capture fraction, the Rayleigh scattering coefficient (γ_R) and the transmission (α) loss in the fibre for 1.55µm are both equal to $4.6 \times 10^{-5} m^{-1}$, $W_p = 1 \times 10^{-9} s$ is the pulse width, $V_g = 2 \times 10^8 m/s$ is the velocity of light in fibre and L is the sensing length of 100m. The Raman backscattered signal level for a heated section of the fibre experiencing a temperature difference of 50°C, increases proportionally to the anti-Stokes Raman signal sensitivity at that temperature, i.e., 0.63%/°C, calculated using equation 16 from section 3.5. Hence the signal level for the heated section increases to 1.297nW resulting in a signal equivalent voltage of $3.89 \times 10^{-5} V$. With noise equivalent voltage $\left(NEV_{\text{det.}}\right)$ of

$6.75\times10^{-4}V$, signal to noise ratio of 0.057 is achieved in the absence of any averaging. With 2^{20} averages, the signal to noise ratio improves to 59 resulting in a temperature resolution of 2.7°C.

5.2.2 B-OTDR

The B-OTDR technique in this discussion exploits the direct detection of the anti-Stokes Brillouin backscattered signal. This is achieved by reflecting off the anti-Stokes Brillouin backscattered signal from a fibre Bragg grating. The grating is assumed to be tuneable, flat topped, 99.9% reflecting, has a sharp transition edge and FWHM of 5GHz.

In the case of the B-OTDR measurements, the signal to noise ratio improves with launch of higher peak power pulses. But, it is important to know the maximum pulse peak powers that can be used without setting up non linear effects, resulting in the deterioration of the of the signal to noise ratio.

GVD, MI and SBS effects can be neglected for reasons similar to those discussed in the previous section. However, since the Brillouin and Rayleigh signals are separated by only 11GHz as against the 100nm separation between the Rayleigh and Raman signals, contamination of Brillouin signal due to SPM related broadening of the Rayleigh signal poses a serious problem. The magnitude of the maximum SPM induced Rayleigh broadening at FWHM, represented by $\delta\omega_{\max}$ is given by equation 3 [1], where $\Delta\omega$ is the 1ns unchirped Gaussian pulse with an initial width of 440MHz at FWHM and $\varphi_{\max}$ is the maximum phase shift in the Rayleigh signal.

$$\delta\omega_{\max} = 0.86\times\Delta\omega\times\varphi_{\max} \qquad (3)$$

The maximum phase shift $(\varphi_{\max})$ is related to the maximum pulse peak power $(P_{\max})$, effective length $(L_{eff} = \text{sensing length} = 100\text{m})$ and $\gamma = 1.1/km.W$ as shown in equation 4 [1].

$$\varphi_{\max} = L_{eff}\gamma P_{\max} \tag{4}$$

Using equation 3 the maximum phase shift term is eliminated from equation 4 and the resulting equation is rearranged in order to develop an equation which directly links the maximum pulse peak powers with the maximum magnitude of spectral broadening of the Rayleigh signal due to SPM, as shown in equation 5.

$$P_{\max} = \frac{\delta\omega_{\max}}{0.86 \times \Delta\omega \times L_{eff} \times \gamma} \tag{5}$$

Equation 5 is then used to estimate the maximum peak power that can be launched whilst allowing for at most a 0.33% contamination in the Brillouin signal collected using the FBG. 0.33% of the Brillouin signal contamination due to SPM translates into a temperature accuracy of 1°C as a function of sensing length.

The Brillouin signal is separated by 11GHz from the Rayleigh signal. SPM related broadening of the Rayleigh signal has similar broadening effects on the Brillouin signal too. But since the Rayleigh signal is 60 times stronger than the anti Stokes Brillouin signal, experimentally the grating is positioned so as to minimise the collecting of the Rayleigh signal even if it leads to losing some of the Brillouin signal. In this discussion, the grating is assumed to be positioned such that the edge of the grating sits half way between the Rayleigh and the Brillouin signals.

The Rayleigh signal is represented by a Gaussian function with a FWHM of 0.44GHz (~1ns Gaussian pulse), normalised using the peak value of the function. This Rayleigh signal is numerically broadened under the influence of SPM. The broadened signals are subsequently normalised using the peak value of the un-broadened Rayleigh signal. Broadening of the Rayleigh signal leads to its overlap with the FBG filter. Rayleigh power in this overlapping area is calculated using equation 6.

$$P_{overlap} = \frac{a}{A} \times P_R \tag{6}$$

Where, a is the area under the overlap region and A is the area under the broadened Rayleigh and P_R is the Rayleigh signal power. Equation 7 is used to estimate the percentage which the Rayleigh power corresponding to the overlap region constitutes of the Brillouin power, i.e., $P_{Brillouin} = P_R / 60$. This percentage represents contamination in the Brillouin power due to the Broadened Rayleigh.

$$\%_{\text{Contamination}} = \left(\frac{a}{A} \times 60 \right) \times 100 \tag{7}$$

Using the limit of 0.33% as the tolerable Brillouin signal contamination, the maximum allowable broadening of the Rayleigh signal under the influence of SPM, is simulated as shown in figure 1.

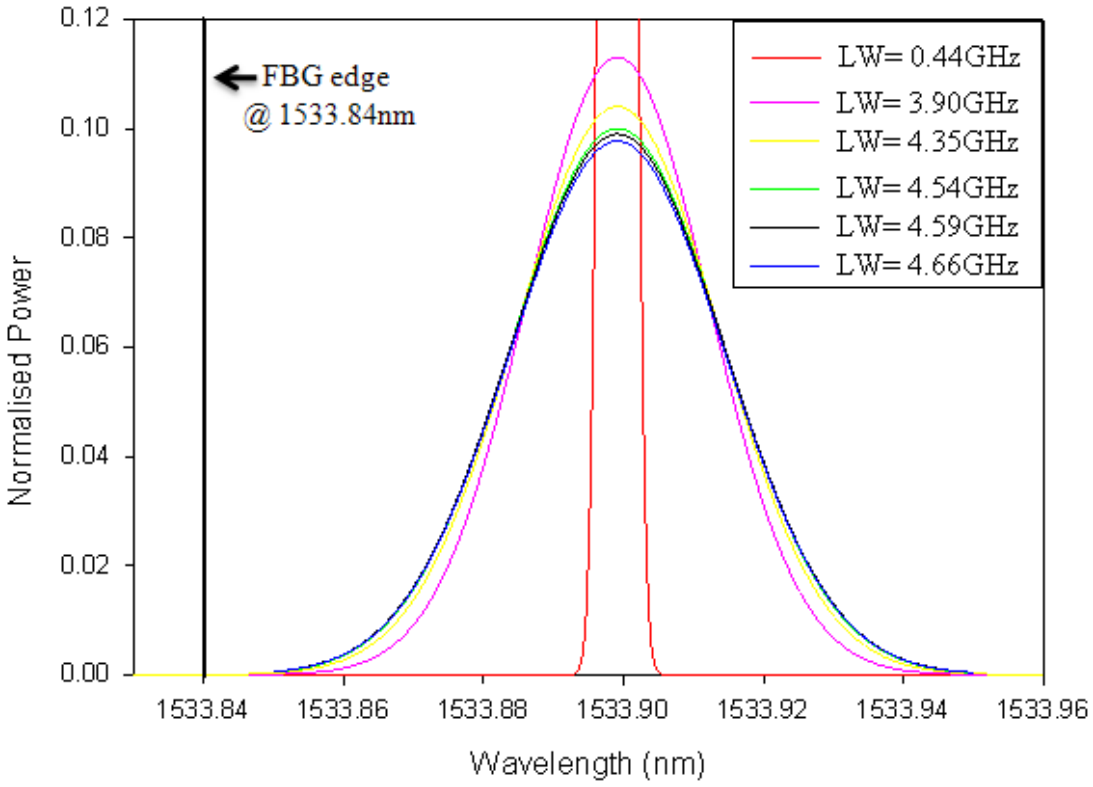

Figure 1. The sharp transition edge of the FBG in black separated by 11GHz of the numerically estimated Gaussian function plots, representing broadening of the Rayleigh signal due to SPM

Corresponding to the plots shown in figure 1, table 1 summarises the percentage contamination of Brillouin signal and the FWHM value of the broadened Rayleigh signal. Equation 12 of chapter 3 is used to convert the spectral width in wavelength corresponding to the broadened Rayleigh signals shown in figure 1, to its equivalent FWHM values in frequency domain shown in table 1.

Peak power (W)	**FWHM values of Rayleigh signal (GHz)**	**Percentage contamination (%)**
….	0.44	0
83.1251	3.90	0.016
93.9362	4.35	0.13
98.5009	4.54	0.28
99.7021	4.59	0.33
101.3838	4.66	0.43

Table 1. Peak pulse power resulting in broadening of the Rayleigh signal, leading to percentage contamination of the Brillouin signal collected by the FBG

Since the FWHM value of a 1ns Gaussian pulse is 0.44GHz, the FWHM value corresponding to signal contamination of 0.33% results in $\delta\omega_{\max} = 4.15GHz$. Using this value of $\delta\omega_{\max}$ in equation 5, the maximum peak power that can be launched to interrogate a sensing length of 100m whilst tolerating a temperature error of 1°C along the sensing length, is calculated to be 99.7W.

The strength of the spontaneous Brillouin anti-Stokes signal is 60 times weaker [2] than the backscattered Rayleigh signal. So equation 8 can be used to calculate the Brillouin anti-Stokes backscattered signal power for launched pulse peak powers of 99.7W over a sensing length of 100m.

$$P_{Brillouin} = \frac{P_{Rayleigh}}{60} = \frac{\frac{1}{2} \times P_{pk.} S \gamma_R W_p V_g \exp(-2\alpha L)}{60} = 8.95nW \qquad (8)$$

Where, all the symbols used in equation 8 have the same meaning as described for equation 2 in section 5.2.1 and the Brillouin power calculated, is for the unheated section of the sensing fibre. The Brillouin backscattered anti-Stokes power for a heated section experiencing a temperature change of 50°C, undergoes an increase by an amount proportional to 0.33%/°C [2], resulting in 10.43nW of signal power or a signal equivalent voltage of $3.13 \times 10^{-4} V$. Signal to noise ratio of 0.46 is achieved for the heated section in the absence of any averaging.

Moreover, due to the narrow linewidth (~35MHz) of the spontaneous Brillouin signal [1, 2] and its spectral overlap with the gain bandwidth of the erbium amplifier, the Brillouin backscattered signal can be optically amplified. Using a 30dB gain optical amplifier introduces two other important sources of noise, i.e., ASE-ASE beat noise and signal-ASE beat noise. These noise sources are considered along with the noise floor of the detector whilst estimating the total noise.

The noise equivalent current for the ASE-ASE best noise and signal-ASE beat noise terms is given by equations 9 and 10 [3]. Table 2 shows the value of the various quantities used in equations 9 and 10, together with the noise equivalent current values corresponding to the ASE-ASE and signal-ASE beat noise sources.

$$NEI_{ASE-ASE} = \sqrt{4R^2 S_{ASE}^2 B_{opt.} B_{elec.}} \qquad (9)$$

$$NEI_{sig.-ASE} = \sqrt{4R^2 GP_s S_{ASE} B_{elec.}} \qquad (10)$$

Quantity	**Value**
Optical ASE power per unit bandwidth $\left(S_{ASE}\right)$	$\frac{10^{-3} W}{3.7\times10^{12} Hz}$
Optical signal power for the heated section $\left(P_S\right)$	$5.86\times10^{-9} W$
Optical gain 30dB (G)	1000
Responsivity (R)	$1 A/W$
Optical bandwidth $\left(B_{opt.}\right)$	$3.5 GHz$
Electrical bandwidth $\left(B_{elec.}\right)$	$0.3 GHz$
Noise equivalent current for the ASE-ASE beat noise $\left(NEI_{ASE-ASE}\right)$	$5.5\times10^{-7} A$
Noise equivalent current for the signal-ASE beat noise $\left(NEI_{sig.-ASE}\right)$	$1.4\times10^{-6} A$

Table2. Various quantities and their respective values used in equations 9 and 10

With the detector responsivity of A/W, the detector gain can also be represented as 30,000V/A. Using this value of detector gain in equations 11 and 12, the noise equivalent voltages of 0.016V and 0.04V are calculated for the ASE-ASE and signal-ASE beat noise terms respectively. Equation 13 is then used to calculate the total noise equivalent voltage $\left(NEV_{total}\right)$ of 0.04V.

$$NEV_{ASE-ASE} = NEI_{ASE-ASE} \times 30000V/A \quad (11)$$

$$NEV_{sig.-ASE} = NEI_{sig.-ASE} \times 30000V/A \quad (12)$$

$$NEV_{total} = \sqrt{\left(NEV_{sig.-ASE}\right)^2 + \left(NEV_{ASE-ASE}\right)^2 + \left(NEV_{\det.}\right)^2} \quad (13)$$

In the absence of averaging, the 30dB optical amplification of the signal, increases the signal equivalent voltage from $3.13\times10^{-4}V$ to 0.313V, resulting in an increase in the signal to noise ratio to 7.8 from 0.46. But optical amplification of 30dB together with 2^{11} averages results in a temperature resolution of less than 1°C.

5.3 Conclusion

Over short sensing lengths of 100m, with 10cms of spatial resolution capability and without averaging the signal to noise ratio for the B-OTDR measurements (0.46) is better than that of the R-OTDR measurements (0.057). However, with 2^{20} averages, signal to noise ratio for the R-OTDR measurements increases to 59, resulting in a temperature resolution of 2.7°C. But the narrow spectral linewidth of the spontaneous Brillouin signal (~35MHz) qualifies for optical amplification, as against the broadband spontaneous Raman signal (~50nm) [1]. Even in the absence of any averaging, B-OTDR benefits from optical amplification, resulting in an increase in the signal to noise ratio to 7.8, which is 21.3dB better than the R-OTDR. However, 30dB of optical amplification coupled with only 2^{13} averages results in less than 1°C

of temperature resolution during the B-OTDR measurements. Fewer averages during the B-OTDR measurements also reduce the detection time of the technique, eventually making it more attractive than the R-OTDR technique. This conclusion is consistent with the improved performance of the temperature compensated high spatial resolution distributed strain measurements of chapter 4, where the B-OTDR technique was used in combination with the BOCDA as against the R-OTDR in combination with BOCDA used in chapter 3.

The SPM induced broadening of the Rayleigh signal leads to a temperature accuracy of 1°C along the sensing length. Collection of the Brillouin anti-Stokes signal relies heavily on the characteristic and positioning of fibre Bragg gratings. So the appropriate design features of the FBG, i.e., sharp transition, flat topped, high reflectivity, and high out band suppression, are all crucial in order to decide the placement of the FBG relative to Brillouin and Rayleigh signals in order to achieve the predicted claims for the B-OTDR technique.

5.4 References

[1] G.P. Agarwal, ‘‘Nonlinear Fibre Optics’’, Third Edition, Academic Press (2001)

[2] S. M. Maughan, PhD Thesis, University of Southampton (2001)

[3] K. De Souza and T. P. Newson, ‘‘Signal to noise and range enhancement of a Brillouin intensity based temperature sensor’’, *Optics Express*, 12(12), 2656-2661 (2004)

Chapter 6

6. Evaluation of Brillouin coefficients under combined temperature and strain influence

6.1 Introduction

To date, sensing rigs used for Brillouin scattering based distributed strain and temperature measurements have comprised separate sections of sensing fibre subjected to either temperature or strain influences [1 – 12]. Interpretation of such experiments have been based on the premise that the Brillouin coefficients used to describe the influence of strain or temperature remain constant under circumstances where a sensing fibre is subjected to the combined influence of both temperature and strain. This chapter experimentally investigates this premise.

6.2 Theory

6.2.1 The Brillouin coefficients

The change in Brillouin frequency and power due to strain and temperature has been represented by the matrix equation 1 [6, 7]

$$\begin{bmatrix} \Delta v_B \\ \Delta I_{BI} \end{bmatrix} = \begin{bmatrix} C_{Bv}^{\varepsilon} & C_{Bv}^{T} \\ C_{BI}^{\varepsilon} & C_{BI}^{T} \end{bmatrix} \begin{bmatrix} \Delta\varepsilon \\ \Delta T \end{bmatrix} \quad (1)$$

Where C_{Bv}^{ε}, C_{Bv}^{T} are the Brillouin frequency coefficients and C_{BI}^{ε}, C_{BI}^{T} are the Brillouin power coefficients for strain and temperature respectively, with Δv_B and ΔI_{BI} representing the change in peak Brillouin frequency and Brillouin anti-Stokes power with temperature and strain. Inverse of matrix equation 1 allows for values of strain $(\Delta\varepsilon)$ and temperature (ΔT) to be determined.

$$\begin{bmatrix} \Delta\varepsilon \\ \Delta T \end{bmatrix} = \frac{1}{\left| C_{Bv}^{\varepsilon} C_{BI}^{T} - C_{BI}^{\varepsilon} C_{Bv}^{T} \right|} \times \begin{bmatrix} C_{BI}^{T} & -C_{Bv}^{T} \\ -C_{BI}^{\varepsilon} & C_{Bv}^{\varepsilon} \end{bmatrix} \begin{bmatrix} \Delta v_B \\ \Delta I_{BI} \end{bmatrix} \quad (2)$$

Equation 2 highlights that in order to estimate strain or temperature, it requires knowledge of the Brillouin coefficients which so far have been measured by varying only one parameter, for example strain, whilst keeping the other constant i.e. temperature or vice versa. The assumption has been that these coefficients are independent of the other parameter.

6.2.2 Brillouin frequency and intensity measurements

The Brillouin frequency measurements were made using the well established Brillouin optical correlation domain analysis (BOCDA) technique [8, 9, 10], which has been described in the previous chapters.

The Brillouin intensity measurements were made using the Brillouin optical time domain reflectometry technique (B-OTDR). Depending upon the spatial resolution required to interrogate the measurand, laser pulses of a certain pulse width were launched into the sensing fibre. The time duration between the launched pulses was

chosen so as to allow only for a single pulse and the corresponding scattering from it to propagate through the sensing fibre at any time. As the pulse propagated through the sensing fibre, light was scattered from the frozen imperfections in the fibre (Rayleigh scattering), the acoustic phonons (Brillouin scattering) and the optical phonons (Raman scattering).

The backscattered Brillouin anti-Stokes signal was filtered using tuneable fibre Bragg gratings and converted into an electrical signal through a photo receiver and displayed as a decay trace on the oscilloscope. The decay trace represented the change in Brillouin anti-Stokes power as a function of distance along the sensing fibre. Using the correct bandwidth electronics, the measurand, i.e., strain or temperature under investigation, was spatially resolved.

6.3 Experimental Setup and Procedure

6.3.1 Experimental Setup and procedure for Brillouin frequency measurement

The experimental set up for the Brillouin frequency measurements is shown in figure 1(a) with the detail of the sensing fiber layout in 1(b).

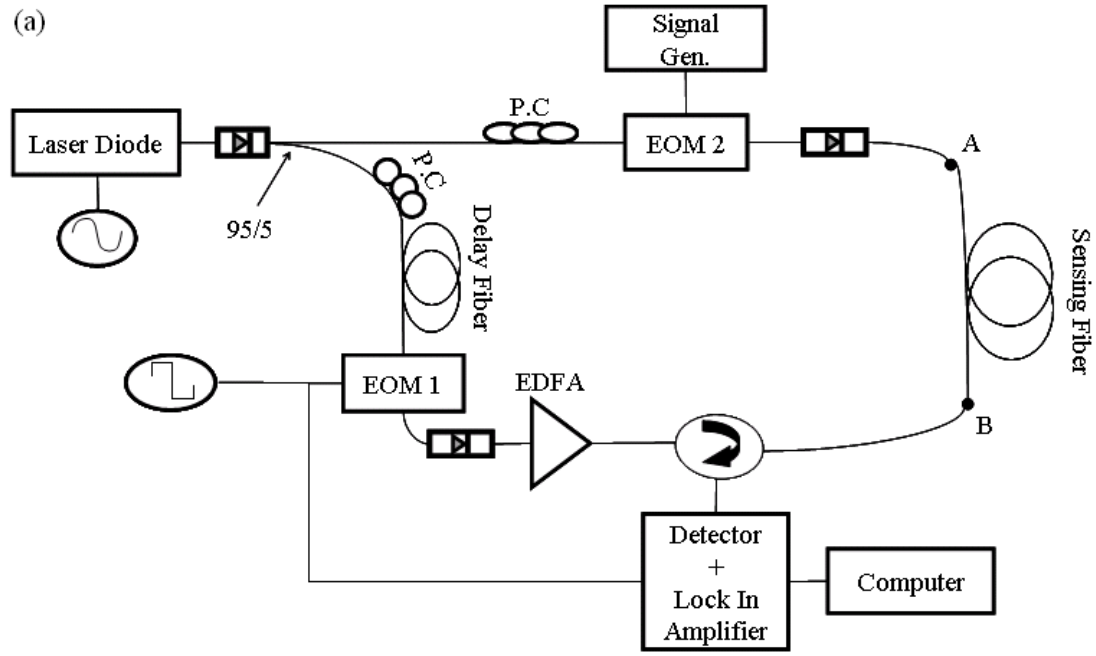

Figure 1a. The experimental set up for the Brillouin frequency measurements

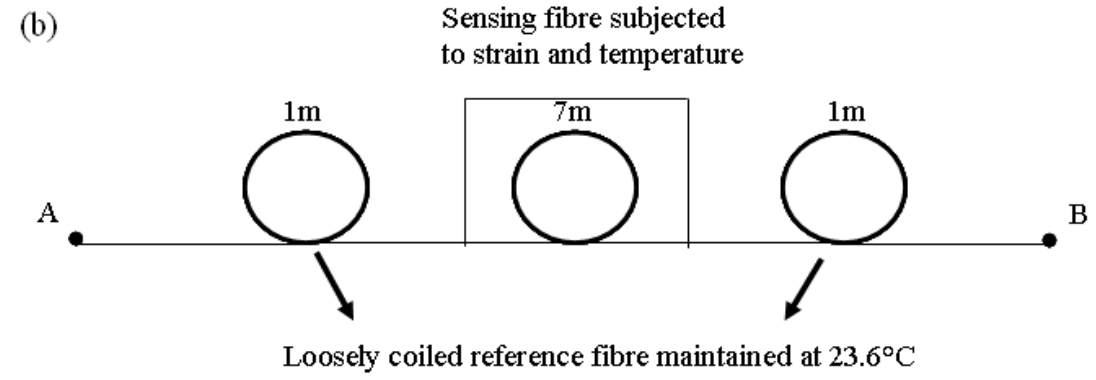

Figure 1b. Detail of the 7m of sensing fibre along with reference fibres.

The 7m section of sensing fibre was a standard single mode telecommunication fibre with an effective area~ 80μm^2, loss ~ 0.20dB/km and dispersion ~17 ps/km.nm at 1550 nm. The sensing fibre was arranged on a strain rig consisting of pulleys which could be placed in an environmental chamber in order to allow for the fibre to be

strained at different temperatures, as shown in figure 2. The remaining two sections of 1m each were loosely coiled and maintained at 23.6°C.

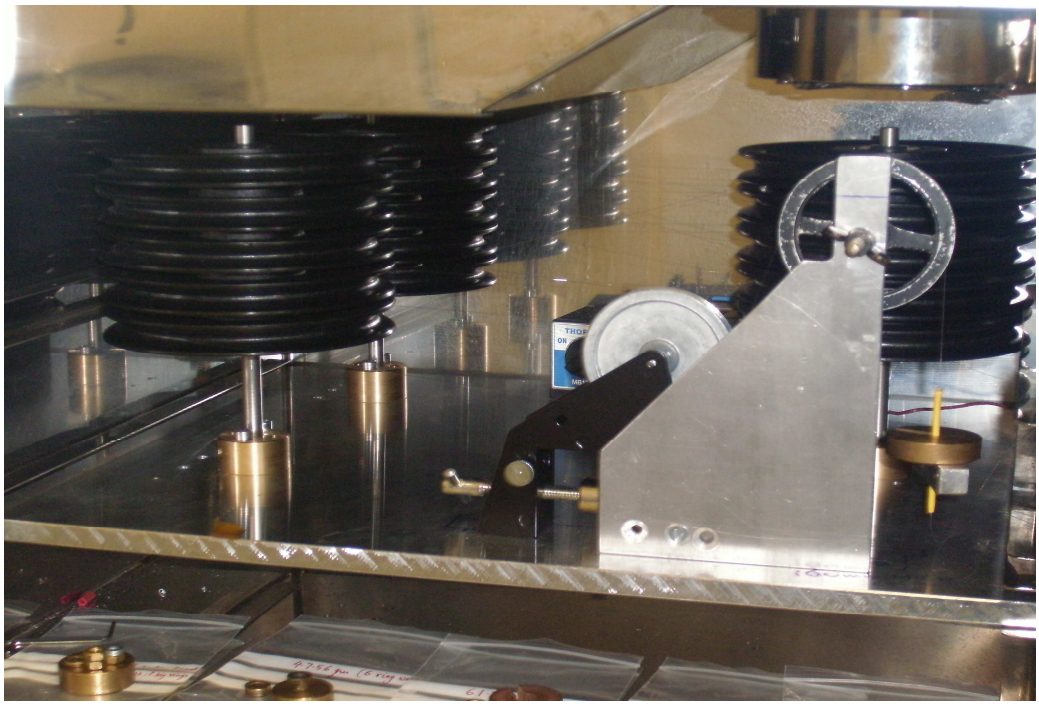

Figure 2. The inside of the environmental chamber with the arrangement for straining the 7m section of sensing fiber using weights

The injection current of the laser diode (linewidth ~ 5MHz, 1550nm) was modulated to achieve a frequency variation Δf of 8 GHz with sinusoidal sweep rate f_m of 74.4 kHz. This combination of Δf =8GHz and f_m =74.4 kHz resulted in a spatial resolution of 1.8m. A signal generator was used to provide a 30kHz (square wave) signal to the EOM1 which also served as a reference signal to the lock-in amplifier, of 100kHz bandwidth. EOM2 was driven by a synthesizer to generate side bands corresponding to the expected Brillouin frequency shift of ~10GHz - 12GHz. The Brillouin signal was detected using a 1GHz detector with responsitivity of 0.95A/W.

6.3.2 Experimental Setup and procedure for the Brillouin intensity measurement

The experimental set up for Brillouin intensity measurements is shown in figure 3a with the detail of the sensing fiber layout in figure 3b. A pulse width of 30ns was used to achieve an adequate signal to noise. This corresponded to a spatial resolution of 3m. To accommodate this increased spatial resolution, the fibre either side of the 7m section was increased from 1m to 10m. An additional 40m long loosely coiled fibre was added to the sensing fibre and maintained at 50°C to facilitate tuning of the FBG filters to the centre of the Brillouin frequency shift.

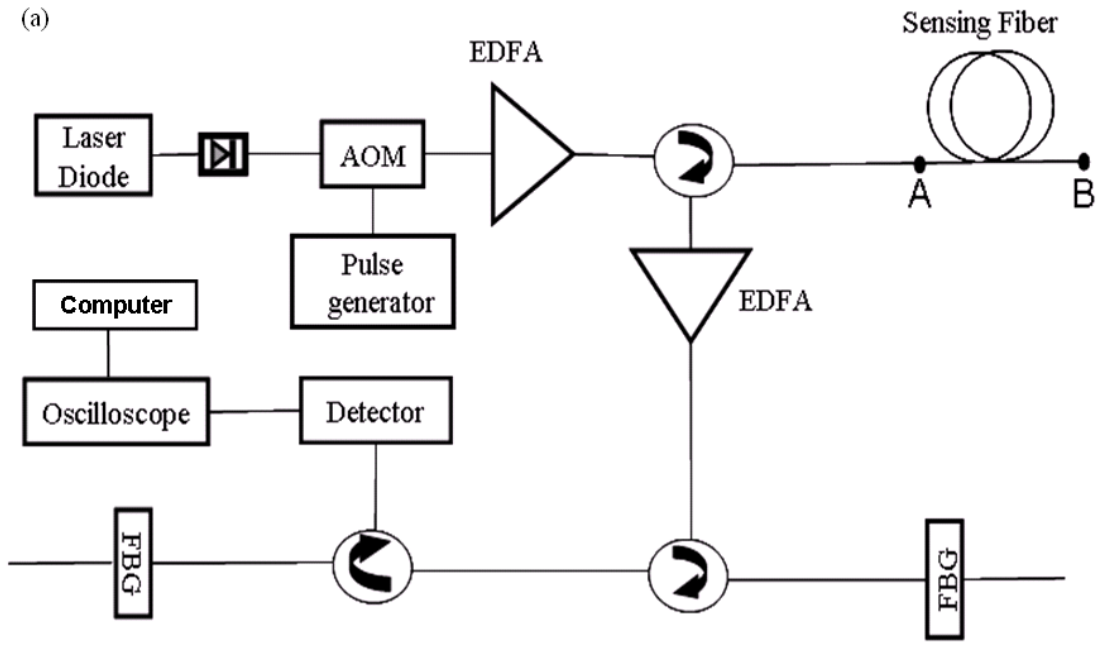

Figure 3a. The experimental set up for the Brillouin intensity measurements

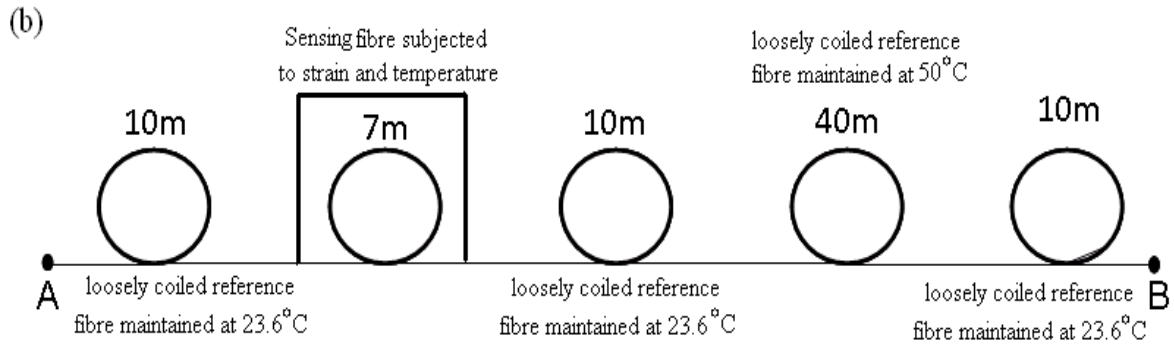

Figure 3b. Detail of the sensing fibre along with reference fibres

The output of the laser diode (linewidth ~ 5 MHz, 1533.95nm) was pulsed using an acousto-optic modulator to achieve 30ns rectangular shaped optical pulses at a repetition rate of 1MHz. These were amplified to peak powers of 1W before being launched into the sensing fiber. The backscattered anti Stokes Brillouin signal was amplified and filtered using two tunable narrow gratings (3dB bandwidth of 3.5GHz).

The grating characteristic, shown in figure 4, was acquired by shining an ASE source onto the grating and collecting the reflected light from the grating on an optical spectrum analyser set at a resolution of 20MHz over 1GHz span. The reflectivity of these gratings varied less than 0.03% over the temperature range of 23.6°C – 69.5°C. The filtered Brillouin backscattered signal was detected using a 200MHz bandwidth detector. Strain in the environmental chamber was imposed by applying weights using a pulley system as shown in figure 2.

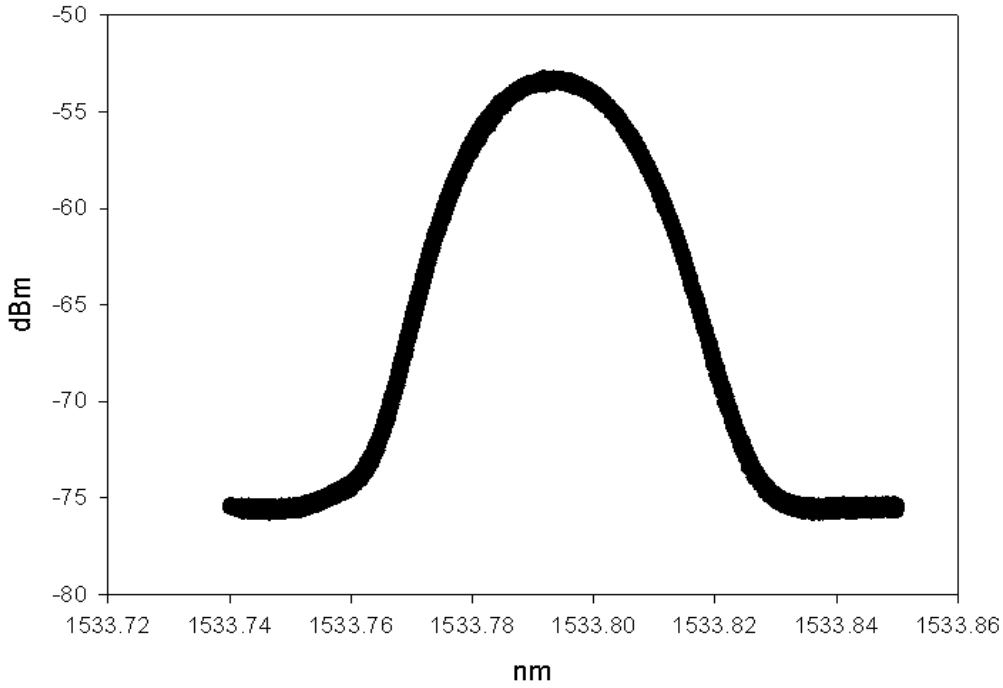

Figure 4. The reflection spectrum of the 3.5GHz (3dB linewidth) tunable grating

The backscattered anti-Stokes Brillouin traces for varying temperatures at fixed values of strain, i.e., 275με, 567με, 828με, 1120με, 1285με, 1463με were collected and normalised using the anti-Stokes Brillouin traces collected at room temperature under similar influences of strain. Traces normalised in this manner were used to estimate the Brillouin intensity coefficient for temperature at different values of strain i.e., 275με, 567με, 828με, 1120με, 1285με, 1463με.

Similarly the backscattered anti-Stokes Brillouin traces for varying strain at fixed values of temperature, i.e., 29.8°C, 39.6°C, 49.3°C, 59.6°C, 69.5°C were collected and normalised using the backscattered anti-Stokes Brillouin traces collected at 0με under similar temperature influences. These normalised traces were used to estimate the Brillouin intensity coefficient for strain at different values of temperature i.e., 29.8°C, 39.6°C, 49.3°C, 59.6°C, 69.5°C.

Data from the frequency based Brillouin optical correlation domain analysis experiments and the intensity based anti-Stokes Brillouin optical time domain reflectometry experiments was collected and analysed by a personal computer.

6.4 Results

6.4.1 Results of Brillouin frequency measurement

Plots in figure 5, show the shifts in peak Brillouin frequency corresponding to applied strain at fixed values of temperature imposed to the 7m section of the sensing fiber.

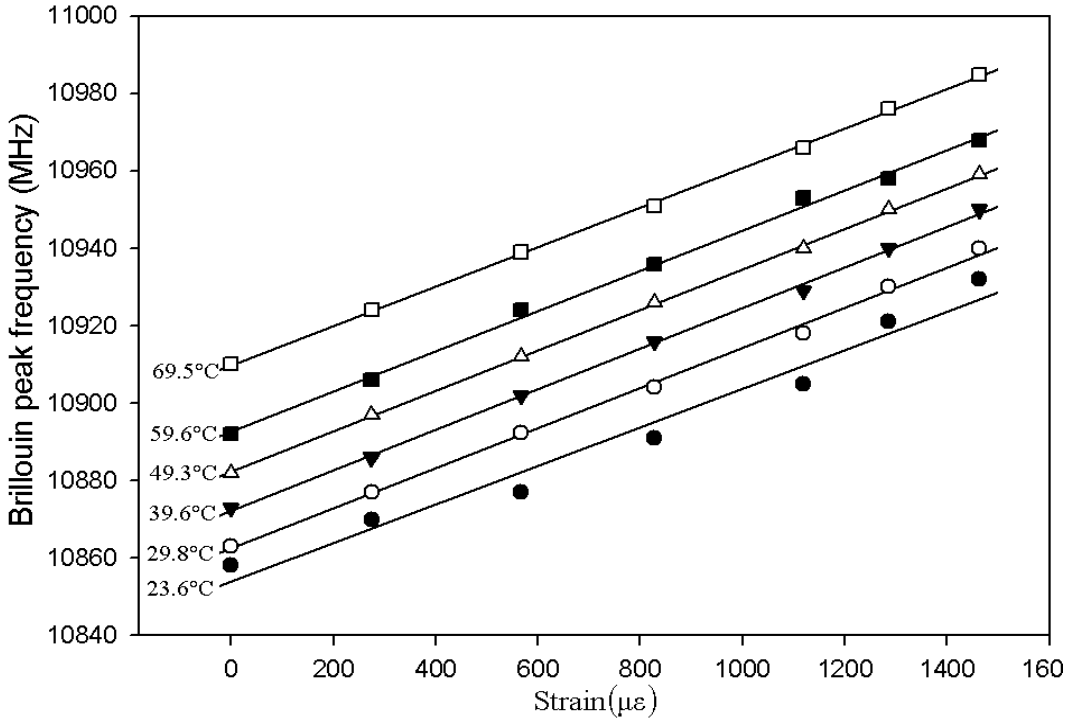

Figure 5. The plots for changes in peak Brillouin frequency with strain at different values of temperature

Plots in figure 6, show the shifts in peak Brillouin frequency corresponding to applied temperature at fixed values of strain imposed to the 7m section of the sensing fiber.

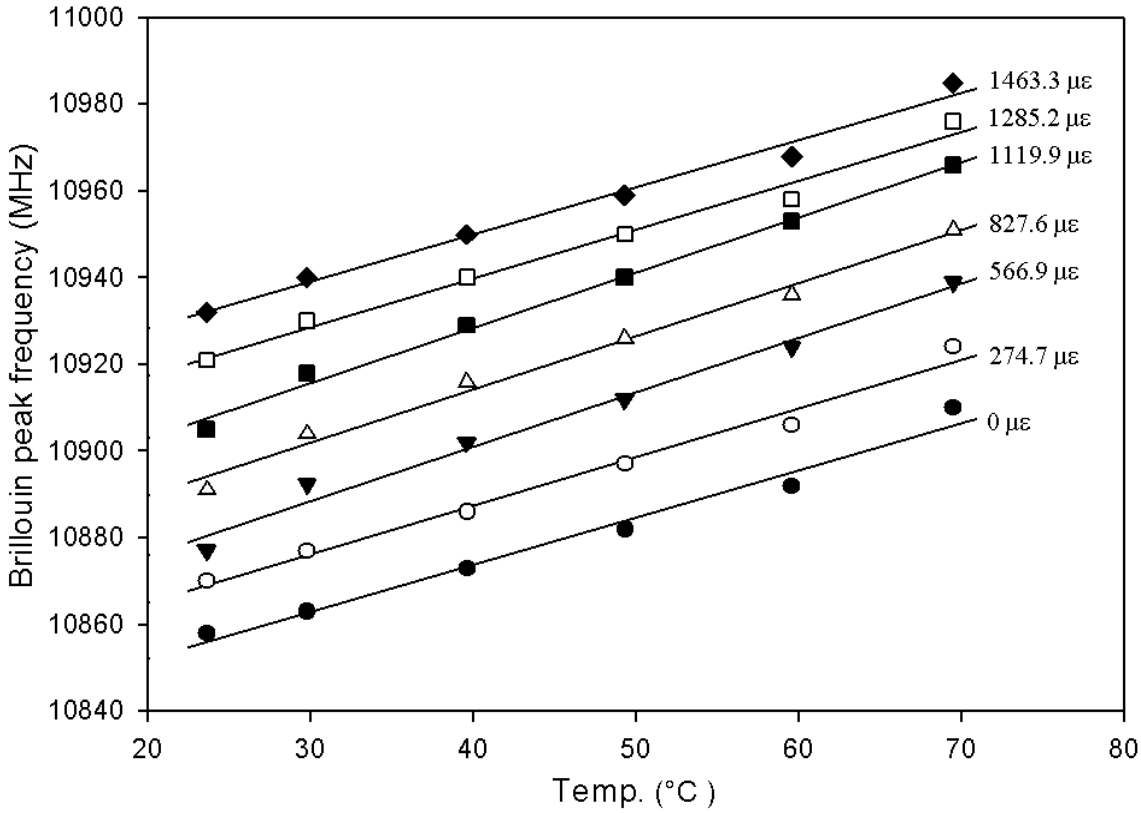

Figure 6. The plots for changes in peak Brillouin frequency with temperature at different values of strain

6.4.2 Results of Brillouin intensity measurement

Plots in figure 7, show the percentage changes in Brillouin anti-Stokes intensity with temperature at fixed values of strain imposed to the 7m section of the sensing fiber.

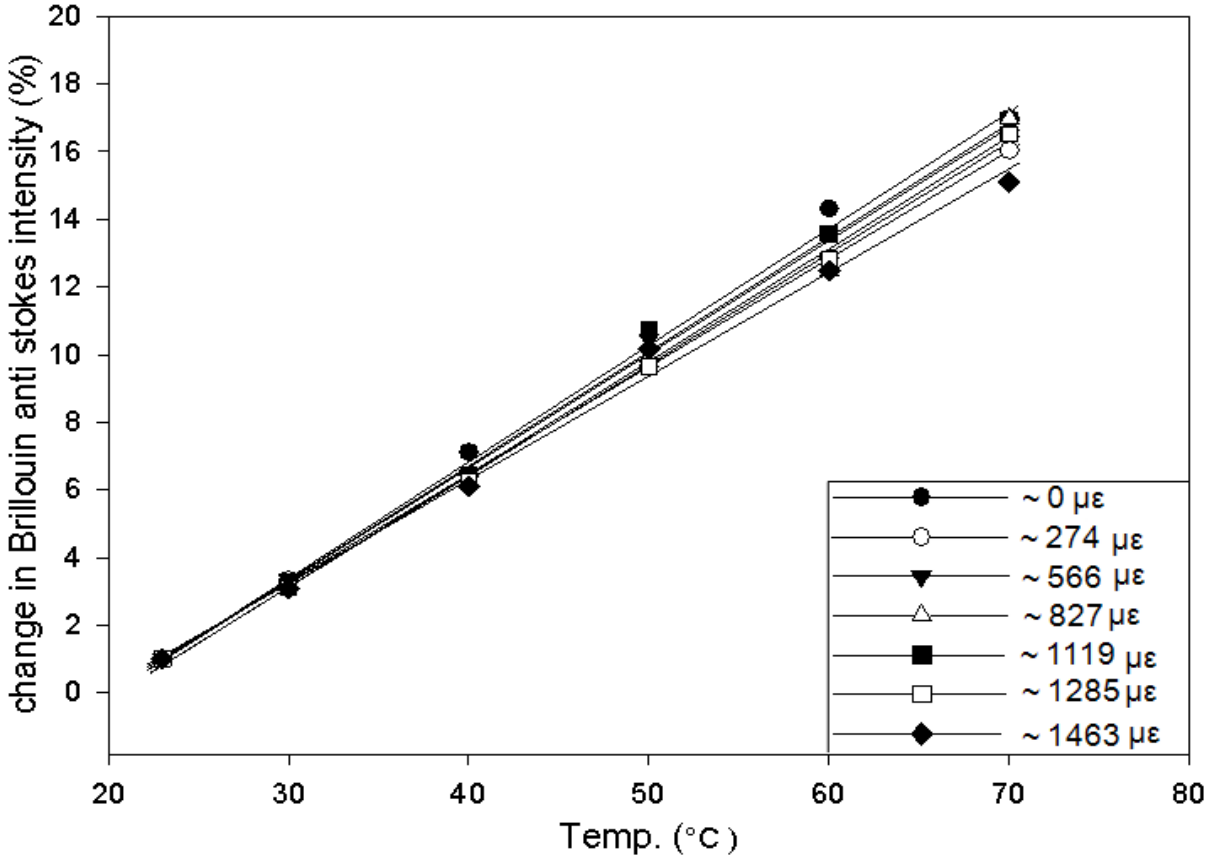

Figure 7. The plots for percentage change in anti-Stokes Brillouin power with temperature at different values of strain

Plots in figure 8, show the percentage changes in anti-Stokes Brillouin intensity with strain at fixed values of temperature imposed to the 7m section of the sensing fibre.

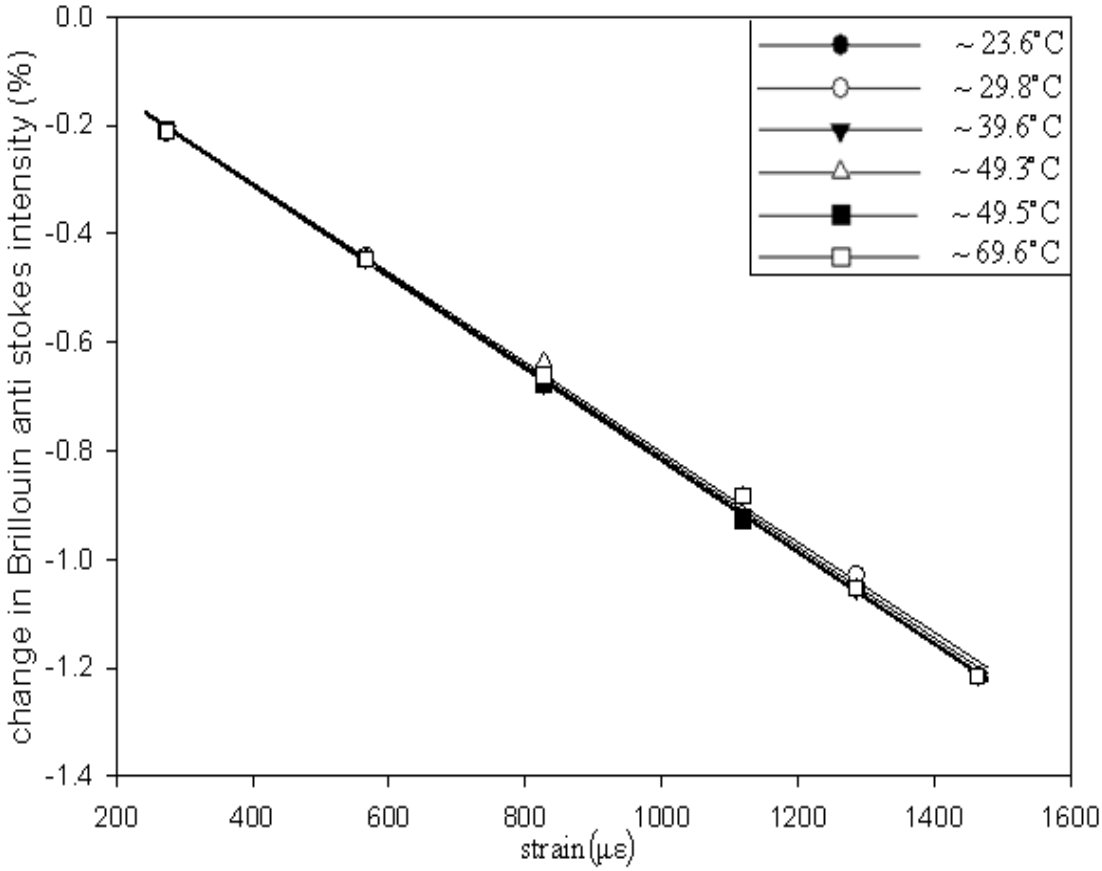

Figure 8. The plots for percentage change in anti-Stokes Brillouin power with strain at different values of temperature

The strain imposed by applying weights to the fibre, between temperature range of 23.6°C to 69.5°C, was computed using the corresponding Young's modulus values from the plot shown in figure 9.

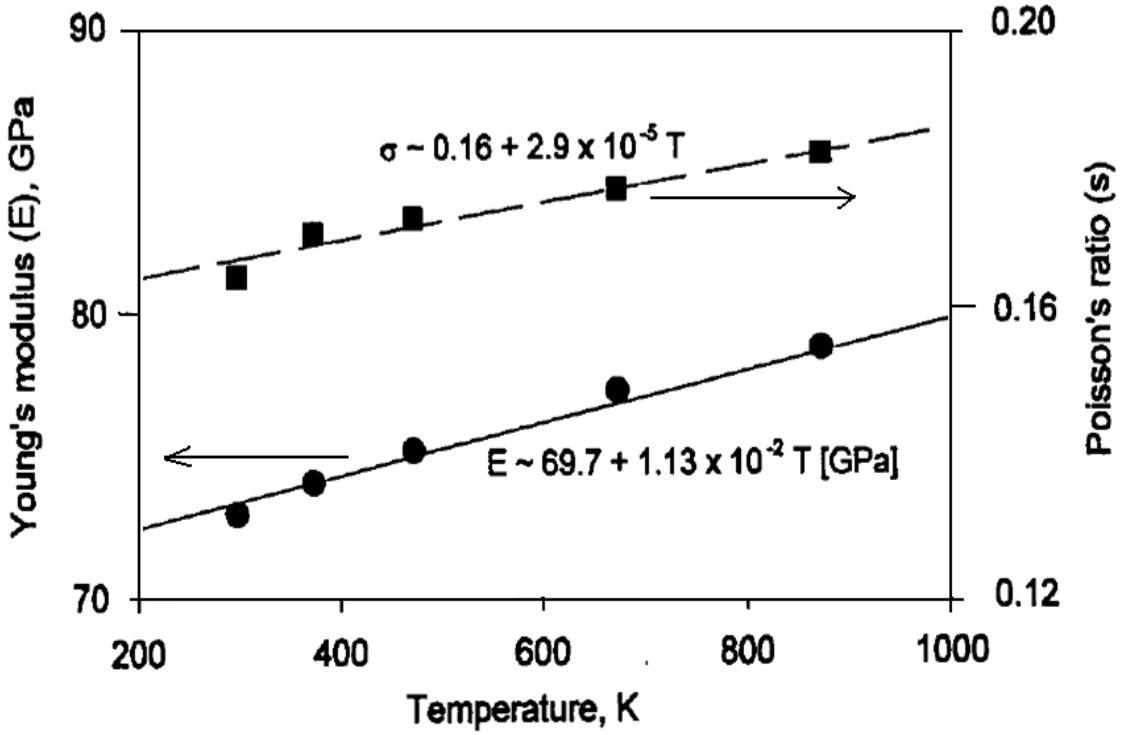

Figure 9. The variation of Young's modulus and Poisson ratio of bulk silica with temperature [13]

6.4.3 Summary of Results

Plots in figures 10 to 13 show the variation in Brillouin coefficients under combined temperature and strain influence plotted with the error bars depicting 1 standard deviation.

Figure 10 shows the Brillouin frequency coefficient for temperature under different values of applied strain, while figure 11 shows Brillouin frequency coefficient for strain under different values of imposed temperature.

The value of slope, calculated from the linear regression fit, provides an estimate of the variation in the Brillouin frequency coefficient for temperature under different

strains and also of the Brillouin frequency coefficient for strain under different temperature.

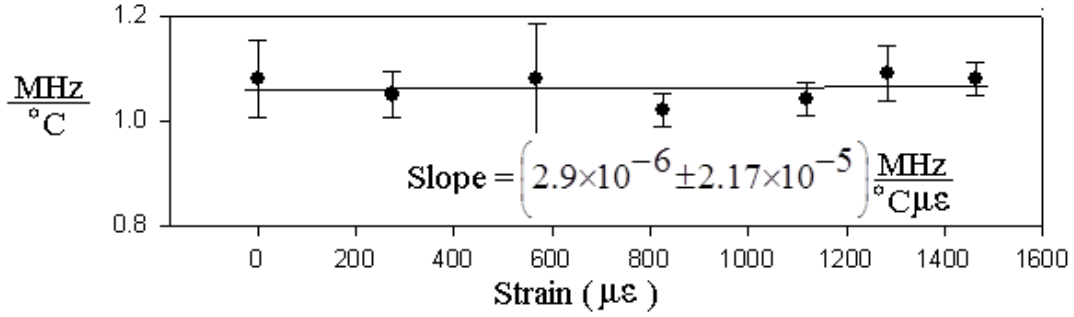

Figure 10. The variation of Brillouin frequency coefficient for temperature at different values of strain

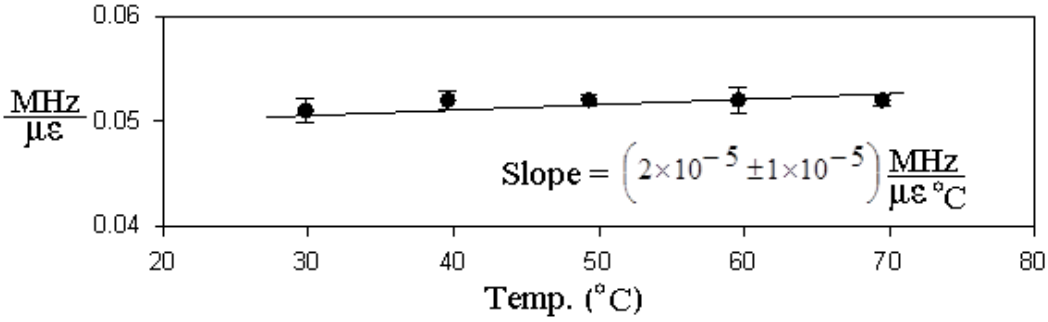

Figure 11. The variation of Brillouin frequency coefficient for strain at different values of temperature

On inspection, the presence of noise as seen in the trace at 23.6°C of figure 5 was found to manifest itself as the uncertainty in the data of figure 9 at 23.6°C.The noise was due to the insufficient settling time of the environmental chamber at 23.6°C during opening and closing of the chamber for imposition of new strain. Hence this data point was excluded. Exclusion of the data at 23.6°C in figure 11 resulted in the change in the value of the slope from $5.2 \times 10^{-5} \frac{MHz}{\mu\varepsilon\ ^{\circ}C}$ to $2 \times 10^{-5} \frac{MHz}{\mu\varepsilon\ ^{\circ}C}$.

Figure 12 shows the Brillouin power coefficient for temperature under different values of applied strain, while figure 13 shows Brillouin power coefficient for strain under different values of imposed temperature.

The value of slope, calculated from the linear regression fit in these plots, provides an estimate of the variation in the Brillouin power coefficient for temperature under different strains and also of the Brillouin power coefficient for strain under different temperatures.

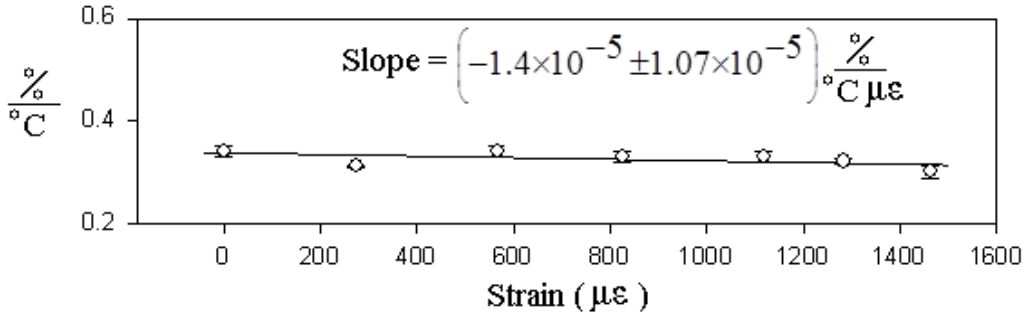

Figure 12. The variation of Brillouin intensity coefficient for temperature at different values of strain

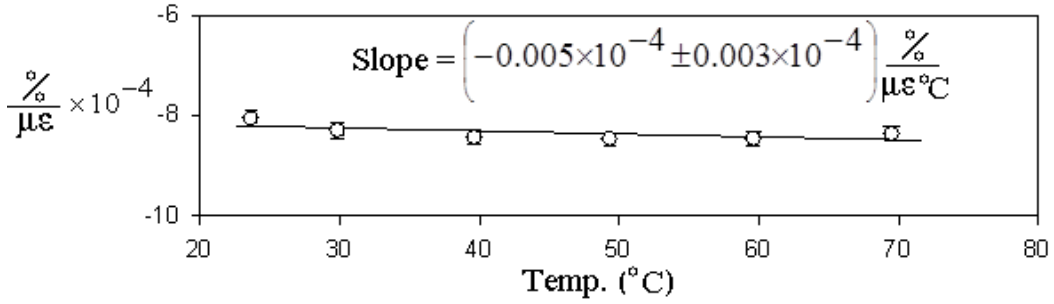

Figure 13. The variation of Brillouin intensity coefficient for strain at different values of temperature

The four Brillouin coefficients under a simultaneously varying temperature and strain environment are extracted using the plots shown from figures 10 – 13. These coefficients are summarised in table 1.

Brillouin frequency coefficient for temperature as a function of applied strain $C_{B\nu}^{T}(\varepsilon) = \left[1.06\left(1 + \left[2.73 \times 10^{-6} \pm 2.04 \times 10^{-5}\right]\varepsilon\right)\right] \frac{MHz}{^{\circ}C}$
Brillouin frequency coefficient for strain as a function of temperature $C_{B\nu}^{\varepsilon}(T) = \left[0.048\left(1 + \left[4.16 \times 10^{-4} \pm 2.29 \times 10^{-4}\right]\Delta T\right)\right] \frac{MHz}{\mu\varepsilon}$
Brillouin intensity coefficient for temperature as a function of strain $C_{BI}^{T}(\varepsilon) = \left[0.33\left(1 - \left[4.24 \times 10^{-5} \pm 3.24 \times 10^{-5}\right]\varepsilon\right)\right] \frac{\%}{^{\circ}C}$
Brillouin intensity coefficient for strain as a function of temperature $C_{BI}^{\varepsilon}(T) = \left[-8.07 \times 10^{-4}\left(1 + \left[6.19 \times 10^{-4} \pm 3.71 \times 10^{-4}\right]\Delta T\right)\right] \frac{\%}{\mu\varepsilon}$

Table 1. Summary of the four Brillouin coefficients under a simultaneously varying temperature and strain environment

6.5 Discussions

Observing the Brillouin frequency coefficient for temperature and strain, it can be inferred that a MHz change in Brillouin frequency can result either as a consequence of a degree rise in temperature or due to 20με of increase in the value of applied strain. With regards the Brillouin intensity, every degree rise in temperature results in almost 0.3% increment in the level of backscattered Brillouin intensity, however an increase in the value of applied strain, reduces the Brillouin intensity by a small percentage. The Brillouin scattering mechanism is based upon generation of acoustic phonons. In order to understand the behaviour of the Brillouin coefficients it is useful to represent acoustic phonon density by a Maxwell- Bolztman statistic, given by equation 5 and the Brillouin frequency shifted acoustic phonons by equation 6.

$$N_i = \sum_i N_i \exp\left(-\frac{h\nu_i(T,\varepsilon)}{kT}\right) \tag{5}$$

Where N_i is the acoustic phonon density in state i, $\sum_i N_i$ is the total number of phonons, $h\nu_i(T,\varepsilon)$ is the energy of the acoustic phonons in state i at temperature T in Kelvin and strain ε in micro strain and k is the Boltzman constant.

$$\nu_B(T,\varepsilon) = \frac{2\times n(T,\varepsilon)\times V_A(T,\varepsilon)}{\lambda_p} \tag{6}$$

Where, ν_B is the Brillouin frequency shifted acoustic phonons generated by an optical pump at a wavelength of λ_p, travelling at an acoustic velocity of V_A in a medium with an effective refractive index of n.

Both the refractive index and the acoustic velocity terms in equation 6 are temperature and strain dependent [14]. If the frequency increase is due to strain then the population density of phonons is expected to be reduced as a result of their high energy level. This leads to the observed reduction in the anti Stokes Brillouin backscattered intensity with strain. On the other hand if the frequency increase is due to temperature then the observed increase in the anti Stokes Brillouin backscattered power indicates that the population density even at the higher frequency is greater as a result of the increase in thermal energy.

The straight line fit to the data shown in plots of figures 10 – 13 resulted in the four Brillouin coefficients corresponding to a thermally controlled (23.6°C - 69.5°C) variable strain (0.2με - 1.4mε) environment. Consider a situation where a Brillouin intensity change of 15% and a Brillouin frequency change of 100MHz is experimentally observed. Using the uncorrected Brillouin coefficients in equation 7 and 8, the change in strain and change in temperature values of 1024με and 48°C are computed.

$$\Delta\varepsilon = \frac{C_{BI}^{T}(\varepsilon).\Delta\nu_{B} - C_{Bv}^{T}(\varepsilon).\Delta I_{BI}}{\left|C_{Bv}^{\varepsilon}(T)C_{BI}^{T}(\varepsilon) - C_{BI}^{\varepsilon}(T)C_{Bv}^{T}(\varepsilon)\right|} \tag{7}$$

$$\Delta T = \frac{C_{Bv}^{\varepsilon}(T).\Delta I_{BI} - C_{BI}^{\varepsilon}(T).\Delta\nu_{B}}{\left|C_{Bv}^{\varepsilon}(T)C_{BI}^{T}(\varepsilon) - C_{BI}^{\varepsilon}(T)C_{Bv}^{T}(\varepsilon)\right|} \tag{8}$$

Using the values for the change in strain (1024με) and change in temperature (48°C) in table 1, the corrected Brillouin coefficients are estimated. These corrected Brillouin coefficients are then used in equation 7 and 8, resulting in the change in strain and change in temperature values of 907.5με and 49.9°C. These values of the change in strain and change in temperature are used again in table 1 in order to

estimate another set of corrected Brillouin coefficients, which are used in equations 7 and 8 resulting in the change in stain and change in temperature values of 958.5με and 49.9°C. The process is iterative and continues until the percentage variation between two successively computed values for the change in strain and change in temperature is 1% or less. Table 2, summarises the impact of iterations on the percentage variations between the two successively calculated change in strain and change in temperature values.

Number of Iterations	Change in strain	Percentage variation between successive iteration	Change in temperature	Percentage variation between successive iteration
1	1024με		48°C	
2	963.7με	-5.8%	50.1°C	4.19%
3	958.5με	-0.5%	49.9°C	-0.39%

Table 2. Results for the change in strain and the change in temperature values together with percentage variation in them between successive iterations

According to table 2, for the frequency change of 100MHz and percentage change in intensity of 15%, the true values for the change in strain and change in temperature are computed to be 958.5με and 49.9°C respectively. The value for the change in strain was achieved at the end of the third iteration, when the percentage variation for the change in strain value, between the second and the third iteration reduced to 0. 5%. The value for the change in temperature was also achieved at the end of the third iteration, when the percentage variation for the change in strain value, between the third and the second iteration reduced to 0.39%.

The percentage error in the four Brillouin coefficients under simultaneously imposed strain $(\Delta\varepsilon)$ and temperature (ΔT) change of 0.1% and 50°C, is calculated and summarised in table 3.

Error in Brillouin coefficient	**Error for** $(\Delta T = 50^{\circ}C; \Delta\varepsilon = 1000\mu\varepsilon)$	**Error (%) for** $(\Delta T = 50^{\circ}C; \Delta\varepsilon = 1000\mu\varepsilon)$
Error in Brillouin frequency coefficient for temperature under 0.1% strain $\delta C_{B\nu}^{T}(\varepsilon)$	$\left(2.9\times10^{-3} \pm 0.02\right)\frac{MHz}{^{\circ}C}$	0.2 ± 2
Error in Brillouin frequency coefficient for strain under temperature change of 50°C $\delta C_{B\nu}^{\varepsilon}(T)$	$\left(1.3\times10^{-3} \pm 7.7\times10^{-4}\right)\frac{MHz}{\mu\varepsilon}$	2.9 ± 1.6
Error in Brillouin intensity coefficient for temperature under 0.1% strain $\delta C_{BI}^{T}(\varepsilon)$	$\left(-0.014 \pm 0.0106\right)\frac{\%}{^{\circ}C}$	4.2 ± 3.24
Error in Brillouin intensity coefficient for strain under temperature change of 50°C $\delta C_{BI}^{\varepsilon}(T)$	$\left(-3.5\times10^{-5} \pm 2\times10^{-5}\right)\frac{\%}{\mu\varepsilon}$	4.3 ± 2.5

Table 3. Percentage errors in Brillouin coefficients under a simultaneous change in temperature and strain of $\Delta T = 50°\text{C}$ and $\Delta\varepsilon = 1000\mu\varepsilon$

6.6 Conclusions

The four Brillouin coefficients under a simultaneously varying temperature and strain environment are shown in table 1. For a frequency change of 100MHz and an intensity change of 15%, an iterative process involving estimation of the corrected Brillouin coefficients and their application in equations 7 and 8 resulted in the estimation of 958.5με as the true value for the applied strain and 49.9°C as the estimate for the true value for the change in temperature.

Table 2 provides an insight into the percentage error in the four Brillouin coefficients under a simultaneously imposed step change in temperature of 50°C and strain of 1000με. Errors in the individual Brillouin coefficients provide an insight into one of the key sources of errors during the estimation of the applied strain and the change in temperature values. But since the four coefficients are linked with each other, any one Brillouin coefficient cannot be studied in isolation in order to quantify the source which has the dominant contribution to the error in the estimation of the applied strain and the change in temperature values. It is certainly motivation for future work.

6.7 References

[1] T. Horiguchi, O. Kurashima and M. Tateda, ‘‘Tensile strain dependence of Brillouin frequency shift in silica optical fibers’’, *IEEE Photonics Technology Letters*, 1(5), 107-108 (1989)

[2] T. Kurashima, T. Horiguchi, and M. Tateda, ‘‘Thermal effects on the Brillouin frequency shift in jacketed optical silica fibers’’, *Applied Optics*, 29(15), 2219 – 2222 (1990)

[3] P. C. Wait and T. P. Newson, ‘‘Landau Placzek ratio applied to distributed fibre sensing’’, *Optical Communications*, 122, 141-146 (1996)

[4] K. De Souza, P. C. Wait and T. P. Newson, ‘‘Characterisation of strain dependence of the Landau-Placzek ratio for distributed sensing’’, *Electronics Letters*, 33(7), 615-616 (1997)

[5] T. R. Parker, M. Farhadiroushan, V. A. Handerek and A. J. Rogers, ‘‘Temperature and strain dependence of the power level and frequency of spontaneous Brillouin scattering in optical fibers’’, *Optics Letters*, 22(11), 787 – 789 (1997)

[6] H. H. Kee, G. P. Lees and T. P. Newson, ‘‘An all-fiber system for simultaneous interrogation of distributed strain and temperature sensing using spontaneous Brillouin scattering’’, *Optics Letters*, 25(10), 695-697 (2000)

[7] S. M. Maughan, H. H. Kee and T. P. Newson, ‘‘Simultaneous distributed fibre temperature and strain sensor using microwave coherent detection of spontaneous Brillouin backscatter’’, *Measurement Science and Technology*, 12, 834–842 (2001)

[8] K. Hotate, and M. Tanaka, ‘‘Distributed fiber Brillouin strain sensing with 1-cm spatial resolution by correlation-based continuous-wave technique’’, *IEEE Photonics Technology Letters*, 14(2), 179-181 **(**2002)

[9] K. Y. Song and K. Hotate,‘‘Enlargement of measurement range in a Brillouin optical correlation domain analysis system using double lock-in amplifiers and a

single-sideband modulator'', *IEEE Photonics Technology Letters*, 18(1-4), 499-501 (2006)

[10] K. Y. Song, Z. He and K. Hotate, ''Distributed strain measurement with millimeter-order spatial resolution based on Brillouin optical correlation domain analysis'', *Optics Letters*, 31(17) 2526-2528 (2006)

[11] M. Belal, Y. T. Cho, M. Ibsen and T. P. Newson ''A temperature compensated high spatial resolution distributed strain sensor'', *Measurement Science and Technology*, 21 (2010)

[12] M. A. Soto, G. Bolognini, F. D. Pasquale, and L. Thévenaz, ''Simplex-coded BOTDA fiber sensor with 1 m spatial resolution over a 50 km range'', *Optics Letters*, 35(2), 259 – 261 (2010)

[13] K. De Souza, PhD Thesis, University of Southampton (1999)

[14] P. C. Wait, PhD Thesis, University of Southampton (1996)

Chapter 7

7. Summary, Discussion, Conclusion and Future Work

7.1 Summary

The critical review in chapter 2 revealed that the design of a high spatial resolution temperature compensated distributed strain sensor remained a key and challenging problem for distributed sensing yet to be solved. The problem was solved here in this thesis by exploring the possibility of combining the high spatial resolution Brillouin frequency measurements with the intensity measurements of Raman, as well as Brillouin. These explorations were then followed by a calibration experiment for the Brillouin coefficients, in order to facilitate reliable measurements even under a simultaneously varying temperature and strain influence.

The combinatory scheme of Brillouin frequency (BOCDA) with the anti-Stokes Raman intensity (R-OTDR) measurements yielded a temperature compensated distributed strain resolution of 46με with spatial resolution of 24cms, for a sensing length of 135m. The data during the R-OTDR was averaged 2^{22} times. Improvements in the values of strain and spatial resolution were observed in the combinatory scheme of Brillouin frequency and the anti-Stokes Brillouin intensity measurements, where 22με of temperature compensated strain resolution was achieved with 10cms of spatial resolution, over a sensing length of 131m. The B-OTDR data was also averaged 2^{22} times. Table 1 summarises the independent achievements of the B-OTDR and R-OTDR techniques and also the value of temperature compensated strain resolution and spatial resolution achieved by the two techniques in combination with the BOCDA.

Parameters	R-OTDR	B-OTDR
Spatial Resolution	24cms	7cms
Sensing Length	135m	131m
Temperature Resolution	2°C	0.95°C
Strain resolution in combination with BOCDA	46με	22με
Temperature compensated spatial resolution	24cms	10cms
Data Averages	2^{22}	2^{22}

Table 1. Performance outcome of the R-OTDR and the B-OTDR techniques

Improvements in various sensor parameters were found using the second technique, i.e., BOCDA + B-OTDR, but some of the improvements could potentially be attributed to improved experimental set up. Hence, in order to identify which technique is more apt for high spatial resolution distributed temperature measurements at short sensing lengths, performance of both R-OTDR and B-OTDR techniques was theoretically examined over similar sensor parameters, i.e., sensing length of 100m, spatial resolution of 10cms and a temperature error of less than 1°C. The outcome of the theoretical analysis identified the B-OTDR technique superior to the R-OTDR, with 21.3dB improvement in the signal to noise ratio.

The re-characterization of the Brillouin coefficients under a temperature controlled variable strain environment highlighted the necessity of using corrected Brillouin coefficients in the estimate of the true values of the applied strain and the change in temperature. The value of the applied strain and the change in temperature estimated using the iteratively computed corrected Brillouin coefficients was calculated to be 911.2με and 49.7°C, for a frequency change of 100MHz and an intensity change of 15%. However for a similar change in frequency and intensity the uncorrected

Brillouin coefficients resulted in 1024με and 48°C as the values for the applied strain and the change in temperature.

7.2 Discussions

In order to design a short range high spatial resolution temperature compensated distributed strain sensor, the combination of the Brillouin frequency and intensity measurements has been identified as the best choice. But since the temperature compensation feature of a sensor based upon such a combinatory scheme relies on the B-OTDR measurements, it is important to study the effects which limit the performance of the B-OTDR.

7.2.1 Factors limiting sensor performance and methods enhancing sensor applicability

Stimulated Brillouin scattering (SBS), group velocity dispersion (GVD), stimulated Raman scattering (SRS), modulation instability (MI) and self phase modulation (SPM) are the key non linear effects that influence the performance of the B-OTDR measurements. Hence, the following sub-sections discuss the threshold limits of the key non linear effects capable of affecting the performance of the B-OTDR measurements. The discussion also aims at identifying means of improving the B-OTDR results achieved in chapter 4 and hence the combined performance of the high spatial resolution temperature compensated distributed strain sensor. In order to further strengthen the sensor applicability, loss compensation schemes are also discussed.

7.2.1.1 SBS

Using $g_B = 5\times10^{-11}$ m/W at $\lambda = 1.55\,\mu$m and $A_{eff} = 80\times10^{-12}\,\mu m^2$, the SBS threshold for a 0.5ns pulse, expressed in equation 1 [1], is calculated to be 336W.

$$P_{Th.}^{SBS} = \frac{21\times A_{eff}}{L_{eff}\times g_B} \qquad (1)$$

Since the product of the Brillouin gain (g_B) and its linewidth $\left({}^{Br}\Delta\nu_{LW}\right)$ is a constant, the SBS threshold for 0.5ns Gaussian shaped pulses, would be $440\text{MHz}/{}^{Br}\Delta\nu_{LW}$ times bigger than the value calculated in equation 1, i.e., 4.2KW, where the natural Brillouin linewidth $\left({}^{Br}\Delta\nu_{LW}\right)$of 35MHz [1, 2] is considered. The high SBS threshold peak power value ties in with the theoretical understanding of generation of SBS, where 8ns – 10ns [1] is the typical decay time of the acoustic waves responsible for seeding the SBS effect, and hence pulses much shorter than the acoustic decay time would require much high peak powers in order to generate stronger acoustic waves capable of seeding the SBS. Hence for all practical purposes the role of SBS effects from short duration pulses over short sensing lengths is neglected, because other non linear effects have much lower threshold limits and hence they influence the decision on the use peak powers that can be used for the B-OTDR experiments.

7.2.1.2 GVD

For a given pulse width, equation 2 [1] gives an estimate of the lengths over which GVD effects contribute towards influencing the shape and the width of the pulses.

$$L = \frac{T_o^2}{|\beta_2|} \qquad (2)$$

Where, $\beta_2 = -17\, ps^2/km$ is the value of the fibre parameter and T_o is the half pulse width at half maximum [1]. So for a 0.5ns (HWHM) Gaussian pulse the GVD effect sets in over 14,705km. However the sensing lengths used in the B-OTDR experiments are 0.13km and hence the GVD related effects can also be neglected over such sensing lengths.

7.2.1.3 SRS

SRS, unlike the SBS, builds up as a function of sensing length and hence such effects impact the temperature accuracy of the B-OTDR measurements. Equation 3 [1] helps estimate the SRS threshold. 135W is the estimate for SRS threshold over 0.13Km of sensing length.

$$P_{Th.}^{SRS} = \frac{16 \times A_{eff}}{L_{eff} \times g_R} \qquad (3)$$

where $g_R = 7 \times 10^{-14}$ m/W at $\lambda = 1.55\,\mu m$, $A_{eff} = 80 \times 10^{-12}\,\mu m^2$ and $L_{eff} = 135$m. The SRS threshold power is much smaller than the peak threshold power for the SBS. But in order to decide the powers to be used in order to improve the existing signal to noise results of the B-OTDR measurements, it is important to compare the threshold peak powers for SPM with that of SRS. This is because both the SPM and SRS effects influence the accuracy of temperature measurements, i.e., they build up as a function of sensing length. Hence the effect which has a lower threshold would

determine the peak power that can be launched whilst maintaining a certain degree of temperature accuracy.

With the SRS threshold value of 135W for 0.13km of sensing length, it must also be pointed out that during the R-OTDR experiments in chapter 3, 240W peak power pulses were used instead, over nearly the same sensing length. Hence it is noteworthy that the process of normalisation carried out on the backscattered anti-Stokes Raman signal corresponding to higher temperature by using the room temperature anti-Stokes Raman backscattered signal, proved beneficial in correcting for modest pump depletion caused by the onset of SRS as against using the Rayleigh signal at the Raman wavelength, which is not only incapable of accounting for pump depletion effects but also suffers from the coherent Rayleigh noise.

7.2.1.4 SPM and MI

During the B-OTDR experiments of chapter 4, it emerged that peak powers in excess of 2W lead to reduction in the signal to noise ratios. Theoretical performance analysis of the B-OTDR over 0.1km of sensing length in chapter 5 indicated that 100W peak power pulses could be used before SPM related contamination of signal results in noise increase in excess of 0.33%. However, in that theoretical treatment, due to use of dispersion shifted fibres, with zero dispersion wavelength as the wavelength of operation, i.e., 1.53µm, MI effects were neglected. Hence, during the B-OTDR experiments in chapter 4, MI would have been the main limitation of peak powers, i.e., less than 2W.

MI takes place when the operating wavelength is in the anomalous dispersion regime $(D > 0, \beta < 0)$, i.e., usage of sensing fibre with positive dispersion value of 17ps km^{-1} nm^{-1} at the wavelength of operation. Detrimental effects due to the onset of MI were shown by Alahbabi et al [3] over long sensing range (>20km) and their work also highlighted the advantages of using fibres with zero or negative dispersion

value at the wavelength of operation, which could hence utilize launch of higher peak powers resulting in improved signal to noise.

Figure 1, shows the gain spectra of modulation instability for three levels of power for an optical fibre with a value of $\beta = -20\,ps^2/km$ and $\gamma = 2km^{-1}W^{-1}$ [1].

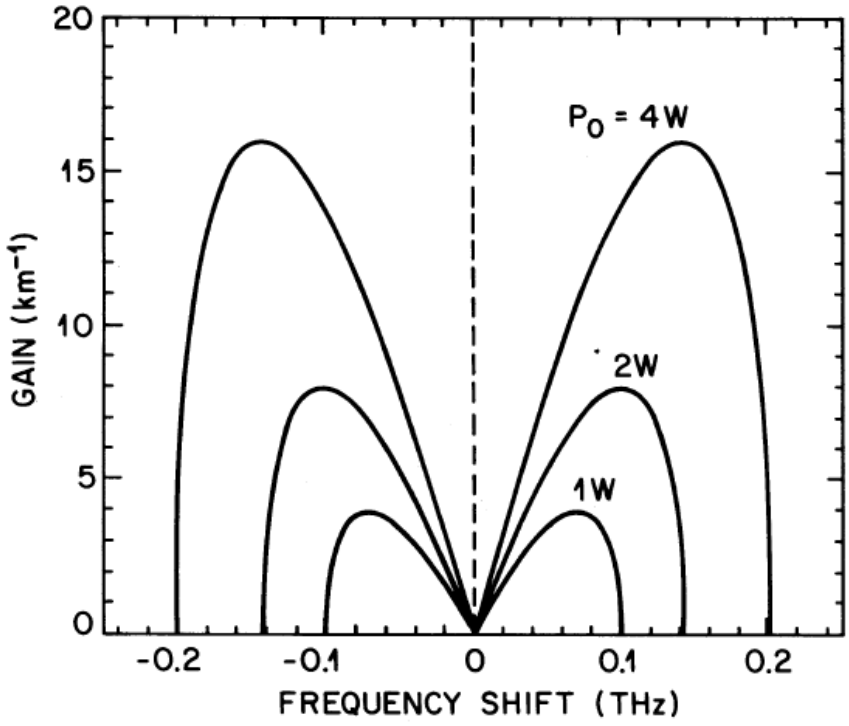

Figure 1. Shows the gain spectra of modulation instability for the three levels of power [1]

Plots in figure 1 illustrate the increase in gain at the Brillouin frequency shift ~ 11GHz due to MI corresponding to peak powers in excess of 1W. This situation can be avoided by using fibre with zero dispersion or even negative dispersion value [3] at the wavelength of operation.

The theoretical study of the SPM related broadening effects of the Rayleigh signal in chapter 5, identified the necessity of the sharp transition edge together with a flat top requirement of the fibre Bragg grating, used during the collection of the anti-Stokes Brillouin signal. The study predicted a temperature accuracy of 1°C over the sensing length of 0.1km, using peak pulse powers of 99.7W. Hence, use of 76.10W peak pulse power would deliver a similar level of temperature accuracy over 0.13km of sensing length.

In comparison to all the other non linear effects, the threshold powers corresponding to SPM, emerges as the lowest pulse peak power that can be used safely without deteriorating the signal to noise of the B-OTDR measurements. Hence use of 76.10W of peak pulse power would improve the existing signal level in the B-OTDR results of chapter 4 by 15.8dB and in the absence of optical amplification this increase in peak power would not only improve the signal to noise ratio but also reduce the averaging time, resulting in the possible applicability of the sensor for high spatial resolution temperature compensated dynamic strain measurements.

7.2.1.5 Loss compensation

In the previous experimental chapters, the technique of normalizing the R-OTDR measurements for elevated temperatures against room temperature measurements has proven beneficial in cancelling out the length dependent pump depletion effects occurring as a consequence of SRS and similarly in the case of B-OTDR a similar normalisation protocol tackles the problem leading to deterioration of the signal to noise as a function of length due to MI and SPM related effects. But it is the insensitivity of the Rayleigh signal to temperature and strain effects, which is recognised as a preferred choice for normalization of Brillouin [4] and Raman signals [5] over long distances.

In the case of B-OTDR measurements, the normalization carried by the Rayleigh signal is shifted by 0.1nm and is still considered valid because the transmission losses experienced by the two wavelengths separated by such a small amount are

nearly equal. However, the disadvantage with the Rayleigh based normalization protocol is the emergence of uncertainties in the distributed temperature measurements due to coherent Rayleigh noise [4]. Although, the coherent Rayleigh noise (CRN) decreases with increase in the effective line width of the source [4], the high spatial resolution capability of our sensor, indicates a requirement for loss compensation ability with a similar spatial resolution. In order to achieve 1% of coherent Rayleigh noise, source line width in excess of 200nm is required. The challenge is not only in designing a source with such bandwidth requirements but also in finding similar bandwidth optical amplifiers in order to achieve 1ns high peak power pulses. In addition, such a broadband source would also suffer from wavelength dependent bend losses and hence if used to normalize the much narrower, i.e., 35MHz Brillouin signal, it would lead to misleading results. Thus, the idea of exploiting the Rayleigh normalization protocol in order to develop a loss compensation scheme for high spatial resolution temperature compensated distributed strain sensor is rather impractical. The lack of applicability of the Rayleigh normalization protocol to high spatial resolution B-OTDR measurements necessitates the finding for an alternative normalization protocol that can be used to provide reliable loss compensation.

The B-OTDR measurements could also be normalised using the R-OTDR measurements. From the theoretical performance comparison study between R-OTDR and B-OTDR in chapter 5, in terms of better signal to noise ratios B-OTDR emerged better than the R-OTDR. This implies that the signal to noise ratio of the B-OTDR can be reduced to match that of R-OTDR, allowing for a subsequent normalization of the B-OTDR by the R-OTDR. In the future, it would be very useful to identify the fibre losses [6] beyond which this normalization scheme proves to be effective.

7.3 Conclusion

The experimental work in the previous chapters has demonstrated the capability of measuring 22με of temperature compensated distributed strain with under 10cms of

spatial resolution. The discussion following the experimental work clearly identify further improvements in the signal levels of the B-OTDR measurements, resulting in reduced data averaging times. Table 2 summarises the achievements till date in measuring temperature compensated distributed strain. The term STF used in the table below stands for standard telecommunications fibre, while the term PM stands for polarization maintaining fibre.

Ref.	Spatial Res.	Strain Res.	Temp. Res.	Fibre type	Range	Technique Used
[7]	20m	100με	4°C	STF	30km	Coherent detection of spontaneous Brillouin backscatter
[8]	5m	85με	3.5°C	STF	50km	Coherent detection of spontaneous Brillouin backscatter with in line Raman amplification
[9]	1.3m	80με	3°C	STF	6.3km	Microwave detection system for spontaneous Brillouin backscatter
[10]	20cm	9με	0.4°C	PM	6m	DPP-BOTDA
[11]	10cm	12με	0.3°C	PM	8m	BOCDA
[12]	5cm	63με	2°C	STF	18m	BOCDA +BOTDR

Table 2. The achievements of previous techniques with spatial, temperature and strain resolutions respectively

It is also understood that the existing performance capability of the sensor, as demonstrated in chapter 4, can be further enhanced by integrating a loss compensation scheme to the intensity measurements. Such a feature would not only provide immunity to bend losses but would also prove beneficial in quantifying post installation strains in the sensing fibre.

The normalization protocols used during the R-OTDR and B-OTDR measurements, utilising the normalization of elevated temperature measurements against room temperature measurements, has proven beneficial in tackling the effect of deterioration in the signal to noise values as a result of onset of length dependent nonlinear effects, i.e., SRS in the case of R-OTDR and MI and SPM in the case of B-OTDR.

The study of the Brillouin coefficients under a simultaneously varying strain and temperature environment identified corrections to the Brillouin coefficients, which prove necessary in the estimation of the true value of the applied strain and the change in temperature. However, the Brillouin coefficient which has the dominant contribution to error in the estimation of applied strain and change in temperature values needs to be investigated.

7.4 Future Work

With the growing demand on the development of high speed rail networks and other civil structures such as dams, bridges etc., there is also an ever increasing demand for probing the integrity of the structure whilst in use. Incorporating robust and reliable features probing the structure of such high performance engineering projects brings forth the challenge of performing dynamic measurements with true real time capabilities. Much in line with such requirements that the reduced data collection and analysis time achieved with the combinatory technique of BOCDA and BOTDR, presented in chapter 4, makes it very attractive to perform temperature compensated dynamic strain measurements in future. It is also known that for all practical

purposes temperature effects which would vary at low frequencies compared to the higher frequency dynamic strain can be considered virtually d.c. Although this relaxes the high frequency temperature mapping requirement, which at the moment relies on Brillouin intensity measurements and hence requires longer time for signal processing than the strain measurement, it would still require measuring both strain and temperature, i.e., making independent Brillouin intensity and Brillouin frequency measurements.

Alternatively, such a class of engineering problems requiring dynamic strain measurements with temperature compensation can also be tackled exploiting special fibres. Design of such fibres would involve exploiting multiple acousto-optic interactions and their correspondingly different responses to strain and temperature impositions. A sensing fibre with such a characteristic would support an all frequency based temperature compensated distributed strain measurement, thereby reducing the time taken during intensity measurements. Recently much of the work in suppression of the SBS effects has been focussed into exploring various means to influence refractive indices of the propagating acoustic and optical modes in optical fibres. This implies that the optical refractive index can be changed and so is its acoustic refractive index. The acoustic refractive index is defined as $n_a = V_h / V$ [13], where V is the acoustic velocity of the doped material (such as Ge-doped silica) and V_h is the acoustic velocity of the host material (Silica). Table 3 [14] shows a summary of the effect of various dopants on the optical (n_o) and acoustic refractive (n_a) indices when added to pure silica, (assuming $n_a = 1$ for pure silica) [15], with RE representing rare earth and upward arrow sign depicts an increase while the downward arrow sign depicts a decrease in the value of the respective refractive index.

	Ge	P	Ti	B	F	Al	Y	RE
n_o	↑	↑	↑	↓	↓	↑	↑	↑
n_a	↑	↑	↑	↑	↑	↓	↓	↑

Table 3. Shows the effect of dopant on the acoustic and optical index of silica with RE representing rare earth [14]

Figure 2, shows an example where the acoustic velocity profile has been designed such that the Brillouin gain spectrum (BGS) has a multitude of acoustic modes spread across a wide frequency range [14]. The dashed line represents the location of the optical core. The top BGS corresponds to a conventional Ge-doped step-index Er fiber, while the lower plot shows an Er-doped fiber designed to have multiple acoustic modes spread across a wide frequency range. The spectrum in figure 2 is broadened between 11.2GHz to 11.5GHz, which can be attributed to acoustic waveguide loss that tends to broaden the spectrum. Such a spectral broadening is explained as a consequence of change in the longitudinal field in the cladding from evanescent to radiative within an infinite-cladding model [14].

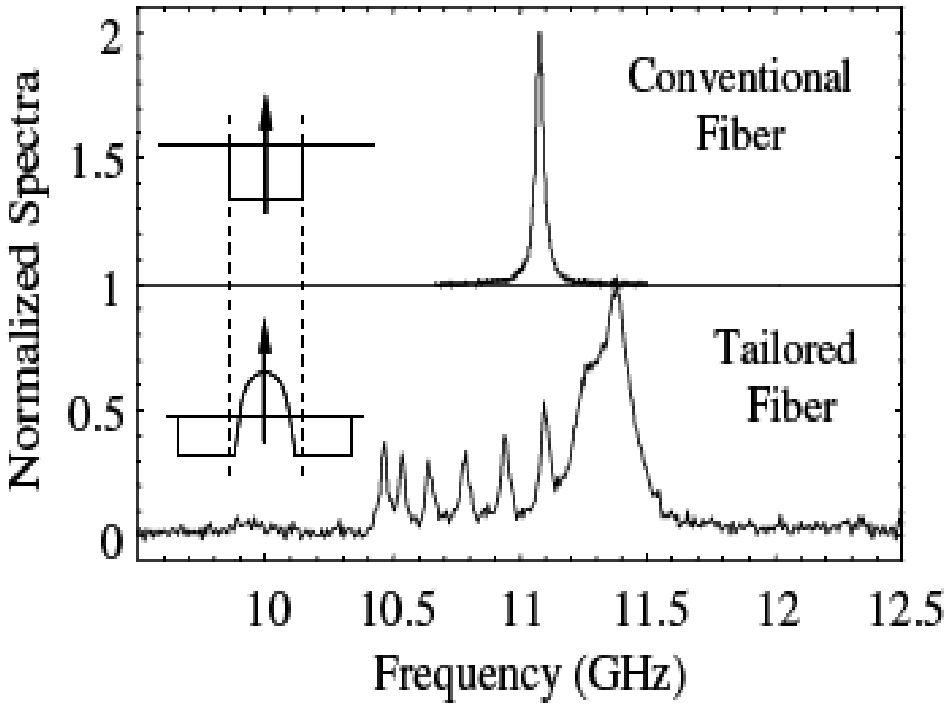

Figure 2. Normalised Brillouin gain spectrum BGS of a conventional (top) and a Brillouin-tailored (bottom) fibre measured at 1534nm. The acoustic velocity profiles are shown and the dashed line shows the location of the core [14]

Whilst the fibre fabrication community has largely focussed on exploiting the broadening of the BGS for high power fibre laser applications that the same concept

finds applications within the distributed sensing community where the multiple peaks as shown in figure 2 of the BGS could potentially have different response to strain and temperature effects. Different responses to temperature and strain based on multiple Brillouin peaks in a BGS would eventually help develop sensors allowing for the temperature compensated distributed strain measuring capabilities, as demonstrated earlier in chapters 3 and 4, except for the fact that it would involve a special fibre.

7.5 References

[1] G.P. Agarwal, ‘‘Nonlinear Fibre Optics’’, Third Edition, Academic Press (2001)

[2] S. M. Maughan, PhD thesis, ORC, University of Southampton (2001)

[3] M. N. Alahbabi, Y. T. Cho, T. P. Newson, P. C. Wait and A. H. Hartog, ‘‘Influence of modulation instability on distributed optical fiber sensors based on spontaneous Brillouin scattering’’, *Journal of the Optical Society of America B*, 21(6), p 1156-1160 (2004)

[4] P. C. Wait and T. P. Newson, ‘‘Reduction of coherent noise in the Landau Placzek ratio method for distributed fibre optic temperature sensing’’, *Optics Communications*, 131, p 285-289 (1996)

[5] H. H. Kee, G. P. Lees and T. P. Newson, ‘‘1.65μm Raman based distributed temperature sensor’’, *Electronics Letters*, 35(21), p 1869-1871 (1999)

[6] D. Marcuse, “Curvature loss formula for optical fibers”, *Journal of the Optical Society of America B*, 66, p 216-220 (1976)

[7] S. M. Maughan, H. H. Kee and T. P. Newson, ‘‘Simultaneous distributed fibre temperature and strain sensor using microwave coherent detection of spontaneous Brillouin backscatter’’, *Measurement Science and Technology*, 12, p 834 (2001)

[8] M. N. Alahbabi, Y. T. Cho and T. P. Newson, ‘‘Long-range distributed temperature and strain optical fibre sensor based on the coherent detection of spontaneous Brillouin scattering with in-line Raman amplification’’, *Meas Measurement Science and Technology*.**,** 17**,** p 1082 (2006)

[9] M. N. Alahbabi, N. P. Lawrence, Y. T. Cho and T. P. Newson, ‘‘High spatial resolution microwave detection system for Brillouin-based distributed temperature and strain sensors’’, *Measurement Science and Technology*, 15, p 1539 (2004)

[10] Y. Dong, L. Chen, and X. Bao, “Demonstration of Brillouin distributed discrimination of strain and temperature using a polarization-maintaining optical fiber”, *IEEE Photonics Technology Letters*, 22(18), p 1364-1366 (2010)

[11] Zou, He and Hotate , “Demonstration of Brillouin distributed discrimination of strain and temperature using a polarization-maintaining optical fiber”, *IEEE Photonics Technology Letters*, 22(8), p 526-528 (2010)

[12] M. Belal and T. P. Newson, ‘‘A 5cm spatial resolution temperature compensated distributed strain sensor evaluated using a temperature controlled strain rig’’, *Optics Letters*, 36(24) (2011)

[13] P. D. Dragic, C. H. Liu, G. C. Papen, and A. Galvanauskas, ‘‘Optical fiber with an acoustic guiding layer for stimulated Brillouin scattering suppression’’, *CLEO/QELS tech. dig.*, p. 1984-1986 (2005)

[14] P. D. Dragic, ‘‘Brillouin suppression by fibre design’’, *Photonics Society Summer Topical Meeting Series, 2010 IEEE*, p 151-152 (2010)

[15] C. K. Jen et al., “Acoustic Characterization of Silica Glasses”, *Journal of American Ceramic Society*, 76, p 712-716 (1993)

LIST OF PUBLICATIONS

Journal Publications:

1. M. Belal, Y. T. Cho, M. Ibsen and T. P. Newson, ‘‘A temperature compensated high spatial resolution distributed strain sensor’’, *Measurement Science and Technology*, 21(1), p 015204 (2010)

2. M. Belal and T. P. Newson, ‘‘Enhanced performance of a temperature compensated submeter spatial resolution distributed strain sensor’’, *IEEE Photonics Technology Letters*, 22(23), p 1705-1707 (2010)

3. M. Belal, Z. Song, Y. Jung, G. Brambilla and T. P. Newson, ‘‘An optical fiber microwire current sensor’’, *Optics Letters*, 35(17), p 3045-3047 (2010)

4. M. Belal, Z. Song, Y. Jung, G. Brambilla and T. P. Newson, **‘‘**An interferometric current sensor based on optical fiber micro wires’’, *Optics Express*, 18(19), p 19951-19956 (2010)

5. M. Belal and T. P. Newson, ‘‘Experimental examination of the variation of the spontaneous Brillouin power and frequency shift under the combined influence of temperature and strain’’, *Journal of Lightwave Technology* (2012)

6. M. Belal and T. P. Newson, ‘‘A 5cm spatial resolution temperature compensated distributed strain sensor evaluated using a temperature controlled strain rig’’, *Optics Letters*, 36(24), p 4728-4730 (2011)

7. X. Zhang, M. Belal, G. Y. Chen, Z. Song, G. Brambilla and T. P. Newson, ‘‘Compact optical microfiber phase modulator’’, *Optics Letters*, 37(3), p 320-322 (2012)

Conference Publications:

1. M. Belal and T. P. Newson, ‘‘Temperature compensat*ed sub-metre sp*atial resolution strain sensor’’, *CLEO/QELS* San Jose 16-21 May 2010 CFH5
2. M. Belal and T. P. Newson, ‘‘Sub-metre spatial resolution temperature compensated distributed strain sensor’’, *Photon 10* Southampton 23-26 Aug 2010
3. G. Brambilla, Y. Jung, M. Belal, F. Xu, P. Horak, T. P. Newson, D. J. Richardson, ‘‘Optical micro-nano/fibre sensors and resonating sensors’’, *IEEE Sensors* Waikoloa, Hawaii 1-4, Nov 2010 (Invited)
4. G. Brambilla, M. Belal, Y. Jung, T. P. Newson, D. J. Richardson, ‘‘Nanotaper based sensors’’, *IEEE Winter Topicals* Keystone, Colorado 10-12, Jan 2011 (Invited)
5. G. Y. Chen, T. Lee, Y. Jung, M. Belal, G. Brambilla, N. G. R. Broderick, T. P. Newson, ‘‘Investigation of thermal effects on embedded microcoil resonators’’, *CLEO/Europe-EQEC*, Munich 22-26, May 2011
6. G. Brambilla, M. Belal, Y. Jung, Z. Song, F. Xu, T. P. Newson, D. J. Richardson, ‘‘Optical fibre microwire sensors’’, *OFS 21* Ottawa, Canada 15-19 paper 7753-14, May 2011 (Invited)
7. M.Belal and T.P.Newson, ‘‘Performance comparison between Raman and Brillouin intensity based sub metre spatial resolution temperature compensated distribued strain sensor’’, *CLEO/Europe-EQEC*, Munich 22-26, May 2011
8. M.Belal and T.P.Newson, ‘‘Evaluation of a high spatial resolution temperature compensated distributed strain sensor using a temperature controlled strain rig’’, *OFS 21* Ottawa Canada 15-19, 7753-366, May 2011

9. M.Belal and T.P.Newson, ‘‘Experimental examination of the variation of the spontaneous Brillouin power and frequency shift under the combined influence of temperature and strain’’, *OFS 21* Ottawa Canada, 7753-357, 15-19 May 2011

10. G. Y. Chen, M. Belal, G. Brambilla and T. P. Newson, ‘‘High frequency current sensing using optical fiber micro-wire’’, *CLEO/Europe-EQEC* Munich CH6.4, 22-26 May 2011